Fall November 2014

CHARACTERIZATION OF Ca2+ INFLUX PATHWAY(S) DURING MOUSE OOCYTE MATURATION

Banyoon Cheon
bcheon@mcb.umass.edu

CHARACTERIZATION OF Ca^{2+} INFLUX PATHWAY(S) DURING MOUSE OOCYTE MATURATION

A Dissertation Presented

by

Banyoon Cheon

Submitted to the Graduate School of the

University of Massachusetts Amherst in partial fulfillment

of the requirements for the degree of

DOCTOR OF PHILOSOPHY

September 2014

Program in Molecular and Cellular Biology

CHARACTERIZATION OF Ca^{2+} INFLUX PATHWAY(S) DURING MOUSE OOCYTE MATURATION

A Dissertation Presented
by
Banyoon Cheon

Approved as to style and content by:

_____
Rafael A. Fissore, Chair

_____
Pablo E. Visconti, Member

_____
Jesse Mager, Member

_____
Alejandro P. Heuck, Member

_____
Barbara A. Osborne, Director
Program in Molecular and Cellular Biology

ACKNOWLEDGEMENTS

I would like to thank my advisor Dr. Rafael Fissore for his time, funding, and advice to make me achieve Ph.D. I sincerely appreciate all members of dissertation committees, Drs. Pablo Visconti, Jesse Mager and Alejandro Heuck for guiding me and providing helpful idea and discussion about the thesis work. I also like to thank to colleagues of our lab current and past lab members who taught and provide me resources, knowledge, and skills, and all people in VASCI department.

I would like to thank all people who helped and inspired me. Especially for my friends, they gave me such diverse experiences that enriched my mind and life with positive energy and inspired me in many ways. I am really indebted to them.

Lastly, I thank you to my parents and lovely siblings for their endless love, support, and trust. I would like to express my honor and love to my deceased great parents. I wish they could hear my wholehearted appreciation in heaven.

ABSTRACT

CHARACTERIZATION OF CA^{2+} INFLUX PATHWAY(S)

DURING MOUSE OOCYTE MATURATION

SEPTEMBER 2014

BANYOON CHEON, B.E., SEJONG UNIVERSITY

M.A., KOREA UNIVERSITY

Ph.D., UNIVERSITY OF MASSACHUSETTS AMHERST

Directed by Professor RAFAEL A. FISSORE

Ca^{2+} signaling induced at fertilization, also known as oscillations, is essential in mammalian eggs to initiate early embryonic development. The generation of the oscillations relies on optimization of Ca^{2+} toolkit components during oocyte maturation. In this dissertation, we intend to deepen our understanding of how this differentiation of the Ca^{2+} toolkit, especially those components associated with Ca^{2+} influx, is achieved during maturation, and how it contributes to the filling of the ER Ca^{2+} store during the maturation and fertilization.

We first identified the expression and characterized the function of the components of the Store Operated Ca^{2+} Entry (SOCE) during oocyte maturation. We observed that SOCE underwent suppression during maturation concomitant with an increase in $[Ca^{2+}]_{ER}$ content. We demonstrated that the suppression of SOCE coincided with the inability of Stim1, the Ca^{2+} sensor in ER, to form puncta near the PM, which prevented interaction with Orai1, the channel on the PM. Consistent with a possible role on Ca^{2+} homeostasis in oocytes, overexpression of Stim1 and Orai1 increased basal Ca^{2+} levels during maturation, especially during the GV stage, but this influx was suppressed in MII eggs. These results suggest that Ca^{2+} uptake during maturation is

closely related to the Ca^{2+} content of the ER. Bypassing this inactivation via expression of mutant versions of Stim1 prevented oocytes from resuming meiosis.

The inactivation of SOCE was due in part to changes in Stim1 organization during maturation. We found that Stim1 reorganization was occurred largely due to CDK1. We confirmed the effect of phosphorylation by expressing several non-phosphorylated mutants of Stim1. These mutants displayed cortical location and puncta, and interact with Orai1, and enhanced Ca^{2+} influx at the MII stage.

Thus, our study also demonstrates that Ca^{2+} influx and SOCE are actively regulated during mouse oocyte maturation by the MII stage, the stage of fertilization. The suppression of SOCE relies on phosphorylations on the C-terminal end of Stim1 by CDK1.Therefore our studies show that down-regulation of Ca^{2+} influx is required for oocyte maturation and meiotic progression, although it is still unclear how the sperm manages to re-activate Ca^{2+} influx after fertilization, and what channel(s) underlie Ca^{2+} influx during fertilization. Future studies should address how this is accomplished and the channel(s) that mediate it.

TABLE OF CONTENTS

Page

LIST OF FIGURES

Figure **Page**

LIST OF ABBREVIATIONS

AP	Antigenic peptide
BSA	Bovine serum albumin
Ca^{2+}	Calcium
CAD	CRAC activation domain
CAMKII	Ca^{2+}-Calmodulin-dependent kinase II
CIP	Calf intestine phosphatase
CZB	Chatot, Ziomek, and Bavister medium
DAG	1,2-Diacyl Glycerol
DMSO	Dimethylsulfoxide
ER	Endoplasmic Reticulum
ERM	Ezrin-radixin-moesin
FSH	Follicule stimulating hormone
Fura-2AM	Fura-2 Acetomethyl Ester
GV	Germinal vesicle stage of meiosis I
GVBD	GV breakdown
HCZB	Hepes-buffered CZB
HRP	Horseradish peroxidase
IP_3	Inositol 1,4,5-triphosphate
IP_3R	IP_3 receptor
LH	Luteinizing hormone
MAP	Mitogen Activated Protein
MI	Metaphase I of second meiosis

MII	Metaphase stage of Meiosis II
mRFP	Modified red fluorescent protein
PIP_2	Phosphatidylinositol 4,5-biphosphate
PLC	Phospholipase C
PM	Plasma membrane
PMCA	Plasma membrane Ca^{2+} ATPase
PMSG	Pregnant mare serum gonadotropin
PN	Pronucleus
PVA	Polyvinyl alcohol
SAM	Sterile α-motif
SERCA	Sarco/endoplasmic reticulum Ca^{2+} ATPase
SOCE	Store operated Ca^{2+} entry channels
Stim1	Stromal interaction molecule 1
TG	Thapsigargin
TL-Hepes	Hepes-buffered tyrode-lactate solution
TRP	Transient receptor potential channel
VGCC	Voltage gated Ca^{2+} channels
WGA	Wheat Germ Agglutinin
YFP	Yellow Fluorescent Protein
$[Ca^{2+}]_i$	Intracellular concentration of free Ca^{2+}
$[Ca^{2+}]_e$	Extracellular concentration of free Ca^{2+}
$[Ca^{2+}]_{ER}$	ER Ca^{2+} concentration

CHAPTER 1

INTRODUCTION

1.1 The Ca^{2+} signaling toolkit

Ca^{2+} signaling controls numerous biological functions of cells such as motility, innate immunity, apoptosis, transmission of neuronal signal, transcription, and fertilization [1, 2]. Those various effects are initiated by numerous different stimuli of cells including electric, hormonal and/or mechanical stimulation, which converge to increase intracellular free Ca^{2+}, ($[Ca^{2+}]_i$) ; the released Ca^{2+} either directly binds and activates target proteins or indirectly activates target proteins by interacting with Ca^{2+} adaptor proteins (Fig. 1-1). To be used as an effective signaling molecule, cells must tightly regulate the levels of baseline $[Ca^{2+}]_i$ resting while at rest or un-stimulated conditions. To accomplish this, cell compartmentalize Ca^{2+} such that there are ~1-2 mM Ca^{2+} in the extracellular space ($[Ca^{2+}]_e$), ~ a few hundred μM in the endoplasmic reticulum (ER) and between 50 to 100 nM in the cytoplasm [1, 2]. These large Ca^{2+} gradients across the plasma membrane, the cytoplasm and the ER are maintained not only by physical barriers, but also by active sequestration/extrusion of Ca^{2+} from the cytoplasm by molecules such as the sarco/endoplasmic reticulum Ca^{2+} ATPase (SERCA) and the plasma membrane Ca^{2+} ATPase (PMCA), and a Na^{+}/Ca^{2+} exchanger [1]. These large Ca^{2+} gradients between compartments are associated with constant leaks of Ca^{2+} into the cytoplasm, which requires the actions of the aforementioned system to maintain it at ~100 nM.

The $[Ca^{2+}]_i$ increases caused by most stimuli rely on two main sources of Ca^{2+}; one source is the ER and the other is Ca^{2+}influx across the PM[2, 4]. Ca^{2+} release from the ER is equivalent to that from the sarcoplasmic reticulum (SR) in muscle cells, although it occurs mostly through inositol-1, 4, 5-triphosphate receptors (IP_3R) instead of ryanodine receptors. IP_3Rs-mediated Ca^{2+} release is activated by the binding of IP_3, which is generated by the hydrolysis of

phosphatidylinositol-(4,5)-bisphosphate (PIP_2) by phospholipase C (PLC) [2]. Increases in $[Ca^{2+}]_i$ mediated by Ca^{2+}influx are made possible by Ca^{2+} entry via Ca^{2+} channels in the PM that respond to different stimuli, including membrane depolarization, extracellular agonists and depletion of the ER. Among these channels there are voltage gated Ca^{2+} channels (VGCCs), transient receptor potential (TRP) channels and Store Operated Ca^{2+} entry channels (SOCE) [1, 3, 5]. Specific stimuli open the aforementioned channels by changing the conformation of the protein and/or subunits, which favors conductivity. Particular cell types possess a specific complement of these channels, which are finely tuned to respond to their physiological functions. Regardless of the source, $[Ca^{2+}]_i$ rises are translated into various cell functions via the activation of downstream proteins [6].

Although the general properties of the Ca^{2+} toolkit required to regulate Ca^{2+} homeostasis is conserved among species and cell types, there are, as already pointed out, specific adaptations so that specific signals as well as specific decoding of these signals can be accomplished for distinct functions. Cells and/or organisms can accomplish this specificity by displaying proteins and enzymes with diverse sensitivities to Ca^{2+}, presence of multiple adaptors, buffering molecules and down-stream target proteins as well as by delivering a Ca^{2+} signal with precise temporal and spatial distribution[3].

1.2 Ca^{2+} roles during mouse oocyte maturation and fertilization

A well-known example of Ca^{2+} signaling is fertilization. Ca^{2+} release plays a critical role during fertilization in all species examined to date [7-10]. $[Ca^{2+}]_i$ is known to increase from ~100 nM in eggs of all species, although the duration and pattern of the $[Ca^{2+}]_i$ varies radically among species [8]. In the mouse, after fusion of the gametes, sperm-induced $[Ca^{2+}]_i$ signal lasts for a few hours and display a pattern of brief $[Ca^{2+}]_i$ rises interspersed among long intervals of basal concentrations, which is referred to as $[Ca^{2+}]_i$ oscillations (Fig.1-2). These long-lasting Ca^{2+}

transients trigger the initiation and completion of several cellular functions including the resumption and completion of meiosis, release of cortical granules [11], and progression of the cell cycle; these events are collectively called "egg activation" [10, 12, 13]. In mammals, the oscillations are thought to be initiated by a sperm-specific phospholipase C (PLC), PLC zeta1 (ζ) [14]. PLCζ is thought to hydrolyze release from ER [15-17]. While the initial $[Ca^{2+}]_i$ responses emanates from the ER, Ca^{2+} influx is required for the persistence of the oscillations, as without $[Ca^{2+}]_e$ oscillations cease prematurely [18]. Downstream of Ca^{2+} rises, well-known effectors such as calmodulin [19, 20], PKC and Ca^{2+}-CaM-dependent kinase II (CaMKII), especially CaMKIIγ, underlie the initiation and completion of most events of egg activation [21, 22].

While $[Ca^{2+}]_i$ oscillations are required for egg activation, additional studies suggest in role in influencing the early steps of embryo development. Moreover, an abnormal pattern of oscillations can lead to abnormal development and even cell death [12, 23-25]. Therefore, to support the precise temporal-spatial pattern of oscillations required for egg activation and embryo development, oocytes optimize the Ca^{2+} toolkit during maturation.

1.3 Differentiation of Ca^{2+} signaling machinery during meiotic maturation

Meiosis is a process during which diploid male or female germ cells reduce their genomic content in preparation for fertilization such that fertilization restores the diploid state required for successful development. The female gamete, oocyte and/or egg, is stored in the ovary in follicles surrounded by different number of layers of somatic cells, the granulosa cells (Fig. 1-3). After the onset of puberty, populations of follicles begin to grow along with oocytes and under the influence of a complex hormonal milieu that includes the gonadotropin hormones FSH and LH. Some of these follicles reach the ovulatory stage, Graafian follicles, which contain a fully grown immature oocyte [26]. This oocyte is arrested in prophase I of meiosis I and possesses a distinctive, large size nucleus, from which its name derives, the germinal vesicle stage [27]

oocyte. Upon release of LH, which will also induce ovulation, the GV oocyte resumes meiosis and initiates the process of maturation. This process can be morphologically determined by observing the dissolution of the germinal vesicle ~ 2 hrs after the LH surge, which is commonly referred to as GV breakdown (GVBD) and is driven by activation of M-phase kinases, CDK1 and Mitogen Activated Protein (MAP) kinase [28, 29]. After GVBD, chromosomes are assembled in a metaphase plate that migrates to the cell cortex and this is followed the release of the first polar body (PB), which contains half of the homologue chromosome present in the oocyte. Release of the PB marks the completion of 1st meiosis, and oocytes then enter the second meiosis where they immediately arrest at the metaphase stage of the second meiosis MII [30, 31]. Besides nuclear maturation, oocytes also undergo cytoplasmic maturation, including optimization of the Ca^{2+} tool kit (Fig.1-4). For example, GV oocytes are endowed with low Ca^{2+} levels in the ER ($[Ca^{2+}]_{ER}$), but by completion of maturation and upon reaching the MII stage, the content of the $[Ca^{2+}]_{ER}$ has increased steadily [32, 33]. The mass of IP_3R1 also increases during maturation and its distribution undergoes marked changes, attaining cortical accumulation [34-36]. Importantly, while many of the molecular mechanisms underlying these changes are known, what remains largely unknown are the mechanisms that lead the increase in $[Ca^{2+}]_{ER}$, including the channels that mediate Ca^{2+} entry from $[Ca^{2+}]_e$. In this vein, it is worth noting that mouse GV oocytes display spontaneous oscillations that terminate around the time of GVBD stage, which is when the first time when a noticeable increase in $[Ca^{2+}]_{ER}$ is detected [33, 37, 38]. These results suggest an association between $[Ca^{2+}]_{ER}$ content and Ca^{2+} influx, and such an association has been reported to underlie Store Operated Ca^{2+} Entry (SOCE), a widespread Ca^{2+} entry mechanism whereby Ca^{2+} influx follows the release of $[Ca^{2+}]_i$, generally associated with activation of the phosphoinositide pathway and production of IP_3 [39, 40]; it is possible that a similar mechanism may play a role in oocytes during maturation and in eggs after fertilization.

1.4 Calcium influx pathways in mouse oocyte

1.4.1 Store Operated Ca^{2+} Entry (SOCE)

SOCE was first proposed as a means for cells to refill Ca^{2+} stores after Ca^{2+} release induced by agonist stimulation caused the depletion of $[Ca^{2+}]_{ER}$ [39] (Fig.1-5a). Subsequent studies showed that depletion of $[Ca^{2+}]_{ER}$ by other mechanisms such as by inhibitors of SERCA such as thapsigargin [41] could also trigger Ca^{2+} influx, which demonstrated the prevalence of this mechanism in somatic cells and its contribution to Ca^{2+} homeostasis [42-45]. The presence of SOCE was first confirmed by electrophysiological means, as its presence elicits unique current properties, which was named I_{CRAC} [40, 45-47]. Nevertheless, the molecular identities for I_{CRAC} remained unknown for many years, until a few years back when the two major components of SOCE, stromal interacting molecule 1 (Stim1), which acts as the ER Ca^{2+} sensor [5, 48, 49] and Orai1, the plasma membrane channel [50, 51], were discovered and characterized (Fig.1-5b,c respectively). Stim1 is a single passing ER resident protein with its N-terminus facing the ER lumen and the C-terminus facing the cytoplasm. Thus, whereas the ER luminal part senses ER depletion, the C-terminus functions to communicate with Orai1. At resting state, Ca^{2+} is bound within the EF hands present on the N-terminus of Stim1, which maintains the sterile α-motif [52] also in the same area of the protein in closed conformation [53]. Upon depletion of the ER store, generally associated with opening of IP_3Rs, Ca^{2+} dissociates from the EF hands, which cause the SAM domain to change conformation so that it can oligomerize. Mutations that disable one of the negatively charged amino acids in the EF hand domain, such as the D76A mutation, cause Stim1 constantly oligomerized near the PM, which very likely engage Orai1, forming an active SOCE complex. Hereafter, these proximal Stim1 oligomers near the PM are referred to as "puncta", whereas the oligomers found deep in the cytoplasm are referred to as "internal patches". Accordingly, it has been proposed that following depletion of $[Ca^{2+}]_{ER}$, Stim1 oligomerization facilitates the migration of the oligomers to posit where the ER meets the PM, which results in the

recruiting and gating of Orai1 (Fig.1-5d) [54-56]. The mechanisms that regulate this Stim1 re-organization are unknown, although it appears to migrate in the ER via free diffusion.

The C-terminus of Stim1 contains domains related to activation and regulation of SOCE. Upon Stim1 oligomerization and puncta formation, C-terminus CRAC activation domain of Stim1 that directly interacts with Orai1 activated SOCE[54, 57, 58]. The role of CAD is further confirmed by the demonstration that expression of soluble CAD alone causes constitutive Ca^{2+} influx, without store depletion, suggesting that it represents the minimal domain required for interaction with Orai1[54]. After the CAD domain, Stim1 contains ~ 200 amino acids among which there are ten putative S/P sites, which are site of phosphorylations for M-phase kinases[59, 60], as well as a site that mediates binding with the microtubule + end binding protein, EB1 [61] and a poly lysine tail [54](Fig.1-6). The poly lysine tail is known to interact with negative charges in the plasma membrane, especially those provided by the phosphatidylinositol 4, 5-bisphospate (PIP_2), and the importance of this mechanism is reflected in the finding that depletion of PIP_2 prevents puncta formation [62, 63]. The role of S/P rich sites also appears important, as during mitosis in somatic cells and during metaphase stages of meiosis in *Xenopus* oocytes and/or eggs, SOCE is strongly inhibited [60, 64-66]. Research in both of these found that the C-terminus of Stim1 is phosphorylated during M-phase stages of the cell cycle, although the functional contribution of this modification to the inactivation of Ca^{2+} entry is contested. Whereas in mitotic cells, truncation of Stim1 such that the molecular cannot be phosphorylated or substitution of all serine residues next to proline to alanine successfully reverse the inactivation of SOCE and makes possible the formation of puncta following depletion of the ER store[59], this is not the case in *Xenopus* eggs[60]. Therefore, this suggests that the role of phosphorylation in the regulation of Stim1 may depend on the on the cell type or cell cycle stage. Given that mammalian oocytes are arrested at MII stage of meiosis and that Ca^{2+} influx is required $[Ca^{2+}]_i$ to support oscillations, it is important to understand how influx is regulated in these cells.

1.4.2 SOCE during oocyte maturation

The activity of SOCE in meiotic cells has only been well characterized in *Xenopus*. It has been shown to be present during the early stages of maturation, the GV stage, but undergoes marked inactivation as oocytes reach the GVBD stage [60, 64]. In mammals, Ca^{2+} influx can be triggered in MII eggs by addition of TG [11, 18, 67], although the mechanism(s) and molecules underlying this Ca^{2+} entry remains to be identified. Further, it is unknown whether the TG-induced influx represents SOCE. Nevertheless, transcripts and protein expression have been reported for both molecules in mouse oocytes and eggs as well as in oocytes of other mammalian species, although some of the results are inconsistent with data in somatic cells and need validation [68-70].

The overall aim of this study was to assess how Ca^{2+} influx/SOCE is regulated during oocyte maturation. We first examined if SOCE was present in oocytes and how changes in its function during maturation were associated with levels of $[Ca^{2+}]_{ER}$. We next confirmed the molecular expression of its components and established their distribution and regulation using cRNAs encoding for Stim1 and Orai1 coupled to a fluorescent protein. We observed that Ca^{2+} influx/SOCE was tightly regulated during maturation and explored the impact of unregulated Ca^{2+} influx during maturation. Lastly, we examined the role of phosphorylation in the regulation of Ca^{2+} influx/SOCE during maturation.

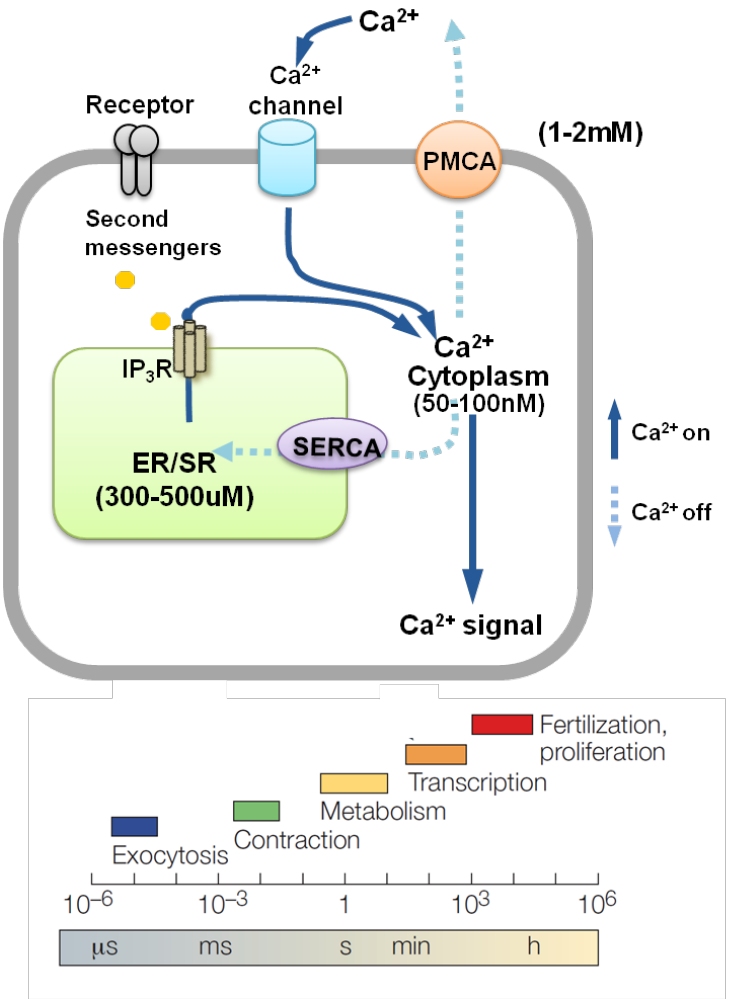

Figure 1-1. Ca^{2+} signaling toolkits

This is a schematic of Ca^{2+} handling machineries in the cell. During Ca^{2+} response is on, two resources contribute to increase $[Ca^{2+}]_{cyt}$: one is opening IP_3R and release Ca^{2+} from ER/SR and/or the other is Ca^{2+} influx across PM. Depending on spatial and temporal needs in the cell, the signal sustain a certain duration. The bottom scale depicts how long Ca^{2+} signal needs to last to exert certain functions. Ca^{2+} level is off through SERCA and PMCA that sequester cytoplasmic Ca^{2+} into ER or pump out to extracellular milieu respectively. [2]

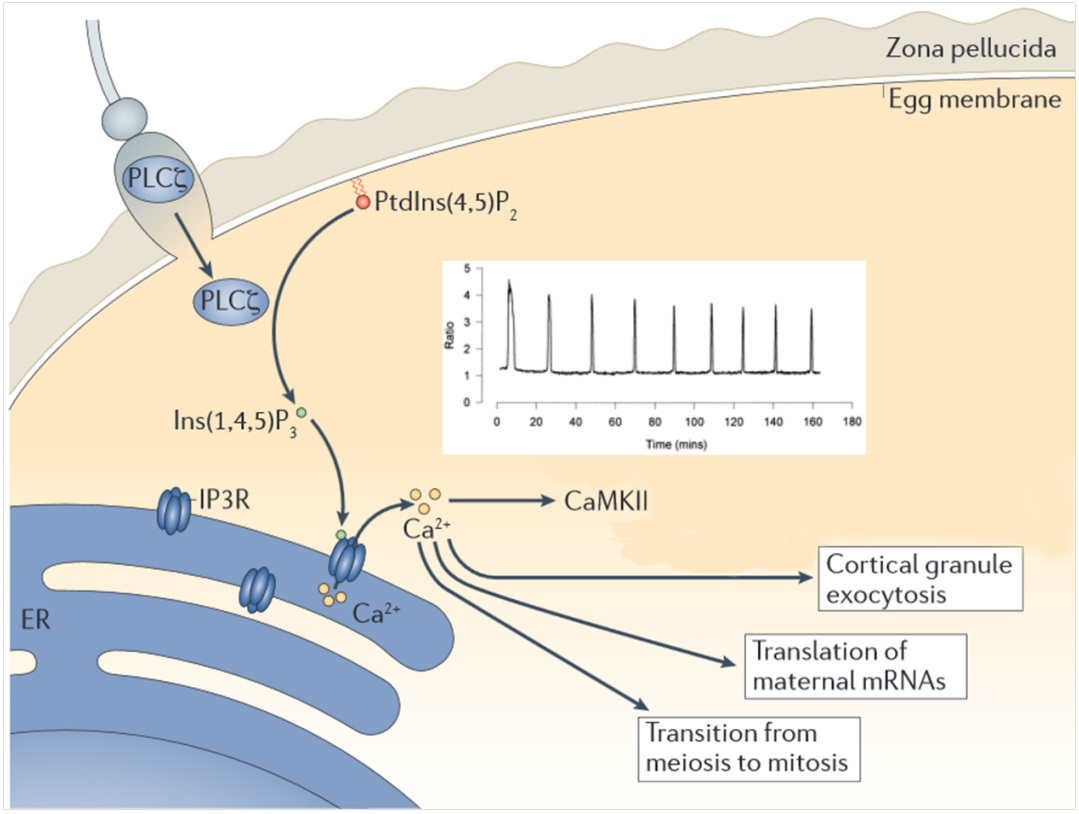

Figure 1-2. Ca^{2+} oscillations after a sperm-egg fusion and subsequent cellular events

After fertilization, release of sperm specific PLC ζ into egg degrades phosphatidylinositol 4,5 biphosphate ($PtdIns(4,5)P_2$) and produce inositol 1,4,5-triphosphoate (IP_3). Its binding to IP_3R opens the channel and release Ca^{2+} from ER, a main Ca^{2+} store in the cell. As shown in an inset, in mouse, the oscillations last more than few hours, stop around 4hr when it forms a pronuculeus (PN) that contain two nucleuses from maternal and paternal genomes. This Ca^{2+} signal involve in a series of cellular events such as activation of calmodulin kinase II (CaMKII), cortical granule exocytosis, translation of maternal mRNA and transition from meiosis and mitosis. adapted from[71].

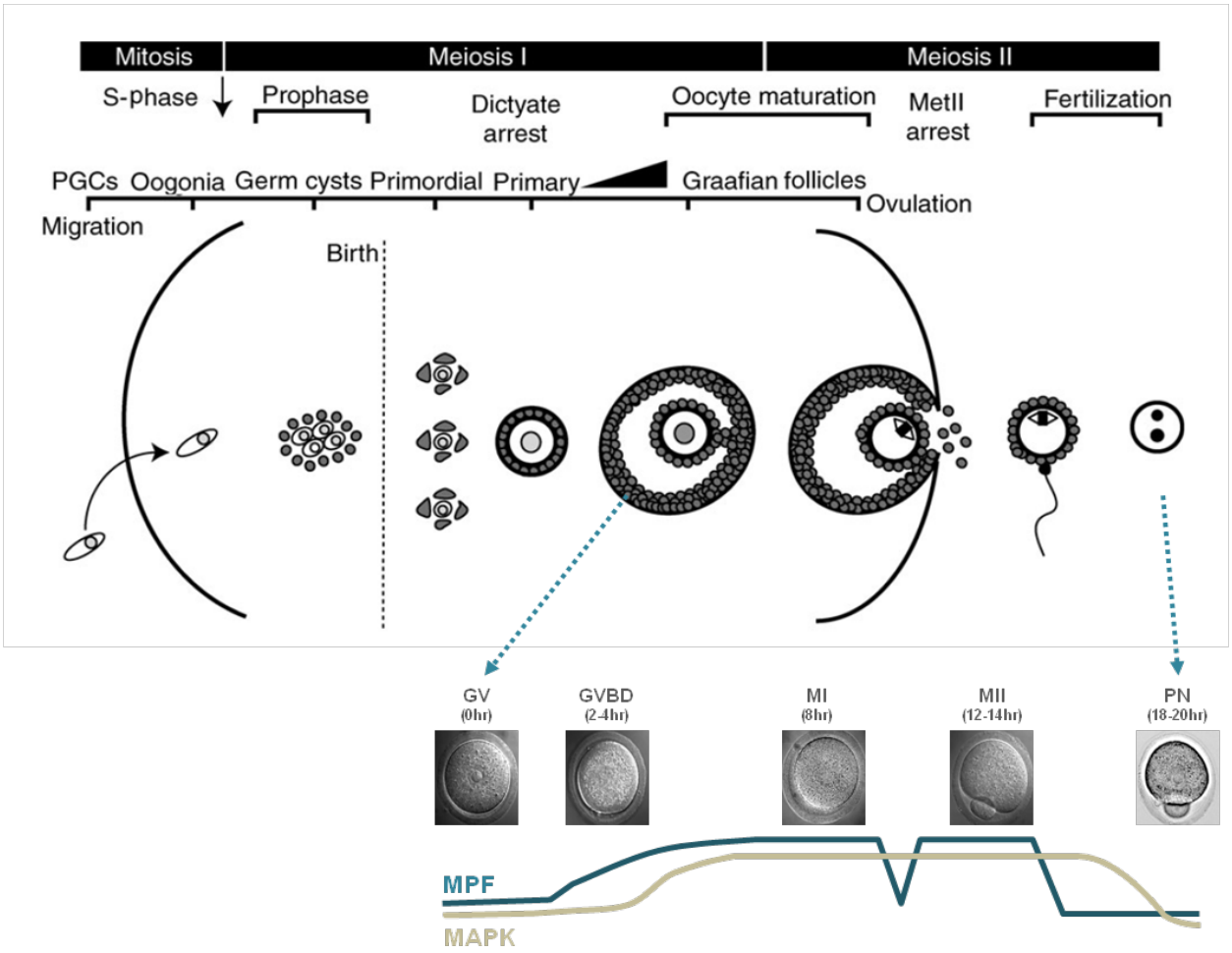

Figure 1-3. Mammalian oocyte maturation and activation [72]

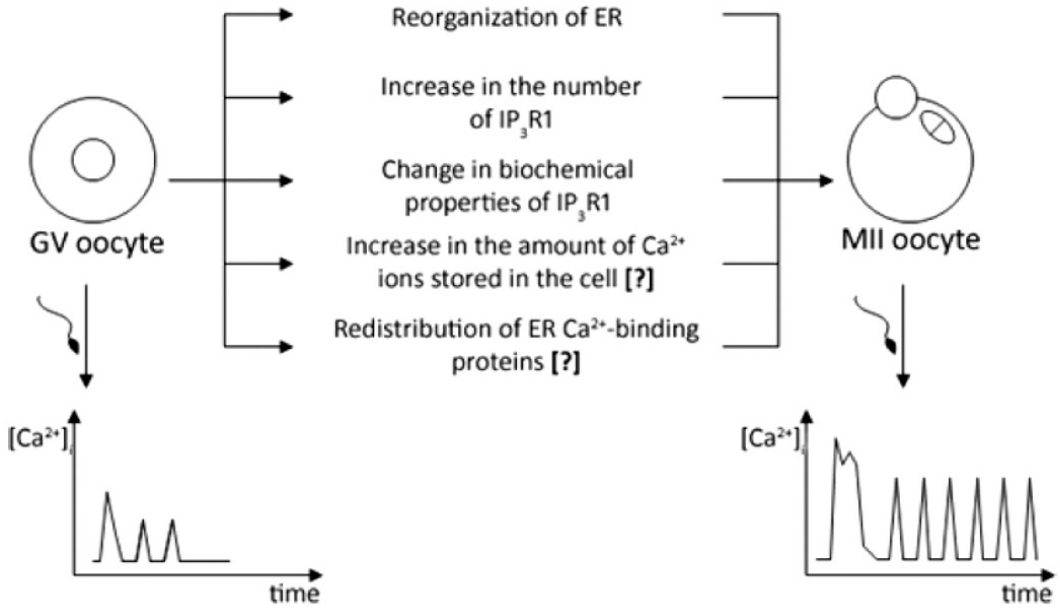

Figure 1-4. Changes in Ca^{2+} machinery during maturation.

An oocyte's ability to generate sperm-induced long-lasting Ca^{2+} oscillations develops during maturation by achieving several changes, including reorganization of the ER, increase the number of IP_3R and increase in the content of ER Ca^{2+} [73]

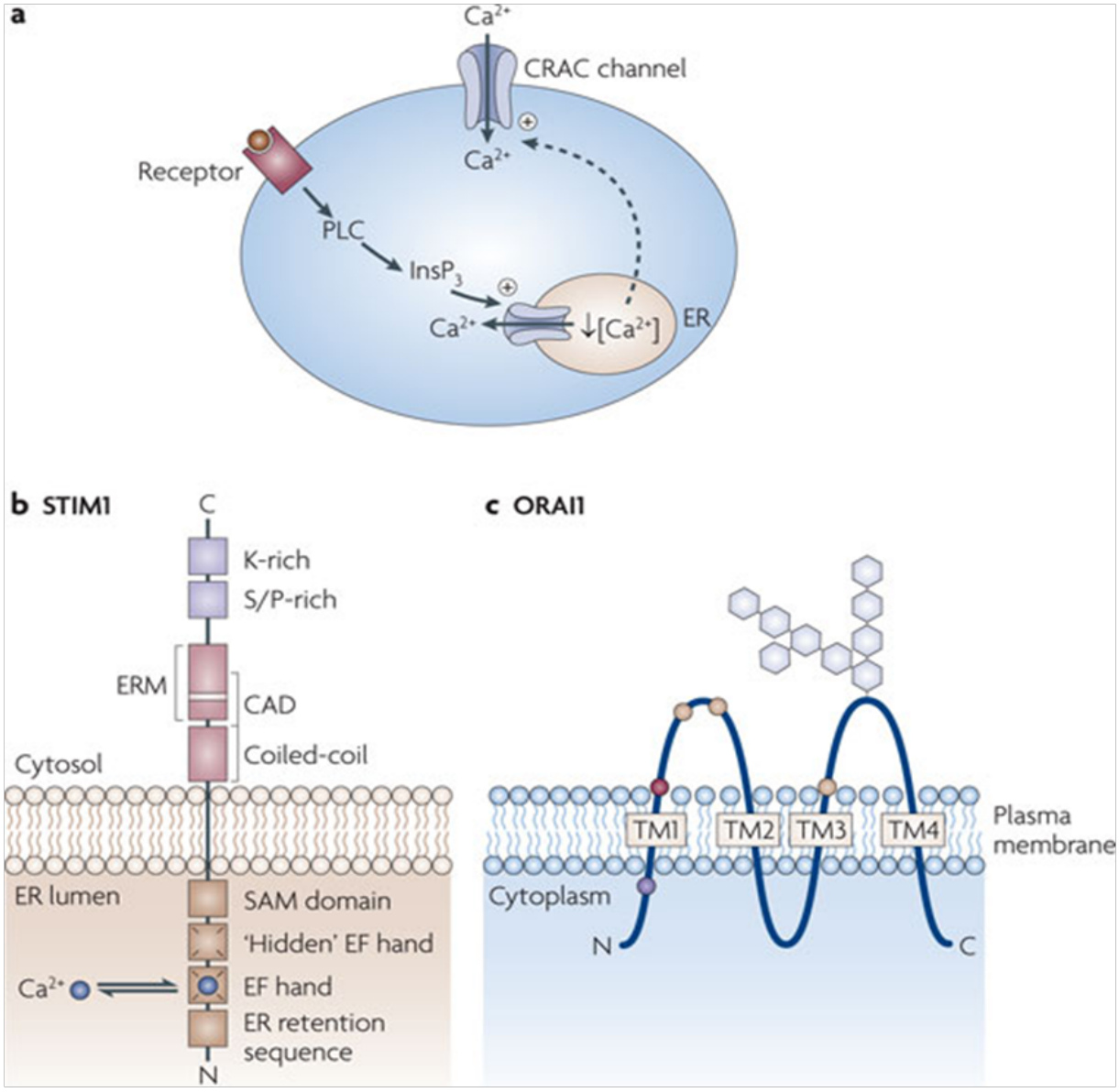
a
Ca2+
CRAC channel
Ca2+
Receptor
PLC
InsP3
Ca2+
↓[Ca2+]
ER
b STIM1
C
K-rich
S/P-rich
ERM
CAD
Coiled-coil
Cytosol
ER lumen
SAM domain
'Hidden' EF hand
Ca2+
EF hand
ER retention sequence
N
c ORAI1
TM1
TM2
TM3
TM4
Plasma membrane
Cytoplasm
N
C

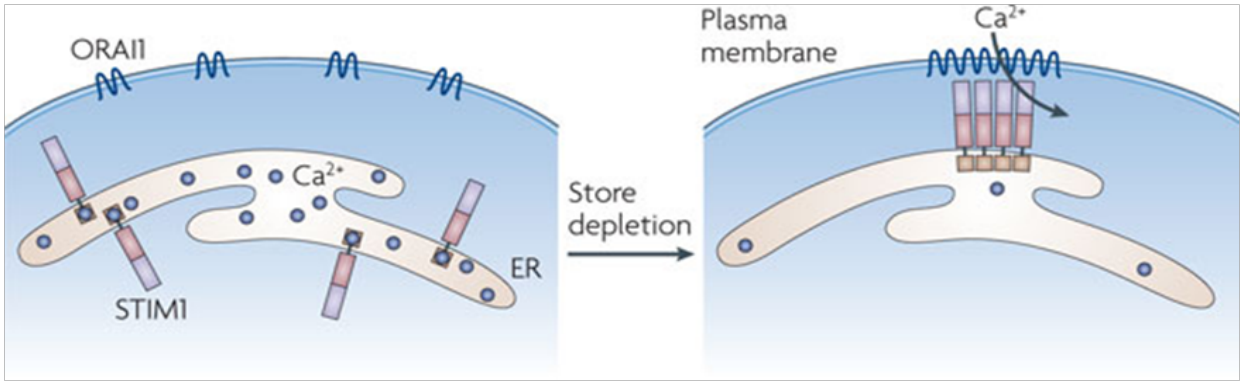
ORAI1
Ca2+
ER
STIM1
Store depletion
Plasma membrane
Ca2+

Figure 1-5. Store Operated Ca^{2+} entry (A) A fall in Ca^{2+} content within the ER, triggered by activation of receptors that stimulate PLC to increase InP_3, leads to the opening of store-operated Ca^{2+} release-activated Ca^{2+} (SOCE) channels in the plasma membrane. These channels are selective for Ca^{2+} and result in a cytoplasmic rise in Ca^{2+} levels. A fall in Ca^{2+} concentration within the store is sensed by stromal interaction molecule 1 (STIM1), which relays this to ORAI1, the pore-forming subunit of the CRAC channel. **(B)**STIM1 spans the ER membrane once. Facing the lumen, and thus being exposed to the Ca^{2+} content of the store, is an EF hand that binds Ca^{2+}, a 'hidden' EF hand that does not bind Ca^{2+} and the sterile α -motif [52] domain that is important in STIM1 oligomerization. Facing the cytoplasm are several predicted functional domains, including two coiled-coil domains, an ezrin-radixin-moesin (ERM) domain, and serine or proline-rich and lysine-rich segments. The CRAC activation domain [74] is essential for the gating of ORAI1. **(C)** Predicted topology of the plasma membrane protein ORAI1. ORAI1 has four transmembrane domains (TM1–TM4), with intracellular amino and carboxyl termini. The purple amino acid represents the single point mutation (R91W) that is seen in CRAC channel-deficient severe combined immunodeficient patients. The red amino acid is glutamate 106.The yellow amino acids represent aspartates 112 and 114 and glutamate 190. Mutations of these latter amino acids affect selectivity, but they might not line the pore. Hexagonal structures represent sugar residues attached to an N-linked glycosylation site (N223). **(D)** In cells with full Ca^{2+} stores, stromal interaction molecule 1 (STIM1) is homogenously distributed in the endoplasmic reticulum (ER) with its EF hand occupied with Ca^{2+}. ORAI1 is dispersed throughout the plasma membrane. Upon stimulation with agonists that increase the levels of cytoplasmic inositol-1,4,5-trisphosphate, the Ca^{2+} content of the store falls. Ca^{2+} dissociates from STIM1 and this results in STIM1 oligomerization and subsequent migration to ER–plasma membrane junctions. At these sites, STIM1 captures diffusing ORAI1 channels. Interaction between the amino and carboxyl termini of ORAI1 with the CRAC activating domain on STIM1 leads to CRAC channel

opening[56] .

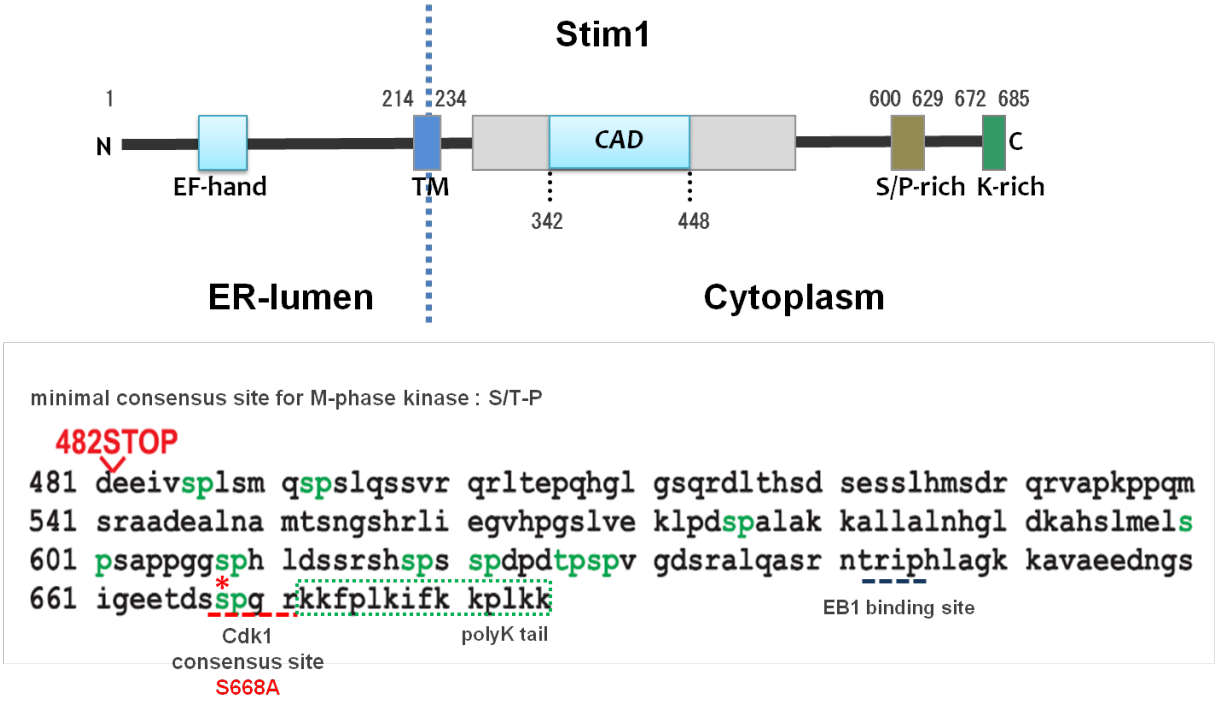

Figure 1-6. Brief schematic of Stim1 C-terminus and its amino acid sequences

CHAPTER 2

MATERIALS AND METHODS

2.1 Collection and preparation of mouse oocytes

Fully grown GV stage oocytes were collected from the ovaries of 6 to 10 week-old CD-1 female mice 44-46 hr after injection of 5 IU of pregnant mare serum gonadotropin (PMSG; Sigma-Aldrich, St Louis, MO; all chemicals from Sigma unless otherwise indicated), as previously described by us [75]. Cumulus intact GVs were recovered into a Hepes-buffered Tyrode's Lactate solution (TL-HEPES) containing 5% fetal calf serum (FCS; Invitrogen, Carlsbad, CA) and supplemented with 100 μM 3-isobutyl-1-methylxanthine (IBMX) to block spontaneous progression of meiosis. Then collected GV oocytes were stored in the incubator for 1.5hr to 2hr in IBMX containing Chatot, Ziomek, and Bavister medium [76] at 36.5°C in a humidified atmosphere containing 6% CO_2 before performing micromanipulation. Also the cumulus cells were removed by passing the oocytes in and out of a fine capillary glass that was slightly larger than the size of GV oocyte. Oocytes were matured *in vitro* for 12-14 hr in IBMX-free supplemented with 3 mg/ml bovine serum albumin (BSA) or 0.02% polyvinyl alcohol (PVA, average molecular weight 30,000–70,000) under paraffin oil. *In vivo* matured MII oocytes were collected from the oviducts 12-14 hr after administration of 5 IU human chorionic gonadotropin, which was injected 46-48 hr after PMSG. All procedures were performed according to research animal protocols approved by the University of Massachusetts Institutional Animal Care and Use Committee.

2.2 Generation of constructs and mRNA preparation

Human Stim1-YFP (hStim1-YFP) and human Orai1 (hOrai1) were generously provided by Dr. T. Meyer (Stanford University) and Dr. M. Trebak (Albany Medical College),

respectively. hStim1-YFP was subcloned into a pcDNA6/Myc-His B vector (Invitrogen) between the restrictions sites AgeI and XbaI. The hOrai1 insert was amplified by PCR and ligated to the N-terminus of the mRFP-bearing pcDNA6/Myc-His B vector (Dr. D. Alfandari, UMass Amherst) between EcoRI and XhoI restriction sites. Constitutively active hStim1, D76A hStim1-YFP, and hStim1-482 stop were generated either by substituting D76 to A or introducing the stop codon after amino acid 481 using the QuickChange® Site-Directed Mutagenesis Kit (Stratagene, La Jolla, CA), as previously reported [48, 59]. Prior to performing *in vitro* transcription reactions, the sequences of all new constructs and presence of targeted mutations were verified by DNA sequencing. Constructs were linearized outside of the coding region with PmeI and *in vitro* transcribed using T7 mMESSAGE mMACHINE Kit (Ambion, Austin, TX). A Poly (A)-tail was added to the mRNAs using a Tailing Kit (Ambion). All mRNAs were prepared to final concentrations of 1.5 μg/μl, aliquoted and frozen at -80°C until use.

2.3 Microinjection of mRNAs

Microinjections were performed as described previously by our laboratory [75]. Prior to injection, cRNAs were heat-denatured, centrifuged and the top 1.2 μl used to prepare microdrops from which glass micropipettes were loaded by aspiration. cRNAs were delivered into oocytes using pneumatic pressure (PLI-100 picoinjector, Harvard Apparatus, Holliston, MA). When cRNAs were injected simultaneously, as in the case of hOrai1–mRFP+hStim1-YFP or hOrai1-mRFP+D76A hStim1-YFP, cRNAs were mixed immediately prior to the injection procedure in 1 to 3 molar ratios, respectively, to allow similar protein expression, which was estimated by comparing fluorescence intensities. When injections were performed in GV oocytes and to allow for maximal translation, oocytes were kept in CZB+IBMX for 6 hr, after which IBMX was removed to allow the commencement of maturation. Germinal vesicle breakdown (GVBD) and

metaphase I (MI) stage oocytes were maturated for 4 and 8 hr, respectively, while MII oocytes were matured for 12-14 hr in CZB.

2.4 $[Ca^{2+}]_i$ measurements and Ca^{2+} reagents

$[Ca^{2+}]_i$ monitoring was performed as previously reported in our laboratory [75]. In brief, Fura-2 acetoxymethyl ester (Fura-2AM) was loaded by incubating oocytes in a HEPES-buffered CZB solution (HCZB) containing 1.25 μM Fura-2AM for 20 min at room temperature (RT). Oocytes were then immobilized on glass-bottom dishes (MatTek Corp., Ashland, MA) and placed on the stage of an inverted microscope (Nikon). Fura-2 fluorescence was excited with 340 nm and 380 nm wavelengths every 20 sec and emitted light was collected at wavelengths greater than 510 nm by a cooled Photometrics SenSys CCD camera (Roper Scientific, Tucson, AZ). Acquisition of fluorescence ratios and rotation of the filter wheel were controlled by the Simple PCI software (C-imaging system, Cranberry Township, PA).

To examine the role of Ca^{2+} influx on refilling of $[Ca^{2+}]_{ER,}$ IBMX-treated GV oocytes were placed either in CZB medium with and without 1.7 mM $CaCl_2$, allowed to mature for 4hr after which oocytes were placed in nominal Ca^{2+} free-HCZB, and after a 5 min interval $[Ca^{2+}]_{ER}$ levels were assessed by adding thapsigargin (TG; Calbiochem, San Diego, CA), an inhibitor of the sarco-endoplasmic reticulum Ca^{2+}-ATPase (SERCA) pump, that induced Ca^{2+} leak with unknown mechanism. TG induced Ca^{2+} rises regarded as $[Ca^{2+}]_{ER}$ content that could be estimated from the area under the curve of the $[Ca^{2+}]_i$ rise using Prizm software (GraphPad Software, La Jolla, CA). To estimate SOCE and to assess the effect of $[Ca^{2+}]_{ER}$ on hStim1-YFP distribution, oocytes were followed by the method in Bird et al. Prior to adding 10 μM TG, oocytes were placed in Ca^{2+}-free HCZB supplemented with 1 mM EGTA. When $[Ca^{2+}]_i$ returned to near baseline values,~35 min after TG addition, 5 mM $CaCl_2$ was added to the medium and the amplitude of the $[Ca^{2+}]_i$ rise caused by the addition was used to estimate SOCE

2.5 Western blotting procedures

To detect endogenous/exogenous Stim1 and Orai1, protein lysates were prepared from 200/20-45, respectively, GV or MII oocytes. Oocytes were washed in Dulbecco's Phosphate buffer saline (DPBS) and lysed in 2X sample buffer and stored at -20°C until use. Heat-denatured proteins (95°C for 3 min) were separated by 7.5% or 10 % SDS–PAGE and transferred to PVDF membranes (Millipore, Bedford, MA). Membranes were blocked with 6% skim milk dissolved in PBS+0.1% Tween-20 (PBST) for 2 hr at 4°C. Two different antibodies were used against Stim1, one raised to recognize the N-terminus (1:100, BD Biosciences, San Jose, CA) and the other to identify the C-terminus end of the molecule (1:500, ProSci Inc., Poway, CA) for which a blocking antigenic peptide (AP) was available. Orai1 was detected using an anti-Orai1 antibody (1:300, ProSci Inc.) raised against the C-terminus of the molecule and an AP was also available for this antibody. For these experiments, equal volumes of AP (ProSci Inc.) and of the specific antibody were incubated for 2hr at 4°C, after which this mixture was used to complete the western blotting procedure. In all samples, an anti-actin antibody was used to detect actin reactivity, which was used as a loading control (1:500, Millipore). Blots were incubated overnight at 4°C with primary antibodies and goat anti-mouse or –rabbit antibodies conjugated with horseradish peroxidase (HRP) were used as secondary antibodies (1:2000, Biorad, Hercules, CA) and incubated for 1 hr at RT. The membranes were then exposed to chemiluminescence reagents (NEN Life Science Products, Boston, MA) and the signal assessed using a Kodak 440 Image Station (Rochester, NY). The same anti-Stim1 antibodies were used to detect exogenously expressed hStim1-YFP (n=45), which were also detected using an anti-GFP antibody (1:1000, MBL, Woburn, MA).

Phosphatase treatment was carried out on WT hStim1-YFP expressing GV and MII oocytes/eggs. Samples were washed in DPBS and placed in phosphatase buffer (50mM Tris-HCL, 100mM NaCl, 10mM $MgCl_2$ and 1mM DTT) supplemented with a protease inhibitor cocktail (Roche, Indianapolis, IN); control samples were also supplemented with 50 mM β-

glycerophosphate to inhibit endogenous phosphatases. All samples were lysed by repeated cycles of freezing and thawing using liquid nitrogen, and 0.5 U of calf intestine phosphatase (CIP, NEB, Ipswich, MA) was added to the indicated groups; all samples were incubated at 37°C for 30 min. The reaction was stopped by addition of 2X-sample buffer, after which western blotting was performed as described above.

2.6 Plasma membrane staining

To estimate the proximity of hStim1-YFP puncta to the plasma membrane [77] during the different stages of maturation, the PM of oocytes/eggs was stained using 10 μg/ml wheat germ agglutinin conjugated with Alexa Fluor® 633 (WGA-Alexa 633, Invitrogen) according to manufacturer's instructions. Prior to staining, the zona pellucida was removed using Tyrode's acidic solution, pH 2.5, to facilitate the diffusion of the stain. Image J free NIH software was used to quantify the distances of the hStim1 puncta to the PM in μm, the diameters of hStim1 aggregates, and to draw the line scan to compare hOrai1 PM distribution.

2.7 Live-imaging of oocytes using confocal microscope

Oocytes/eggs expressing proteins tagged with fluorescent proteins were collected at variable times of maturation and attached to bottom-glass dishes dish while incubated in BSA-free HCZB medium. Fluorescence was examined using a LSM 510 META confocal microscope (Carl Zeiss Microimaging Inc., Jena, Germany) outfitted with a 63x1.4 NA oil immersion lens. Images were taken at the equatorial and cortical regions of oocytes/eggs.

2.8 Statistics analysis

Statistic analyses were performed using Prism software (GraphPad, La Jolla, CA). All data are presented as mean± standard error of the mean (S.E.M). Mean data were compared using unpaired *t*-test or ANOVA, as appropriate. Categorical values such as those generated by maturation rates were analyzed using the Chi-square test. P values <0.05 were considered significant.

CHAPTER 3

Ca^{2+} INFLUX AND THE STORE-OPERATED Ca^{2+} ENTRY PATHWAY TO UNDERGO REGULATION DURING MOUSE OOCYTE MATURATION

3.1 Introduction

Changes in the $Ca^{2+}]_i$ represent an important signaling mechanism involved in a wide range of cellular events including muscle contraction, secretion, neurotransmission and cell death [3]. $[Ca^{2+}]_i$ signaling also plays a dominant role during fertilization in all species examined to date Swann, Saunders [7], [8-10]. In mammals, the sperm-induced $[Ca^{2+}]_i$ signal adopts a pattern of brief $[Ca^{2+}]_i$ rises interspersed among long intervals of basal concentrations that is referred to as $[Ca^{2+}]_i$ oscillations. The oscillations are thought to be initiated by a sperm-specific PLC zeta1 (ζ), following fusion of the gametes [14]. PLCζ is thought to hydrolyze PIP_2 resulting in the production of IP_3, the ligand for IP_3R1, the Ca^{2+} channel located in the ER, the egg's' main Ca^{2+} store [15-17]. Activation of this pathway causes the initial intracellular Ca^{2+} release, but persistence of the oscillations requires Ca^{2+} influx, as without $[Ca^{2+}]_e$ only a few rises occur following sperm entry [18]. Notwithstanding the importance of Ca^{2+} influx, the mechanisms that underlie it during mammalian fertilization are presently unknown.

Fertilization in most vertebrate species happens at the MII, although changes in Ca^{2+} homeostasis that occur prior to this stage during maturation enable eggs to mount $[Ca^{2+}]_i$ oscillations. Fully grown mammalian oocytes are arrested at the germinal vesicle stage [27] and are endowed with $Ca^{2+}]_{ER}$ low in Ca^{2+} reserves. As maturation ensues following the LH surge, $[Ca^{2+}]_{ER}$ increases steadily until the MII stage [32, 33], enhancing IP_3R1-mediated Ca^{2+} release and promoting the acquisition of fertilization-like oscillations [34, 35]. The mechanism(s) that underlie this increase in $[Ca^{2+}]_{ER}$ and the plasma membrane channels that underpin the Ca^{2+} influx

remain unknown, although insights may be gleaned from the spontaneous $[Ca^{2+}]_i$ oscillations displayed by GV oocytes [37, 38]. These oscillations require Ca^{2+} influx and terminate approximately as the resumption of meiosis commences [38], which is when with the first increase in $[Ca^{2+}]_{ER}$ content is noted [33]. These results both predict an association between $[Ca^{2+}]_{ER}$ content and Ca^{2+} influx, which is reminiscent of the mechanism thought to underlie SOCE [39, 42], and active regulation of Ca^{2+} influx during maturation.

SOCE was first proposed as a means for cells to refill Ca^{2+} stores following Ca^{2+} release induced by agonist stimulation [39]. Subsequent studies showed that depletion of $[Ca^{2+}]_{ER}$ caused by inhibitors of the SERCA pumps such as thapsigargin [41] also triggered Ca^{2+} influx, demonstrating the prevalence of SOCE in somatic cells [42-45]. Subsequent electrophysiological studies revealed unique properties of this current, which was named I_{CRAC} [42, 45-47]. While unknown for many years, the molecular effectors of SOCE have now been identified and two components, Stim1, which acts as the ER Ca^{2+} sensor [5, 48, 49] and Orai1, the PM channel that mediates Ca^{2+} influx upon Stim1-induced oligomerization [50, 51], are thought to coordinate Ca^{2+} influx after Ca^{2+} release. The presence of SOCE has been well characterized during the early stages of maturation in *Xenopus* oocytes [60], and Ca^{2+} influx has been described in mammalian eggs during fertilization and after addition of TG [11, 18, 67], although the mechanism(s) and molecules underlying this Ca^{2+} entry remains to be identified. Consistent with this, detection of transcripts for Stim1 and Orai1 has been reported in mammalian oocytes, although the protein expression and cellular distribution during maturation requires additional characterization [68-70, 78].

While Ca^{2+} influx is required for $[Ca^{2+}]_i$ oscillations at the GV stage, its contributions to the filling of $[Ca^{2+}]_{ER}$ have not been carefully examined. Further, the role of $[Ca^{2+}]_i$ changes during oocyte maturation remains unclear. For instance, in mouse GV oocytes suppression of spontaneous oscillations with the Ca^{2+} chelator BAPTA-AM did not affect resumption of meiosis, although it caused cell cycle arrest at metaphase I (MI) of meiosis [32]. In porcine and bovine

oocytes, addition of BAPTA-AM prevented resumption of meiosis and removal of $[Ca^{2+}]_e$ precluded progression of meiosis beyond the MI stage [79, 80]. Remarkably, in *Xenopus* oocytes where SOCE is inactivated during maturation [65], increased Ca^{2+} influx by elevation of $[Ca^{2+}]_e$ and persistent increase in $[Ca^{2+}]_i$ delayed resumption of meiosis and caused spindle abnormalities [81]. Whether enhanced Ca^{2+} influx and persistent elevation of basal $[Ca^{2+}]_i$ affect the initiation or progression of maturation in mammalian oocytes has not been examined.

In this study in mouse oocytes we investigated whether Ca^{2+} influx contributes to the filling of $[Ca^{2+}]_{ER}$ during maturation and if it is differentially regulated during this process. We also researched whether SOCE contributes to this influx as well as the expression of the molecular components of SOCE and their regulation during maturation. Lastly, we evaluated the impact of persistently elevated $[Ca^{2+}]_i$ on resumption and progression of meiosis.

3.2 Results

3.2.1 Spontaneous Ca^{2+} influx is suppressed during maturation in parallel with the increase of ER Ca^{2+} store.

To gain insight into the mechanism and molecular effectors that mediate Ca^{2+} influx in mouse oocytes and eggs, we ascertained whether Ca^{2+} influx across the PM was required for the increase in $[Ca^{2+}]_{ER}$ that occurs during the transition from the GV to the GVBD stage [33]. To accomplish this, GV oocytes were allowed to transition to the GVBD stage in the presence/absence of extracellular Ca^{2+} (1.7mM). $[Ca^{2+}]_{ER}$ levels were estimated following addition of TG 4 hr after the removal of IBMX. In the presence of extracellular Ca^{2+}, $[Ca^{2+}]_{ER}$ increased significantly in GVBD oocytes (Fig. 3-1A, left and right upper panel), although this was not the case when maturation was initiated in nominal Ca^{2+} free medium (Fig.3-1A, right lower panel). These results therefore demonstrate that $[Ca^{2+}]_e$ is required for $[Ca^{2+}]_{ER}$ increase during maturation.

We next examined whether the Ca^{2+} entry pathway(s) that mediates Ca^{2+} influx in GV oocytes is also functional in MII eggs, as both of these cellular stages are known to support oscillations. We incubated GV oocytes and MII eggs in nominal Ca^{2+} free media and shortly thereafter 2mM and 5mM $CaCl_2$ were sequentially added while $[Ca^{2+}]_i$ responses were monitored. While most GV oocytes responded to the addition of $CaCl_2$ by displaying a noticeable $[Ca^{2+}]_i$ rise and in some cases oscillations (Fig. 3-1B, left panel), MII eggs displayed no such changes (Fig. 3-1B, middle panel). We next examined whether the Ca^{2+} entry at the GV stage could be abrogated by pretreatment with 50μM 2-APB, a pharmacological agent that has been shown to regulate SOCE [82]; addition of 2-APB prevented the increase in $[Ca^{2+}]_i$ following the addition of either concentration of $CaCl_2$ (Fig. 3-1B, right panel).

The inhibitory effect of 2-APB and the low $[Ca^{2+}]_{ER}$ levels in GV oocytes suggested that SOCE may be involved, at least in part, in mediating Ca^{2+} entry in GV oocytes. Accordingly, we investigated whether Ca^{2+} influx at the GV stage could be modified by exposure to TG prior to

$CaCl_2$ add-back, a method commonly used to test SOCE in somatic cells [82, 83]. While 3/20 untreated oocytes showed large and prolonged $[Ca^{2+}]_i$ responses following addition of $CaCl_2$, the majority of oocytes, 9/20 and 8/20 showed moderate or minor responses, respectively (Fig. 3-1C, left). Conversely, TG-exposed oocytes uniformly responded to the addition of $CaCl_2$ with robust $[Ca^{2+}]_i$ responses (Fig. 3-1C, right). Altogether, these results show that in Ca^{2+} entry is functionally regulated during mouse oocyte maturation and that SOCE is one of the underlying mechanisms of Ca^{2+} influx at the GV stage.

3.2.2 $[Ca^{2+}]_{ER}$ content and Ca^{2+} influx undergo distinct regulation during mouse oocyte maturation

The previous findings led us to investigate the function of SOCE throughout oocyte maturation using the TG and $CaCl_2$ add-back method. Addition of TG, as expected, caused an increase in $[Ca^{2+}]_i$ that became gradually higher as maturation progressed (Fig. 3-2A,C; $p<0.05$), which is in agreement with previous reports [18, 33] and suggests increasing $[Ca^{2+}]_{ER}$ contents with progression of maturation. In contrast, following $CaCl_2$ addition, Ca^{2+} influx progressively decreased during maturation, with GV and GVBD stage oocytes displaying greater Ca^{2+} influx than MI and MII eggs (Fig. 3-2A,C; $p<0.05$), demonstrating gradual inactivation of Ca^{2+} entry with progression of maturation.

The inverse relationship between $[Ca^{2+}]_{ER}$ content and Ca^{2+} entry during maturation indicates the participation of SOCE as one of the mechanisms involved in Ca^{2+} homeostasis in mouse oocytes. Remarkably, our results suggest that SOCE is progressively disabled during maturation. To extend these observations, GV stage oocytes were injected with *hStim1*-YFP cRNA, the Ca^{2+} sensor component of SOCE, and the effects of such injections on $[Ca^{2+}]_{ER}$ and Ca^{2+} influx were examined during different stages of maturation. hStim1 and mStim1 are highly homologous sharing ~97% of the amino acids at the whole protein level and 99% of the amino

acids in the CRAC activating domain [74], which is the domain that directly interacts with Orai1 [54]. Therefore, hStim1-YFP overexpression was expected to mimic mStim1 function. Expression hStim1-YFP did not affect $[Ca^{2+}]_{ER}$ content throughout maturation (Fig. 3-2B,C-left panel), at least as estimated by our approach, but clearly enhanced Ca^{2+} influx in all stages of maturation, especially in GV oocytes (Fig. 3-2B,C-right panel; $p<0.05$). To demonstrate that the enhanced influx was due to interaction of hStim1 with endogenous Orai1, oocytes were injected with hStim1-ΔCAD-YFP mRNA, which cannot activate Orai1 [54]; overexpression of hStim1-ΔCAD-YFP failed to enhance Ca^{2+} influx at any stage of maturation (Fig. 3-2D). Collectively, the data suggest that hStim1-YFP over-expression broadly recapitulates the regulation of $[Ca^{2+}]_{ER}$ and Ca^{2+} influx observed in mouse oocytes, suggesting that SOCE is operational during mouse oocyte maturation, although is seemingly inactivated at the most advanced stages of meiosis.

3.2.3 Stim1 and Orai1 are expressed in mouse oocytes

We next examined in mouse oocytes/eggs the expression of the two molecular effectors of SOCE, Stim1 and Orai1. Two different anti-Stim1 antibodies were used for western blotting and both antibodies detected in GV and MII stages a band of ~90kDa (Fig. 3-3A, left and center panels), which is the reported MW of Stim1 [84]; the observed reactivity was likely Stim1's, as pre-incubation of the anti-C-terminus antibody with an antigenic peptide specifically obliterated recognition of this band (Fig. 3-3A, right panel). Expression of Orai1 was also detected in mouse eggs (Fig. 3-3B, left panel) with an ~MW of 56kDa, which while higher than predicted for the native protein, is consistent with the MW of the protein in some mammalian tissues [85]; Orai1 has been shown to be glycosylated in somatic cells (Gwack, 2007 #2;Prakriya, 2006 #85). Pre-incubation of the antibody with its antigenic peptide abrogated the reactivity of the 56kDa band but not that of a prominent higher, non-specific band (Fig. 3-3B, right panel; asterisk), confirming the specificity of the antibody. Further, the same antibody detected expression of hOrai1-mRFP

in oocytes and eggs, where it detected several polypeptides ranging in MW from ~52 to 82 kDa, likely the reflection of various degrees of glycosylation (Fig. 3-3C).

To confirm the functional results obtained by injection of hStim1-YFP cRNA, we examined the expression of hStim1-YFP in GV and MII oocytes. Both anti-Stim1 antibodies recognized a band at ~105kDa, which is consistent with the MW of hStim1 and the added MW of YFP (Fig. 3-3D, left and middle panels); an anti-YFP antibody recognized the same bands (Fig. 3-3D, right panel). Actin was used as loading control, and Western blotting against it revealed approximate equal loading of the samples (Fig. 3-3D, middle lower panel). In all cases, hStim1-YFP migration was retarded in MII eggs than in GV oocytes (Fig. 3-3D), suggesting phosphorylation of hStim1-YFP, as reportedly occurs in *Xenopus* oocytes and in mammalian somatic cells [59, 60]. To ascertain whether this was also the case in our system, hStim1-YPF cRNAs was injected into GV oocytes and these cells matured to the MII stage, at which time lysates were prepared and either left untreated or treated with alkaline phosphatase to induce widespread de-phosphorylation. Compared to untreated controls, the AP-treated hStim1-YPF displayed a smeared migration, which suggests different degrees of phosphorylation, and higher reactivity (Fig. 3-3E), which is possibly due to better antibody recognition, as the antibody's epitope falls within this domain. To confirm this observation we injected hStim1-482stop-YFP cRNA, which encodes for a protein that lacks all the C-term M-phase kinase phosphorylation sites [59]; hStim1-482stop did not undergo a mobility shift during maturation (Fig. 3-3F). Collectively, our data show that the components of SOCE are expressed in mouse oocytes/eggs and that during maturation hStim1 undergoes phosphorylation.

3.2.4 hStim1-YFP and hOrai1-mRFP undergo changes in distribution during oocyte maturation

Such findings led us to examine whether the decline in Ca^{2+} influx during maturation coincided with changes in the cellular distribution of Stim1 and Orai1. To follow their

distribution, oocytes were injected with hStim1-YFP or hOrai1-mRFP mRNAs. All oocytes were injected at the GV stage and remained at this stage in media supplemented with IBMX for variable times so that by 20 hr post injection all stages of maturation could be simultaneously examined. hStim1-YFP underwent marked changes in distribution with progression of meiosis. For example, at the GV stage, hStim1-YFP displayed a "patched" distribution with these patches spread throughout the cell (Fig. 3- 4A). In GVBD oocytes, ~4 hr after removal of IBMX, large internal patches were still observed in most oocytes (Fig. 3-4B, upper) but in ~30% of the cells the distribution of hStim1 became more diffuse, although some patches remained around the spindle area (Fig. 3-4B, lower panel). As maturation progressed, the distribution of hStim1 became more disperse and acquired a pattern consistent with its ER localization (Fig. 3-4C,D, upper panel), although a small number of MI and MII oocytes still showed internal patches of smaller size (Fig. 3-4C, D, lower panel); ER distribution was confirmed by injection of ds-Red ER cRNA (data not shown).

The distribution of hOrai1-mRFP also changed during maturation (Fig. 3-4E, F). For example, at the GV stage, hOrai1-mRFP was highly enriched at the PM, where it formed a near perfect ring around the cell (Fig. 3-4E), while at the MII stage, even though hOrai1-mRFP was still present there, its presence was weaker (Fig. 3-4F); this apparent reduction of hOrai1-mRFP at the PM was accompanied by increased fluorescence in the subcortical area (Fig. 3-4F; line an bar graphs below figures), suggesting recycling of the protein, as already reported in *Xenopus* oocytes [60, 86]. Collectively, these results suggest that the molecular components of SOCE undergo cellular redistribution during maturation.

3.2.5 hStim1 puncta formation and co-localization with hOrai1 decreases during oocyte maturation

Following depletion of $[Ca^{2+}]_{ER}$, Stim1 undergoes oligomerization and migration to the cell cortex nearly reaching the PM where these aggregates, also known as "puncta", recruit and

gate Orai1 [54, 55]. To assess whether the ability of Stim1 to undergo puncta formation and migration to the cortex changed during oocyte maturation, hStim1-YFP-expressing GV and MII oocytes were treated with TG and hStim1-YFP reorganization was observed by confocal microscopy. To estimate the proximity of hStim1-YFP puncta to the PM, a diffusible dye, WGA-Alexa 633, was used to stain the PM. Following treatment with TG, hStim1 in GV oocytes readily formed distinct puncta that aligned along the PM (Fig. 3-5C,E) while this ability was severely reduced at the MII stage along with the size of the puncta (Fig. 3- 5D,F); the line graph to the right of Fig. 3-5E, F shows the reduced intensity of the puncta in MII eggs. It is worth noting that even after TG, hStim1-YFP in MII eggs displayed a reticular organization, which was not observed in GV oocytes.

Research in somatic cells has shown that Stim1 and Orai1 directly interact at the PM [54, 55]. Using simultaneous expression of hStim1-YFP and hOrai1-mRFP mRNAs and confocal microscopy, we examined whether the distribution of these molecules overlapped and if so whether this property changed during maturation. Under resting conditions, hStim1 and hOrai1 showed their expected distributions in GV oocytes and MII eggs (Fig. 3-5G-I, 3-5M-O, respectively) and in GV oocytes some overlap between the molecules was noticeable (Fig. 3-5H,I). Following addition of TG, hStim1 and hOrai1 showed extensive co-localization at the GV stage (Fig. 3-5K,L), although this was not evident in MII eggs (Fig. 3-5Q,R). Collectively, the data show that the organization of hStim1 and hOrai1 follow distinct but parallel redistribution during oocyte maturation that temporally coincides with the decline in Ca^{2+} influx during this process.

3.2.6 Co-expression of SOCE components enhances TG-induced Ca^{2+} influx at all stages of oocyte maturation.

The diminished co-localization of hStim1 and hOrai1 in MII eggs following depletion of Ca^{2+} stores led us to examine whether Ca^{2+} influx was reduced at this stage. We expressed either

component of SOCE alone or in combination and compared $[Ca^{2+}]_i$ responses in GV and MII stages using the TG and $CaCl_2$ add-back method. As shown in Fig. 3-6A, expression of hStim1 alone enhanced influx in both stages of maturation, but to a greater extent in GV than in MII, which is consistent with our previous results. Expression of hOrai1 on the other hand failed to modify influx at either stage, whereas hStim1 and hOrai1 co-expression increased Ca^{2+} influx in both stages, although the $[Ca^{2+}]_i$ rise was considerably smaller in MII eggs, consistent with the reduced co-localization of hStim1 and hOrai1 at this stage.

3.2.7 Expression of SOCE components alters basal Ca^{2+} homeostasis during oocyte maturation

We next examined whether expression/co-expression of the SOCE components changed basal $[Ca^{2+}]_i$ levels under natural regular conditions, i.e., without emptying the stores and under normal external Ca^{2+} concentrations, ~1.7mM $CaCl_2$. In control GV oocytes, basal $[Ca^{2+}]_i$ remained steady, as the fluorescence ratio of ~0.1 remained unchanged until the MII stage (Fig. 3-6B, left panels, upper). Expression of hStim1 increased baseline $[Ca^{2+}]_i$ in GV oocytes ($P < 0.05$), although by the MII stage basal $[Ca^{2+}]_i$ had returned to levels that were indistinguishable from those of non-injected controls (Fig. 3-6B, upper right panels, upper). Co-expression of hStim1 and hOrai1 dramatically increased basal $[Ca^{2+}]_i$ at the GV stage ($P < 0.05$) and although basal $[Ca^{2+}]_i$ levels were reduced by the MII stage they still remained higher than controls (Fig. 3-6B, left panels, lower). Together, these results demonstrate that spontaneous Ca^{2+} influx is differentially regulated during mouse oocyte maturation and is greatest at the GV stage, consistent with the presence of spontaneous oscillations at this stage [38].

To ascertain whether the downturn of Ca^{2+} influx was likely due to increasing levels of $[Ca^{2+}]_{ER}$, we expressed an EF-hStim1 mutant, D76A-hStim1, which is insensitive to $[Ca^{2+}]_{ER}$ levels [48]. Co-expression of D76A-hStim1+hOrai1 increased basal $[Ca^{2+}]_i$ in GV oocytes but

unlike previous treatments, basal $[Ca^{2+}]_i$ did not decrease, and effectively increased, as oocytes progressed to the MII stage ($P < 0.05$; Fig. 3-6B, right panel, lower).

3.2.8 Regulation of Ca^{2+} influx is required to complete oocyte maturation

We then examined whether the distinct basal $[Ca^{2+}]_i$ profiles generated by expression of one or both of the SOCE components had differential effects on the rates of in *vitro* maturation. To accomplish this, control GV oocytes or oocytes injected with the selected cRNAs were momentarily maintained at the GV stage to allow for protein translation, after which *in vitro* maturation proceeded for 14-16hr. The majority of control oocytes, ~80%, resumed meiosis and reached the MII stage (Fig. 3-7A), although oocytes expressing hStim1 or hStim1+hOrai1, which displayed elevated basal $[Ca^{2+}]_i$ at the GV stage, showed reduced rates of maturation with more oocytes remaining arrested at the GV stage ($p<0.05$). Remarkably, oocytes expressing D76A hStim1+hOrai1, which displayed persistent elevation of basal $[Ca^{2+}]_i$, failed to consistently resume meiosis (Fig. 3- 7A).

To examine if the excessive Ca^{2+} influx caused by co-expression of D76A hStim1+ hOrai1 was responsible for the GV arrest, we repeated the above experiment but 2.5 hr after release from IBMX oocytes were transferred to medium containing 0.4 mM $CaCl_2$. Under normal $[Ca^{2+}]_e$, as expected, all control oocytes reached the GVBD stage by 2.5 hr, although only ~25% of oocytes expressing D76AhStim1+hOrai1 did (Fig. 3-7B; $P < 0.05$). Subsequently, all D76A-hStim1+hOrai1 expressing oocytes maintained in normal $[Ca^{2+}]_e$-containing media remained arrested at the GV stage, while cohort oocytes transferred to 0.4 mM $CaCl_2$-containing media progressively underwent GVBD and by 12 hr ~50% had undergone GVBD (Fig. 3-7C); progression of maturation in control oocytes was not affected by 0.4 mM $CaCl_2$ media (Fig. 3-7C). We then examined whether moving oocytes to 0.4 mM $CaCl_2$ media altered basal $[Ca^{2+}]_i$. As shown in Fig. 3-7D and 3-7E, 2 hr after changing media oocytes expressing D76A hStim1+hOrai1 displayed a significantly lower basal $[Ca^{2+}]_i$ ($P < 0.05$), whereas control oocytes

were not affected by the switch. Together, these results suggest that regulation of Ca^{2+} influx and Ca^{2+} homeostasis play a role during normal progression of meiosis in mouse oocytes.

3.3 Discussion

In this study we examined how $[Ca^{2+}]_e$ and Ca^{2+} influx contribute to $[Ca^{2+}]_{ER}$ content during mouse oocyte maturation. We also investigated the presence and function of SOCE and the effect of Ca^{2+} influx misregulation on oocyte maturation. We found that while $[Ca^{2+}]_{ER}$ levels increase during maturation, Ca^{2+} entry declines. We detected expression of Stim1 and Orai1 in oocytes and eggs as well as a change in their distribution such that hStim1-YFP and hOrai1-mRFP only extensively overlapped in GV oocytes after addition of TG. Lastly, expression of hStim1+hOrai1 increased basal $[Ca^{2+}]_i$ in GV oocytes but not in MII eggs, and persistently elevated basal $[Ca^{2+}]_i$ compromised oocyte maturation. In total, our studies demonstrate that Ca^{2+} influx is closely regulated during oocyte maturation and that alteration of Ca^{2+} homeostasis undermines the completion of maturation.

3.3.1 $[Ca^{2+}]_{ER}$, $[Ca^{2+}]_i$ influx and SOCE during mouse oocyte maturation

While $[Ca^{2+}]_{ER}$ levels have been known to increase during mouse oocyte maturation, the source of Ca^{2+} and the Ca^{2+} influx mechanism(s) underlying this increase have not been established. Here we show that $[Ca^{2+}]_e$ is required for the increase in $[Ca^{2+}]_{ER}$ and that as $[Ca^{2+}]_{ER}$ increases during maturation, spontaneous or TG-induced Ca^{2+} influx decreases; Ca^{2+} influx is lowest at the MII stage, which is when $[Ca^{2+}]_{ER}$ is greatest. This relationship between $[Ca^{2+}]_{ER}$ and Ca^{2+} influx, which is especially evident at the GV and GVBD stages, suggests participation of SOCE and is reminiscent of data in *Xenopus* where SOCE-mediated Ca^{2+} entry is abruptly inactivated at the GVBD stage [64, 65]. Our results, unlike those in *Xenopus*, show that SOCE is only partly inactivated by the GVBD stage and can contribute to the increase in $[Ca^{2+}]_{ER}$ during this period. Our results differ from other studies in the mouse showing progressively enhanced SOCE activity during maturation [68, 69].

Several additional findings in our study suggest a role for SOCE during mouse oocyte maturation. For example, addition of 2-APB, a broad-spectrum of SOCE inhibitor [82, 87], abrogated Ca^{2+} influx in GV oocytes. Moreover, both Stim1 and Orai1 were produced by oocytes throughout maturation, and expression of functional hStim1 caused enhanced Ca^{2+} influx, whereas an inactive form, hStim1-ΔCAD-YFP, failed to promote Ca^{2+} influx. In spite of such findings indicating a role of SOCE during oocyte maturation, the progressive inactivation of SOCE during maturation raises questions regarding its contribution to Ca^{2+} influx during fertilization. Recent research in mouse eggs suggests a minor role for SOCE during fertilization, for while it was functional in MII eggs, abrogating its function by pharmacological and molecular means failed to modify sperm-initiated oscillations [88, 89]. Importantly, in porcine oocytes, inactivation of SOCE by siRNA against Stim1 and Orai1 inhibited persistent fertilization-associated oscillations [78, 90]. Altogether, these results suggest that in mammals different Ca^{2+} influx mechanisms regulate $[Ca^{2+}]_{ER}$ during maturation and Ca^{2+} influx during fertilization and future studies should identify these channels and their regulation.

3.3.2 Re-organization of hStim1 and hOrai1 during oocyte maturation

The inactivation of spontaneous and SOCE-mediated Ca^{2+} influx led us to examine whether changes in the distribution of Stim1 and Orai1 could be undermining Ca^{2+} influx. Given the inconsistent results obtained using immunofluorescence to localize endogenous Stim1 (not shown), we used corresponding mRNAs also encoding fluorescent proteins. Marked changes in the organization of these proteins commenced around GVBD. For example, in GV oocytes internal “patches” and peri-GV accumulation highlighted the widespread distribution of hStim1, but after GVBD and for the rest of maturation, hStim1 distribution became diffuse and acquired a reticular, ER-like pattern consistent with its localization. Further, addition of TG, which in GV oocytes caused hStim1 to diffuse to the cortex and form distinct puncta, hardly changed the

distribution of hStim1 in eggs. The distribution of Orai1 also changed, as in GV oocytes it was primarily present on the PM but by MII its PM presence was reduced and its signal in the ooplasm increased. In agreement with these changes, after addition of TG, hStim1 and hOrai1 only co-localized on the PM of GV oocytes. Our results are agreement with those in *Xenopus* oocytes where inactivation of SOCE during maturation was associated with inhibition of Stim1 oligomerization/puncta formation and Orai1 internalization [60, 86]. Nevertheless, our results show that hStim1 still retained certain clustering capacity and Orai1 internalization was incomplete in MII eggs, as even at this stage expression of hStim1+hOrai1 enhanced SOCE activity. Our results also concur with data in somatic cells, where SOCE is downregulated at mitosis [59, 91] and this change was associated with reduced ability of Stim1 to form puncta [59]. Data from studies in mammalian oocytes also support our findings. For example, following depletion of $[Ca^{2+}]_{ER}$ Stim1 displayed some degree of oligomerization in porcine MII eggs [70] and in mouse eggs Stim1 showed conspicuous clusters/puncta organization, although without emptying of the stores, and Orai1 distribution was mostly concentrated to the PM [68].

We did not investigate the mechanisms that regulate Stim1 re-organization in oocytes. Nevertheless, Stim1 was originally described as a phosphoprotein [92] and phosphorylation of its S/T-P consensus sites by M-phase kinases was demonstrated in somatic cells [59, 92, 93] and in *Xenopus* oocytes [60]. We found that exogenous hStim1 was phosphorylated in MII eggs, as it experienced a mobility shift that was reduced by phosphatase treatment. We did not observe similar changes in the endogenous protein, although the comparable temporal inactivation of TG-induced Ca^{2+} influx between uninjected and hStim1 mRNA-injected oocytes suggest common regulatory mechanisms.

3.3.3 Ca^{2+} influx and progression of oocyte maturation

To gain further insight into the mechanisms underlying the brief presence of $[Ca^{2+}]_i$ oscillations in GV stage mouse oocytes [37, 38], we expressed, singly or together, hStim1 and hOrai1 mRNAs and monitored their effects on basal $[Ca^{2+}]_i$ in oocytes and eggs. We found that their combined expression markedly and persistently increased basal $[Ca^{2+}]_i$ in GV oocytes, although by the MII stage, basal $[Ca^{2+}]_i$ levels had returned to near normal levels. These results suggest close regulation of Ca^{2+} homeostasis/influx during the early stages of maturation.

To better understand the role of basal $[Ca^{2+}]_i$ and Ca^{2+} influx on oocyte maturation, we co-expressed D76A hStim1+hOrai1 mRNAs, which increased basal $[Ca^{2+}]_i$ throughout maturation. Under these conditions, progression of maturation was greatly reduced with most oocytes remaining at the GV stage. These effects were due to the inability to inactivate Ca^{2+} influx and decrease basal $[Ca^{2+}]_i$, as lowering external $[Ca^{2+}]_e$ reduced $[Ca^{2+}]_i$ and rescued the ability of these oocytes to undergo GVBD. Similar detrimental effects of elevated basal $[Ca^{2+}]_i$ were observed in *Xenopus* oocytes where enhanced Ca^{2+} influx promoted throughout maturation hindered the progression of meiosis [81]. Therefore, it appears that regulation of Ca^{2+} influx is required for normal progression of oocyte maturation in the mouse, although we did not explore the functional mechanism(s) positively affected by the progressive inactivation of Ca^{2+} entry.

We propose a model whereby mouse GV oocytes exhibit a low but persistent Ca^{2+} influx that contributes to the GV's overall cellular metabolism. Upon resumption of meiosis, Ca^{2+} influx is progressively inactivated to allow for normal progression of meiosis, spindle organization and MII arrest. Future studies in mammalian oocytes should elucidate the mechanism(s) responsible for the inactivation of Ca^{2+} influx, and the identity of the channel(s) that mediate Ca^{2+} entry during maturation and fertilization.

Figure 3-1.

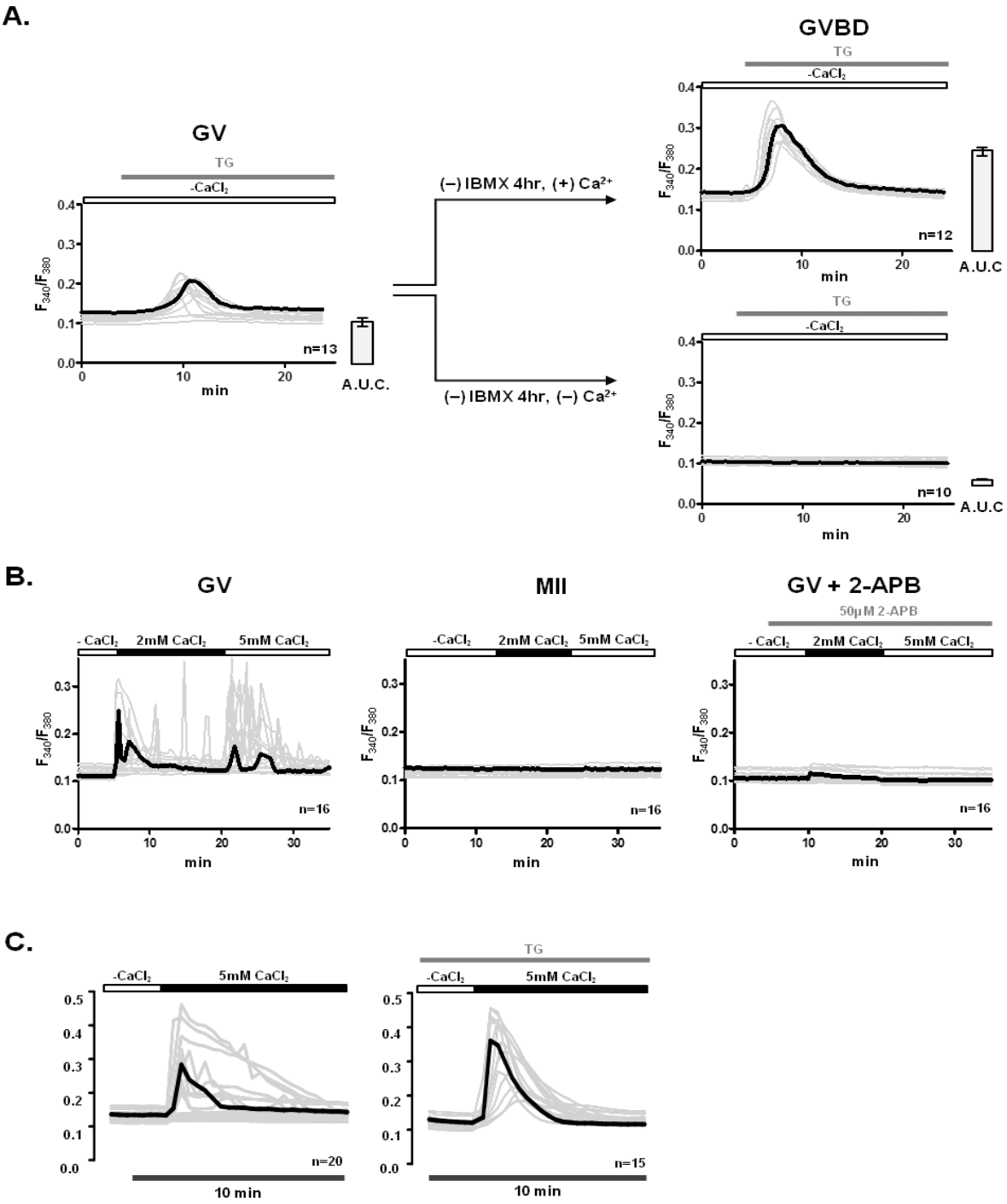
A.
GV
TG
-CaCl2
F340/F380
n=13
A.U.C.
min
(–) IBMX 4hr, (+) Ca2+
(–) IBMX 4hr, (–) Ca2+
GVBD
TG
-CaCl2
n=12
A.U.C
min
TG
-CaCl2
n=10
A.U.C
min
B.
GV
MII
GV + 2-APB
50μM 2-APB
- CaCl2
2mM CaCl2
5mM CaCl2
n=16
min
C.
-CaCl2
5mM CaCl2
TG
n=20
n=15
10 min

Figure 3-1. $[Ca^{2+}]_e$ and Ca^{2+} influx are required to fill $[Ca^{2+}]_{ER}$ in oocytes. The underlying Ca^{2+} influx mechanism(s) are inactivated during maturation and are sensitive to 2-APB and TG at the GV stage. (A) The contribution of extracellular Ca^{2+} to $[Ca^{2+}]_{ER}$ content was estimated in GVBD-stage oocytes after culturing GV oocytes for 4 h in media supplemented with 1.7 mM $CaCl_2$ or without supplementation, nominal Ca^{2+}-free medium. Release of $[Ca^{2+}]_{ER}$ was induced by addition of 10 μM TG. All $[Ca^{2+}]_i$ responses are shown in the graphs, and the bold trace in each graph represents the mean response; bar graphs to the right of each Ca^{2+} panel denote mean ± SEM of $[Ca^{2+}]_{ER}$ content estimated as area under the curve. (B) Spontaneous Ca^{2+} influx was measured in GV oocytes and MII eggs. Oocytes and eggs were placed in Ca^{2+}-free conditions, after which 2 and 5 mM $CaCl_2$ were successively added. Given that only GV oocytes showed Ca^{2+} influx, they were pretreated with 50 μM 2-APB for 5 min before addition of $CaCl_2$ to prevent influx. (C) Ca^{2+} influx was promoted by addition of $CaCl_2$ into GV oocytes with and without prior treatment with TG. GV oocytes were placed in nominal Ca^{2+}-free media or exposed to 10 μM TG for 30 min in nominal Ca^{2+}-free medium to deplete $[Ca^{2+}]_{ER}$, after which 5 mM $CaCl_2$ was added. Representative traces are shown, and bold trace represents mean response.

Figure 3-2

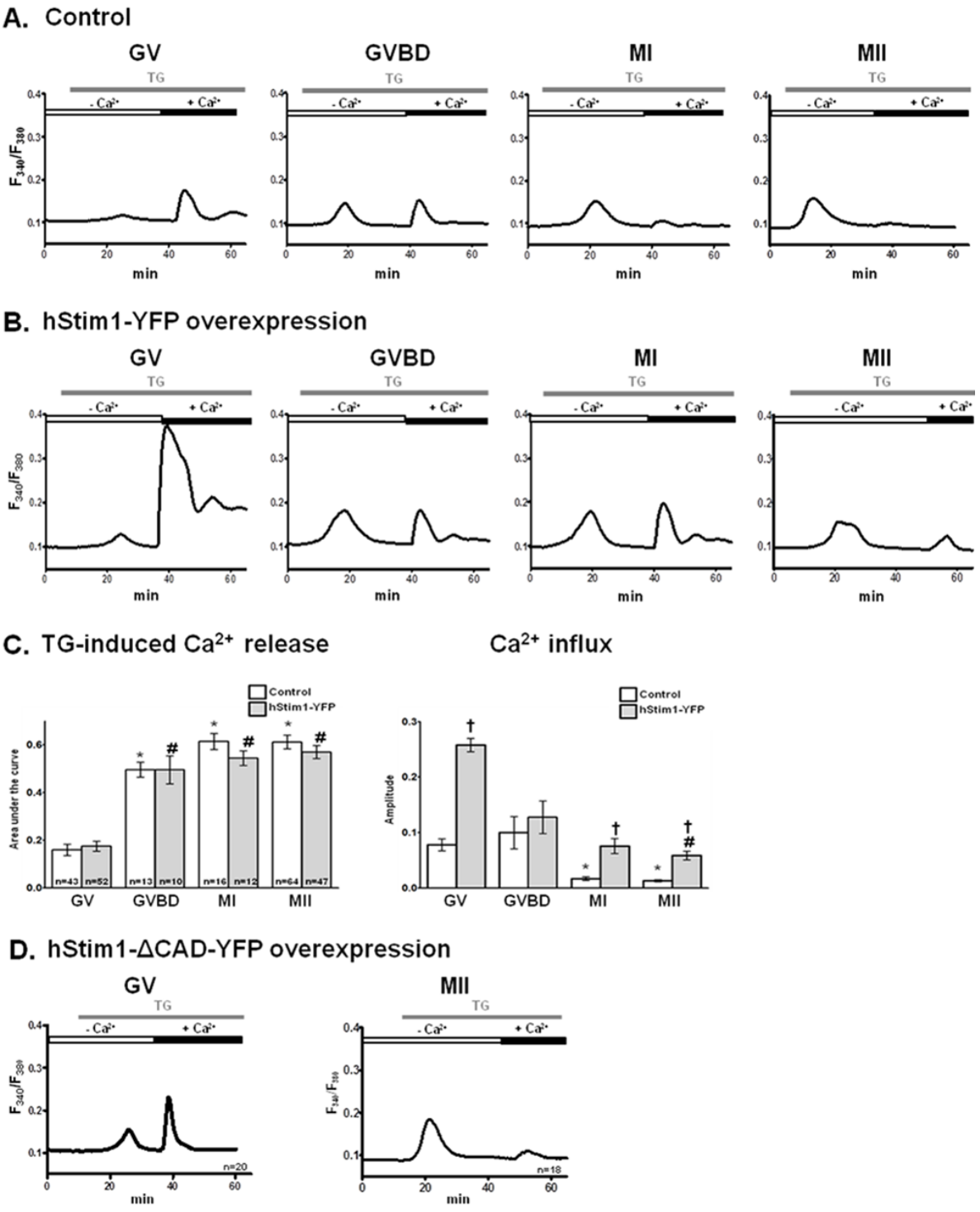
A. Control
GV
GVBD
MI
MII
TG
- Ca2+
+ Ca2+
F340/F380
min
B. hStim1-YFP overexpression
C. TG-induced Ca2+ release
Ca2+ influx
Control
hStim1-YFP
Area under the curve
Amplitude
n=43
n=52
n=13
n=10
n=16
n=12
n=64
n=47
D. hStim1-ΔCAD-YFP overexpression
n=20
n=18

Figure 3-2. $[Ca^{2+}]_{ER}$ content increases, whereas Ca^{2+} influx induced by TG, SOCE, decreases during oocyte maturation. $[Ca^{2+}]_{ER}$ content was estimated from the $[Ca^{2+}]_i$ responses caused by addition of 10 μM TG in oocytes incubated in Ca^{2+}-free medium, and Ca^{2+} influx was estimated by the $[Ca^{2+}]_i$ rise generated by the addition of 5 mM $CaCl_2$ soon after the TG-induced $[Ca^{2+}]_i$ rise had subsided. Representative $[Ca^{2+}]_i$ traces are shown for control oocytes (A) or for oocytes expressing hStim1-YFP (B). (C) TG- and $CaCl_2$-induced $[Ca^{2+}]_i$ changes were quantified, and data are presented in bar graphs as mean ± SEM. Control and hStim1-YFP–expressing oocytes are displayed in open and gray columns, respectively, and the number of oocytes evaluated is shown within each bar. *,#Stages significantly different from the GV-stage values within treatment group. †Significant differences within the same meiotic stage but between treatments ($p < 0.05$). (D) TG-induced $[Ca^{2+}]_i$ responses and subsequent Ca^{2+} influx in oocytes and eggs expressing hStim1-ΔCAD-YFP, an Stim1 variant incapable of interacting with Orai1.

Figure 3-3

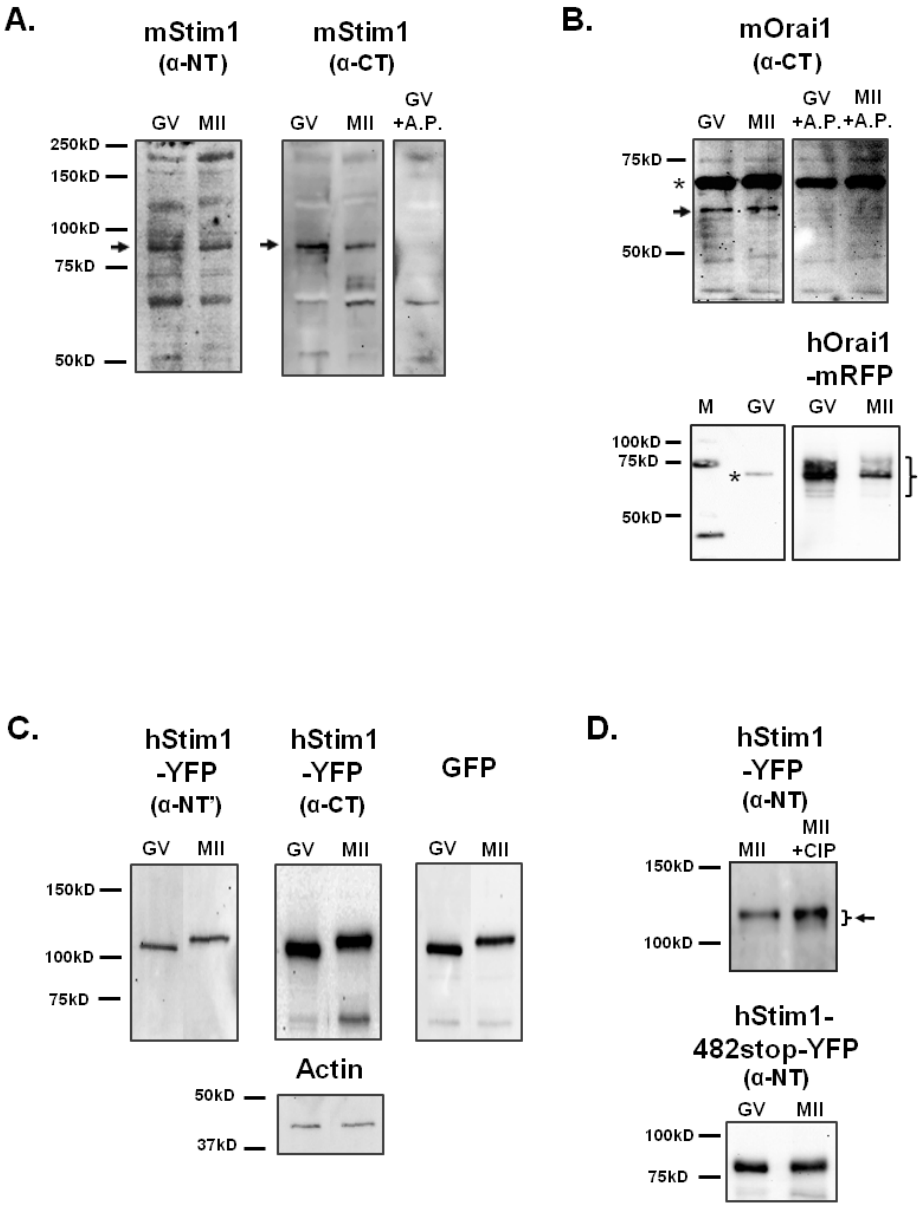
A.
mStim1
(α-NT)
mStim1
(α-CT)
GV MII
GV MII
GV
+A.P.
250kD
150kD
100kD
75kD
50kD
B.
mOrai1
(α-CT)
GV MII
GV MII
+A.P. +A.P.
75kD
*
50kD
hOrai1
-mRFP
M GV
GV MII
100kD
75kD
*
50kD
C.
hStim1
-YFP
(α-NT')
hStim1
-YFP
(α-CT)
GFP
GV MII
GV MII
GV MII
150kD
100kD
75kD
Actin
50kD
37kD
D.
hStim1
-YFP
(α-NT)
MII
MII
+CIP
150kD
100kD
hStim1-
482stop-YFP
(α-NT)
GV MII
100kD
75kD

Figure 3-3. Mouse oocytes express Stim1 and Orai1. (A, B) The expression of Stim1 and Orai1 molecules was probed using lysates of GV oocytes (*n* = 100 and 200, respectively) and MII (*n* = 100 and 200, respectively) eggs and specific antibodies. (A) Left and middle, black arrows point to the band corresponding to Stim1. An antigenic peptide was used to confirm the specificity of the anti–C-terminus Stim1 antibody. (B) Right, black arrow points to the band that represents Orai1. The upper band of ~68 kDa marked with an asterisk is believed to be nonspecific reactivity, as it was not abolished by pretreatment with the antigenic peptide. (C) hOrai1-mRFP expression (*n* = 16 GV oocytes/MII eggs) was analyzed in overexpressing cells using the same antibody. (D) Heterologous expression of hStim1-YFP was demonstrated in lysates of oocytes/eggs (*n* = 45) using the anti–N-terminus and anti–C-terminus Stim1 antibodies and an anti-GFP antibody. The actin protein was probed as a loading control (bottom, middle). (E) To examine the possible phosphorylation of hStim1-YFP in mouse oocytes, lysates of hStim1-YFP–expressing MII oocytes (*n* = 18) were incubated with or without calf intestine phosphatase and then immunoblotted with anti-Stim1 antibody [94]. The presence of hStim1 is denoted by an arrow, and the bracket denotes the presence of polypeptides of different MWs. (F) hStim1–482-stop-YFP–overexpressing GV and MII cells (*n* = 18) were probed with the anti–N-terminus Stim1 antibody, and blots are shown.

Figure 3-4

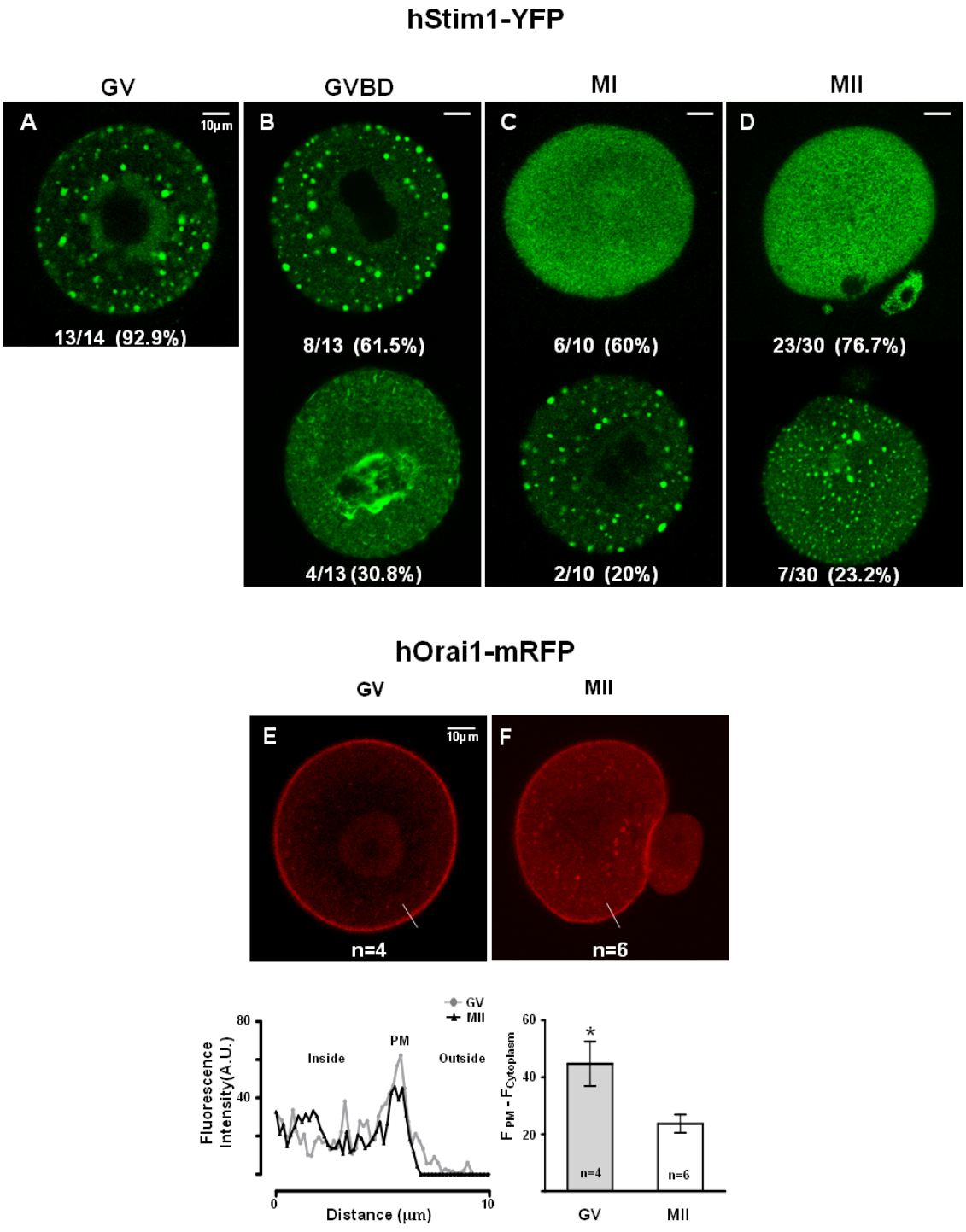
hStim1-YFP
GV
GVBD
MI
MII
A
10μm
B
C
D
13/14 (92.9%)
8/13 (61.5%)
6/10 (60%)
23/30 (76.7%)
4/13 (30.8%)
2/10 (20%)
7/30 (23.2%)
hOrai1-mRFP
GV
MII
E
10μm
F
n=4
n=6
GV
MII
Fluorescence Intensity(A.U.)
80
40
Inside
PM
Outside
0
10
Distance (μm)
60
40
20
F PM - F Cytoplasm
*
n=4
n=6
GV
MII

Figure 3-4. The distribution and organization of hStim1-YFP and hOrai1-mRFP change during oocyte maturation. (A–D) The distribution of hStim1-YFP was examined using confocal microscopy from images taken at the equatorial plane of live hStim1-YFP–expressing oocytes. The number of oocytes examined at each stage is shown at the bottom of each representative image. hStim1-YFP displayed two distinct patterns of organization in all stages of maturation except the GV stage; the most representative configurations are shown, along with the proportion of oocytes/eggs exhibiting the particular pattern. (E, F) The distribution of hOrai1 was examined as in the foregoing in GV and MII oocytes expressing hOrai1-mRFP. Intensity profiles of the line scans drawn in oocytes and eggs are shown below E, and a bar graph displaying the relative intensity of Orai1 signal between PM and cytoplasm is shown below F. Scale bar, 10 μm.

Figure 3-5

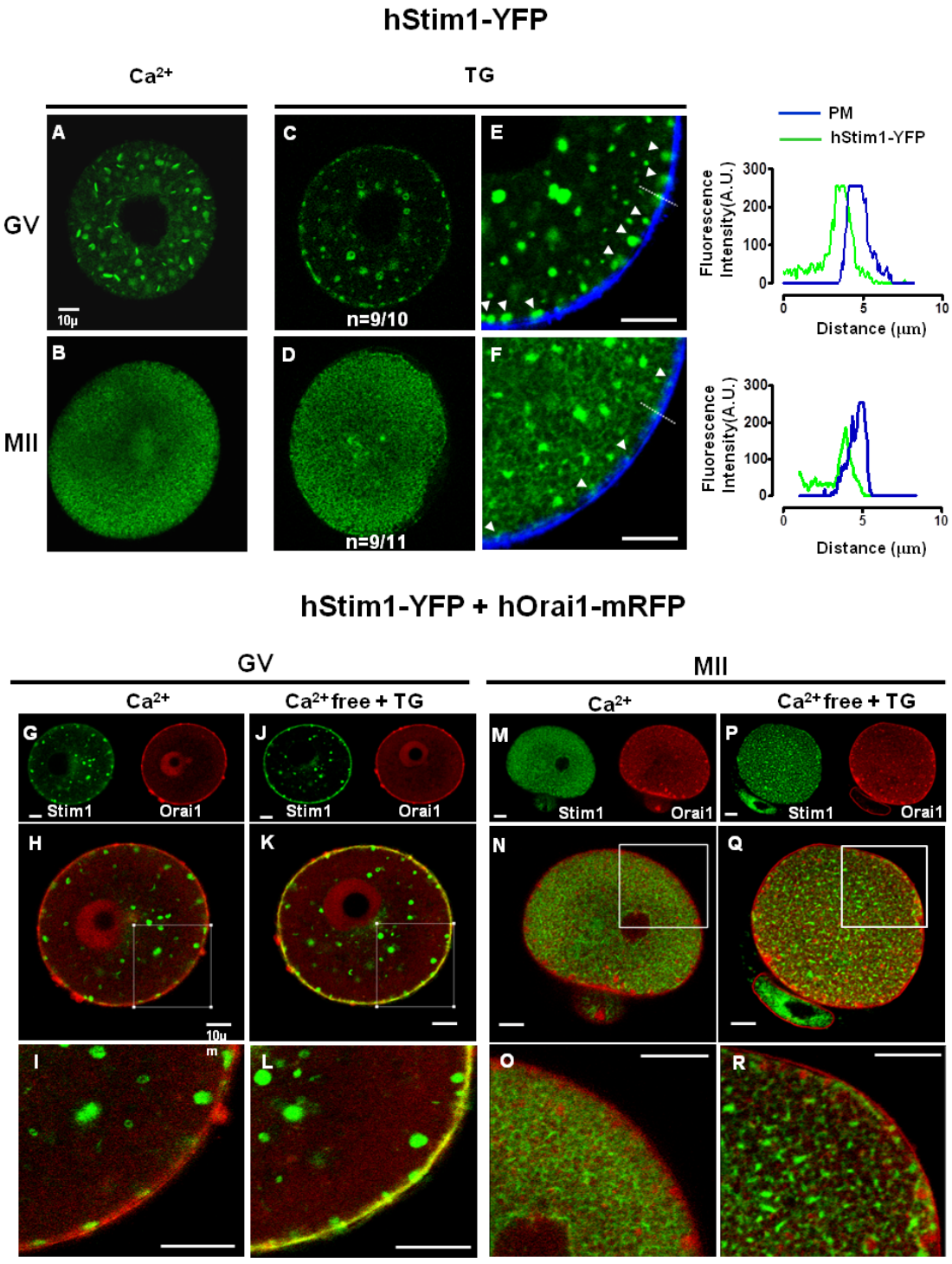
hStim1-YFP
Ca2+
TG
GV
MII
A
B
C
D
E
F
10μ
n=9/10
n=9/11
PM
hStim1-YFP
Fluorescence Intensity(A.U.)
300
200
100
0
0
5
10
Distance (μm)
hStim1-YFP + hOrai1-mRFP
GV
MII
Ca2+
Ca2+free + TG
G
J
M
P
Stim1
Orai1
H
K
N
Q
I
L
O
R

Figure 3-5. hStim1 puncta formation and colocalization with hOrai1 decreases during oocyte maturation. (A, B) Under control conditions, hStim1-YFP forms internal aggregates in GV oocytes, whereas in MII eggs it acquires a more homogenous, ER-like organization. After depletion of $[Ca^{2+}]_{ER}$, hStim1-YFP undergoes "puncta" formation in GV oocytes (C), whereas hStim1-YFP distribution is hardly changed in MII oocytes (D). Arrowheads point to hStim1-YPF puncta (E, F), and line graphs depicting the fluorescence intensity of these puncta, marked with a broken line, are shown to the right of E and F. (E, F) The proximity of the hStim1-YFP puncta/aggregates to the PM was estimated by staining the PM with wheat germ agglutinin–Alexa 664. hStim1-YPF puncta are bigger and more numerous in GV oocytes than in MII eggs. (G–R) Confocal images before and after TG treatment of GV oocytes (G–L) and MII eggs (M–R) expressing hStim1-YFP+hOrai1-mRFP. The same oocytes/eggs were imaged before and after TG. Top, separate fluorescent channels; middle, merged images; bottom, amplified regions of these are. hStim1 and hOrai1 display extensive overlap after the addition of TG in GV oocytes (K, L), but the overlap is negligible at the MII stage (Q, R). Scale bar, 10 μm.

Figure 3-6.

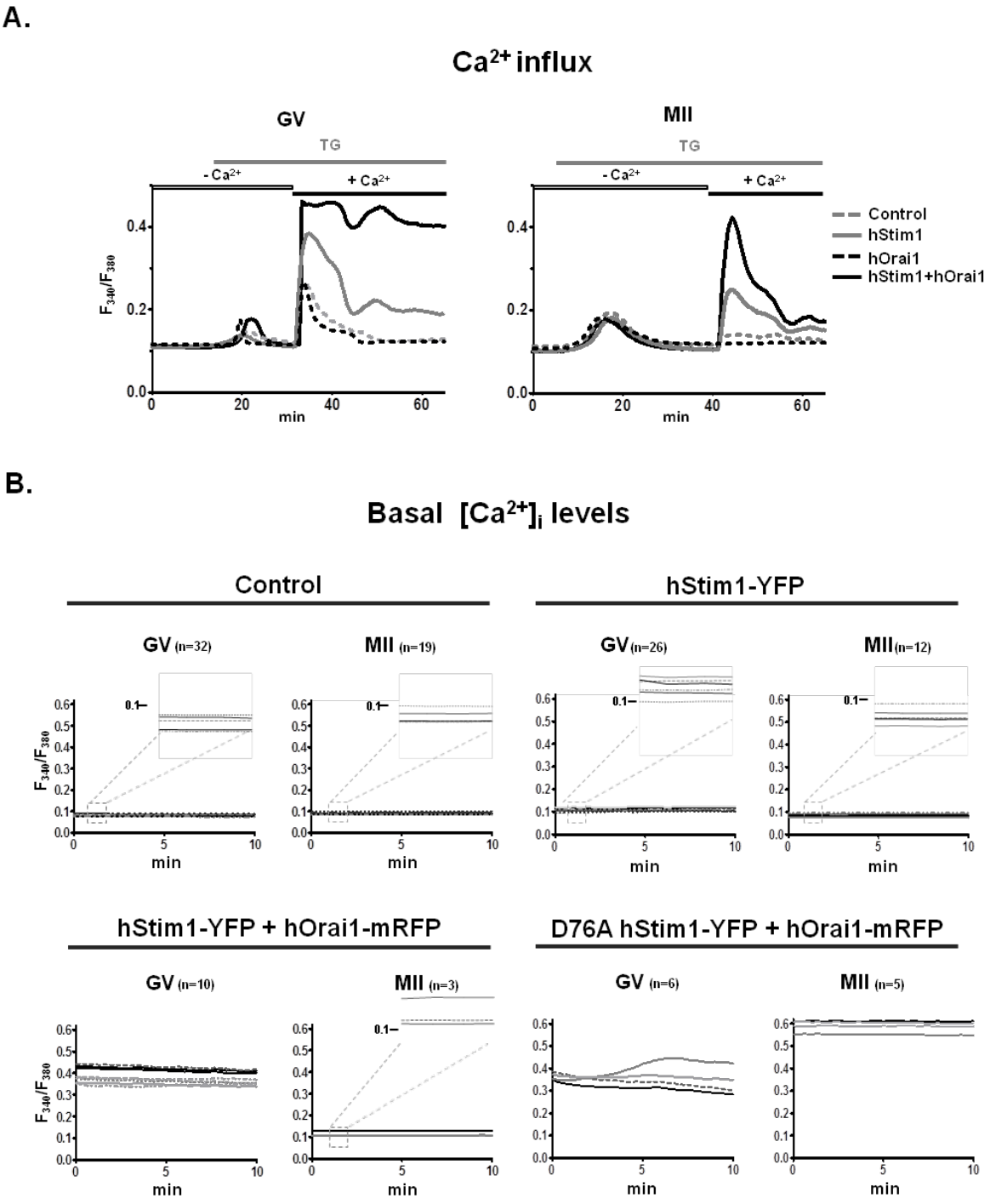
A.
Ca2+ influx
GV
MII
TG
- Ca2+
+ Ca2+
F340/F380
min
Control
hStim1
hOrai1
hStim1+hOrai1
B.
Basal [Ca2+]i levels
Control
hStim1-YFP
GV (n=32)
MII (n=19)
GV (n=26)
MII (n=12)
hStim1-YFP + hOrai1-mRFP
D76A hStim1-YFP + hOrai1-mRFP
GV (n=10)
MII (n=3)
GV (n=6)
MII (n=5)

Figure 3-6. Overexpression of SOCE components alters Ca^{2+} homeostasis. (A) Expression of hStim1-YFP+hOrai1-mRFP increased Ca^{2+} influx in both GV and MII cells after TG and $CaCl_2$ add-back, although the increase was greater and more prolonged in GV oocytes. Expression of hStim1-YFP also increased Ca^{2+} influx in both GV and MII stages but to a lesser extent, whereas hOrai1 had no effect. (B) Expression of hStim1 or hStim1+hOrai1 differentially increased basal $[Ca^{2+}]_i$ during maturation. Baseline $[Ca^{2+}]_i$ traces in control (top, left), hStim1-YFP–expressing (top, right), hStim1-YFP+hOrai1-mRFP–expressing (bottom, left), and D76A hStim1-YFP+ hOrai1-mRFP–expressing (bottom, right) oocytes. Insets in each treatment depict a magnified version of the *y*-axis at the 0.1 mark so that minor differences in basal $[Ca^{2+}]_i$ between GV and MII stages can be appreciated for some of the treatments

Figure 3-7

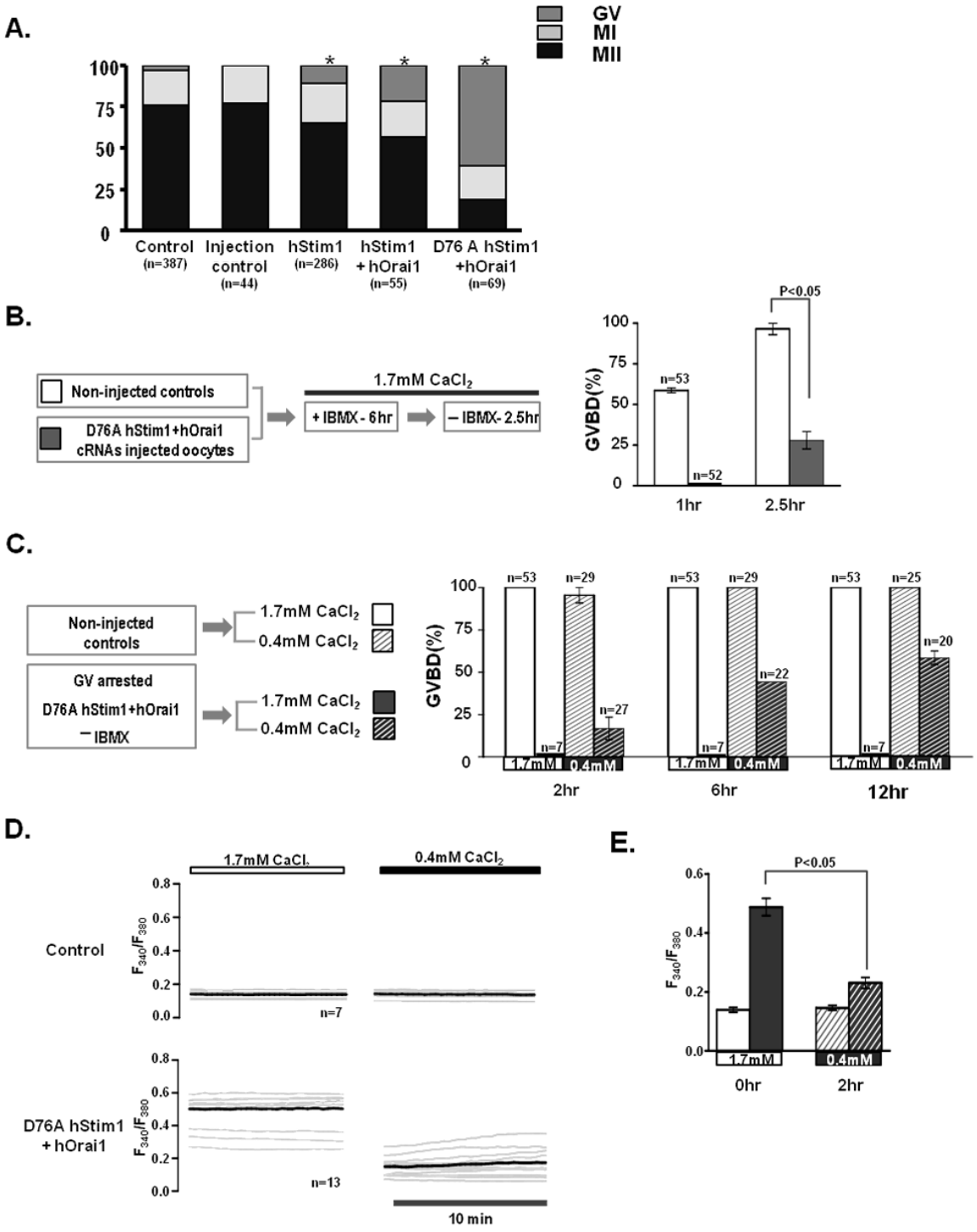
A.
GV
MI
MII
100
75
50
25
0
Control (n=387)
Injection control (n=44)
hStim1 (n=286)
hStim1 + hOrai1 (n=55)
D76 A hStim1 +hOrai1 (n=69)
B.
Non-injected controls
D76A hStim1+hOrai1 cRNAs injected oocytes
1.7mM CaCl2
+ IBMX - 6hr
– IBMX- 2.5hr
GVBD(%)
P<0.05
n=53
n=52
1hr
2.5hr
C.
Non-injected controls
GV arrested D76A hStim1+hOrai1 – IBMX
1.7mM CaCl2
0.4mM CaCl2
n=53
n=29
n=7
n=27
n=22
n=25
n=20
2hr
6hr
12hr
D.
1.7mM CaCl2
0.4mM CaCl2
Control
D76A hStim1 + hOrai1
F340/F380
n=7
n=13
10 min
E.
P<0.05
0hr
2hr

Figure 3-7. Changes in Ca^{2+} homeostasis affect resumption of meiosis and oocyte maturation. (A) Control, sham-injected, and oocytes expressing hStim1-YFP, hStim1-YFP+hOrai1-mRFP, or D76A Stim1-YFP+hOrai1-mRFP were in vitro matured and their maturation rates assessed. Expression of any mRNAs that increased basal $[Ca^{2+}]_i$ even transiently caused a reduction in maturation rates, although expression D76A hStim1-YFP+hOrai1-mRFP nearly completely prevented resumption of meiosis. Asterisks above bars represent treatments that significantly reduced GVBD rates ($p < 0.05$). (B) The effect of coexpression of D76A hStim1-YFP + hOrai1-mRFP on meiotic resumption was investigated as depicted in the flow chart (left), and data are summarized in the bar graph [94]. Expression of D76A hStim1-YFP+hOrai1-mRFP in GV oocytes delayed and mostly prevented GVBD under normal $[Ca^{2+}]_e$ ($p < 0.05$). (C) As before, but selected GV-arrested oocytes were transferred to low-$[Ca^{2+}]_e$ medium (0.4 mM), which partly rescued the arrest caused by expression of D76A hStim1-YFP+hOrai1-mRFP. (D) Ca^{2+} traces depicting the effect of lowering $[Ca^{2+}]_e$ on basal $[Ca^{2+}]_i$ in control and GV-arrested D76A hStim1+hOrai1–expressing oocytes monitored before and 2 h after lowering $[Ca^{2+}]_e$ from 1.7 to 0.4 mM; the bold trace represents the mean of the responses. (E) A bar graph was used to summarize in the same group of oocytes the mean ± SEM change in basal $[Ca^{2+}]_i$ caused by lowering external $[Ca^{2+}]_e$; $p < 0.05$.

CHAPTER 4

THE ROLE OF PHOSPHORYLATION ON STIM1 DISTRIBUTION AND SUBSEQUENT EFFECT IN CALCIUM INFLUX IN MOUSE EGGS

4.1 Introduction

The fertilization-induced Ca^{2+} signal is indispensible for early embryonic development. It controls several important functions required for egg such as the exocytosis of cortical granules, which is responsible for the block to polyspermy, degradation of cytostatic factors that relieves the meiotic arrest of ovulated egg, and is important in driving the egg into interphase and promoting the activation of the embryonic genome [31, 71]. Ca^{2+} release is initiated following the delivery into the ooplasm of a sperm specific PLC_ζ [14], which hydrolyzes a PIP_2 present in egg membranes to generate IP_3 and DAG. The diffusible IP_3 binds its cognate receptor in the ER, IP_3R1, leading to the opening of the channel and Ca^{2+} release into the ooplasm [16, 17]. In the case of mammalian eggs, Ca^{2+} rises occur periodically, ~ every 20 min, and are known as Ca^{2+} oscillations. In mice the oscillations stop around the time of pronuclear formation, but in large domestic species including humans, the oscillations last for more than 8 hr [95, 96].

In mammalian females, follicles are continuously selected for development and growth based on a combination of hormonal stimulation. Upon reaching the graafian stage, which contains fully grown oocytes, these oocytes responds to the LH surge that triggers ovulation and the resumption of meiosis, as these oocytes are arrested at the prophase sate of the first meiotic division, also known as the GV stage. Resumption of meiosis as well as it progression to the MII stage is triggered by activation of the maturation promoting factor, which is composed by the kinase CDK1 and its regulatory subunit, cyclinB1, and the subsequent activation of the mitogen activation protein kinase (MAPK) [28, 29]. During maturation, GV stage oocytes, which possess a large nucleus, undergo GVBD, and progress through the MI stage, where they release the 1st

polar body, after which they become arrested for a second time but this time at a metaphase stage of the second meiotic division; release of this arrest is accomplished by the $[Ca^{2+}]_i$ oscillations induced fertilization [10, 31, 71].Along with nuclear maturation, oocytes also undergo cytoplasmic optimization during maturation, and one of the mechanisms that become finely tuned during this process is the Ca^{2+} signaling machinery. For example, the sensitivity of IP_3R1, i.e., the capacity to release Ca^{2+} in response to IP_3 stimulation, is greatly increased during this period [34, 97]. Similarly, the Ca^{2+} content of the ER, the main Ca^{2+} store in eggs, increases steadily during maturation [32, 33] and the ER also undergoes re-organization and forms prominent cortical clusters [98]. Only following the completion of these adaptation, the Ca^{2+} machinery of the egg is set to deploy the complex $[Ca^{2+}]_i$ oscillations initiated by the sperm. Importantly, one aspect of the Ca^{2+} toolkit that has not been thoroughly investigated in oocytes is how Ca^{2+} enters oocytes during maturation to increase the content of the Ca^{2+} stores, or in eggs, to support the persistence of the oscillations. Our recent study investigated whether different Ca^{2+} influx rates were present during maturation of mouse oocytes [99]. We found that consistent with the low Ca^{2+} content of the ER at the GV stage, at this stage Ca^{2+} influx was the greatest, whereas the opposite was true in MII eggs. This association between the Ca^{2+} content of the internal stores and Ca^{2+} entry brought to mind the store-operated Ca^{2+} entry (SOCE) mechanisms that is thought to be active in many cell types. In addition, the protracted inactivation of SOCE during maturation, suggested active regulation of it in mouse oocytes [99].

SOCE is a ubiquitous Ca^{2+} influx mechanism present in most cell types that is involved in restoring the Ca^{2+} content of the ER after Ca^{2+} has been released from it following agonist stimulation [4, 39, 100, 101]. Two main molecular components are thought to be responsible for SOCE; one that acts as a sensor of the level of concentration of Ca^{2+} in the ER, Stim1[48, 49], and the counterpart Ca^{2+} channel in the plasma membrane Orai1 [51]. Stim1 is an ER resident protein with and its N-terminus facing the ER lumen. This domain contains motifs for sensing the level of Ca^{2+} in the ER, EF-hand, and another one that mediates subunit oligomerization

following depletion of the Ca^{2+} store. The C-terminus part of Stim1 projects into cytoplasm and encompasses several domains, including the domain that interacts and gates Orai1, which is known as CRAC activation domain. Other domains of the cytoplasmic region of Stim1 are the S/P rich domain, which contains multiple phosphorylation motifs and the binding site for the microtubule-plus-end-tracking protein EB1, which makes possible the association with microtubules [61, 102]. Lastly, the poly lysine rich tail (polyK tail) located at very end of the C-terminus makes possible the redistribution of Stim1 to cortical area near the PM [54].

SOCE is activated by depletion of Ca^{2+} from the ER store. This loss of Ca^{2+} causes a conformational change that makes possible intermolecular oligomerization of Stim1. Oligomerization favors translocation of Stim1 to ER-PM junctions, where the ER comes in close apposition to the PM, hence facilitating the interaction of it Orai1. The interaction between Stim1 and Orai1 is direct and is mediated by the CAD domain [54]. The interaction, which causes oligomerization of Orai1, causes Ca^{2+} influx [54].The Ca^{2+} influx is then inactivated by several mechanisms, the molecular details of which remain to be worked out [57, 103, 104]. Inactivation of SOCE also occurs in some cases even before Ca^{2+} influx occurs, as it is observed in somatic cells in mitosis [59, 91] and eggs at the metaphase stage of the second meiosis I [60, 64, 65].This inactivation has been linked to phosphorylation by M-phase kinases in the S/P-rich domain during meiosis and mitosis [59]. Nevertheless, the precise molecular changes induced by phosphorylation that inactivate SOCE remain to be fully elucidated and may be cell-type specific. For example, in *Xenopus* eggs and following Ca^{2+} store depletion, non-phosphorylated Stim1 mutants were unable to form puncta[60], which is required to activate Orai1, whereas in somatic cells, similar mutants rescued puncta formation[59]. Thus, those studies differed in the interpretation of the role of phosphorylation on SOCE inactivation during M-phases of the cell cycle. Given that we have shown that Stim1 becomes phosphorylated in mouse oocytes during maturation, and that SOCE is downregulated during the same period of time[99], an aim of this study was to elucidate the kinases involved in Stim1 phosphorylation and its temporal occurrence

during maturation. Another aim was to examine the role of Stim1 phosphorylation on Stim1 organization and distribution as well as the impact on Ca^{2+} entry in mouse eggs.

4.2 Results

4.2.1 Stim1 is differentially phosphorylated by M-Phase Kinases during mouse oocyte maturation.

TG-induced SOCE activity is progressively inactivated during oocyte maturation ([11, 18, 33] and a similar regulation occurred in oocytes expressing hStim1-YFP cRNA [99]. It was observed that during maturation hStim1 undergoes redistribution that causes reduced localization near the plasma membrane and decreased puncta formation, which are required to engage its channel partner, Orai1 [99]. We confirmed those findings by demonstrating that hStim1 is distinctively rearranged during meiotic maturation, as whereas hStim1-YFP forms large internal patches at the GV stage, (Fig.4-1A), it shows a reticular distribution at the MII stage similar to that of the ER (Fig. 4-1B). Further, treatment with TG and depletion of ER Ca^{2+} induced hStim1-YPF puncta formation in GV oocytes but not in MII eggs (Fig. 4-1 C, D, respectively). This reduced presence of Stim1 near the PM is thought to underlie the decreased function of SOCE in MII mouse eggs.

Inactivation of SOCE has been observed during mitosis in somatic cells and during the late stages of meiosis in *Xenopus* eggs[59, 86] . The molecular mechanism(s) responsible for SOCE inactivation remains to be fully elucidated in these systems, although phosphorylation of Stim1 has been observed both in somatic cells and *Xenopus* eggs [59, 86]. Stim1 phosphorylation has been also detected in mouse eggs, although only after hStim1 expression and without determination of the responsible kinase(s). Thus, we investigated whether it could be attributed to one of the two M-phase kinases, CDK1 and MAPK, which are mostly responsible for driving oocyte maturation (Fig. 4-1E). Phosphorylation has been shown to cause a shift in the electrophoretic mobility of Stim1, which is erased by treatment with an alkaline phosphatase [99], and therefore we used this approach to assume phosphorylation of the protein. In addition, we used the Phos-tag acrylamide method, as its positive charged metals in gel matrix greatly delay the migration of phosphorylated proteins compared to their counterparts [105, 106]. We first

confirmed that the expressed hStim1-YFP protein was phosphorylated during maturation, which was evidenced by the delayed migration of the protein at the MII stage. Importantly, the phosphorylation of hStim1-YFP is cell cycle dependent, as following egg activation, hStim1-YPF regained normal motility suggesting loss of phosphorylation following MII exit (Fig. 4-1F). We next compared the degree of mobility shift of hStim1-YFP using the Phos-tag system, which as it is greatly retarded the migration of thehStim1-YFP in MII eggs (Fig. 4-1G), confirming our previous results. We used this amplifying approach to evaluate endogenous Stim1 phosphorylation, as in a previous study we have failed to note a shift in mobility using conventional acrylamide [99]. Using Phos-tag we observed that mStim1 was phosphorylated during maturation (Fig.S1). These results suggest that mStim1 undergoes the same regulation as hStim1-YFP does, and thus hStim1-YFP can be used to assess the role of phosphorylation on mStim1 distribution and function.

To that end, we first examined the kinase(s) responsible for hStim1-YFP phosphorylation. To accomplish this, GV-arrested oocytes expressing hStim1-YFP were allowed to mature for 4 hr, GVBD, 8 hr, MI, or 14 hr, MII. After those times, oocytes/eggs were treated for 2 hr with U0126, a MAPK pathway inhibitor, Roscovitine, a CDK1 inhibitor, or their combination, prior to preparation of lysates. Western blotting of these lysates and evaluation of the mobility pattern of hStim1-YFP revealed that it experienced significant phosphorylation by the GVBD stage and this phosphorylation seemed to remain unchanged until the MII stage. Of the two inhibitors, U-0126 seemed to have only a mild reversal of the phosphorylation, whereas Roscovitine seemingly fully reversed hStim1-YFP phosphorylation, with the exception of the MII stage, which is possibly due to inactivation of the phosphatase responsible for the dephosphorylation of M-phase kinase targets[107, 108]. In sum, our results suggest that CDK1 is the most important kinase of phosphorylations of hStim1-YFP in mouse oocytes and eggs.

4.2.2 Phosphorylation of hStim1-YFP affects its distribution and ability to interact with hOrai1-mRFP in mouse eggs.

Given the increase in Ca^{2+} ER content that accompanies oocyte maturation, the redistribution of hStim1-YFP during maturation could also be due, at least in part, to the increased levels of luminal Ca^{2+}, which can be sensed by hStim1's EF hand[109-111]. To rule this out, we examined the distribution of a hStim1 variant that is largely insensitive to changes in luminal Ca^{2+} and constitutively localized near plasma membrane, D76A-hStim1[48, 112]. Interestingly, the distribution of D76A hStim1 alone at MII stage did not show any accumulation as puncta near PM, rather spreaded as recticular structure similar to the WT hStim1-YFP at MII stage(Figure S2, left bottom). So to expose hStim1-YFP to thoroughly different phosphorylation environments, D76A hStim1 cRNA was injected into oocytes arrested at the GV stage, where MPF and MAPK activity are absent, or in oocytes after GVBD, ~1.5 to 2 hr post-IBMX, where the activity of M-phase kinases is on the rise (Fig. 4-2A). To evaluate co-localization with hOrai1-mRFP, a dead-pore mutant version of hOrai1, E106A-hOrai1, was used to avoid the large increases in basal $[Ca^{2+}]_i$ caused by the simultaneous expression of Stim1 and Orai1, which compromise maturation competence [99]. The distribution of D76A-hStim1-YFP was greatly affected by the timing of its expression. For instance, GV oocytes expressing D76A hStim1-YFP together with hOrai1-mRFP formed extensive overlay like cortical ring (Figure S2, right), whereas in MII egg injected at the GV stage D76A-hStim1-YFP formed large and uniform puncta closely overlapping with E106A-hOrai1 (Fig. 4-2B), this was not the case in oocytes injected after GVBD, which displayed two patterns of D76A-hStim1-YFP and E106A-hOrai distribution (Fig. 4-2C,D). The first pattern, which was observed in ~50% of these cells, D76A-hStim1-YFP formed puncta, although the size of the puncta were smaller, they were not equally uniform regarding their location near the PM and Orai1 displayed a more diffuse cortical staining whereby in some areas it was not associated with D76A-hStim1 (Fig. 4-2C,D). In the other pattern, D76A-hStim1-YFP failed to form puncta and the degree of overlap with E106A-hOrai1 was greatly

reduced. These results suggest that phosphorylation of Stim1 mediated by M-phase kinases regulate its distribution and its ability to interact with Orai1.

4.2.3 Phosphorylation of a CDK1 site affects the distribution of hStim1 in mouse eggs

The presence of a conserved CDK1 phosphorylation motif on the C-terminal end of Stim1, ^{668}SPGR^{671}, combined with demonstration by mass spectrometry that this site is phosphorylated in mitotic cells [59, 113], and our data showing that the retardation of hStim1 mobility detected by western blotting in oocytes at more advanced stages of maturation was largely overcome by Roscovitine, led us to examine the cellular and functional consequences of expressing a mutant version of the protein, S668A hStim1-YFP. From the standpoint of cellular distribution, expression of S668A hStim1-YFP in eggs maintained under basal Ca^{2+} conditions resulted in a proportion of eggs showing large internal clusters, which were absent in WT hStim1-YFP (Fig.4- 3 A, C, E), and most eggs displaying altered ooplasmic organization characterized by a reticular pattern comprised of longer strings than those observed in eggs expressing WT hStim1-YFP (Fig. 4-3C, E). In addition and even in this basal state, cortical accumulation near the PM could be observed in S668A hStim1-YFP expressing eggs, but not in eggs expressing wild WT hStim1-YFP (Fig. 4-3 A, C, E). Treatment with TG caused internal cluster formation in all eggs (Fig. 4-3B, D, F), although the clusters were bigger in S668A hStim1-YFP expressing eggs than in the WT hStim1-YFP expressing eggs. In addition, treatment of TG caused puncta formation in S668A hStim1-YFP expressing cells, but not in their counterpart control eggs (Fig. 4-3B, D, F and insets). We next examined using western blotting whether S668A hStim1-YFP altered the mobility shift observed in MII eggs expressing WT hStim1-YFP. The mobility pattern of S668A hStim1-YFP was not greatly different than from WT hStim1-YFP (Fig. 4-3G), suggesting multiple phosphorylations of hStim1. Lastly, we ascertained the functional impact of this phosphorylation. Eggs expressing S668A hStim1 showed a consistent but not significant

increase in the amplitude and integrated Ca^{2+} influx induced by TG exposure and Ca^{2+} add back than eggs expressing WT hStim1-YFP (Fig. 4-3H). Altogether, the results show that phosphorylation of the ^{668}SPGR CDK1 consensus modifies at least the cellular distribution of hStim1 in mouse eggs.

4.2.4 C-term phosphorylation consensus sites and the poly-K tail regulate hStim1 distribution and function in eggs

Research shows that the C-terminal end of hStim1 undergoes multiple phosphorylations in somatic cells and in *Xenopus* eggs [59, 60], which is consistent with the partial effect of the S668A mutation on hStim1 distribution and function. Thus, to get a deeper insight into the role of phosphorylation on Stim1 function and distribution, we generated a 482 stop mutant that lacked the 204 amino acids encompassing the ten phosphorylation consensus sites for MAPK/MPF (S/T-P) but maintained the sequences required to interact with hOrai1 [59]; 482stop-hStim1-YFP migration pattern was not affected by the cell cycle, suggesting that all phosphorylation sites have been removed [99]. Expression of this mutant greatly altered the distribution of hStim1 in MII eggs, as even at resting state, it accumulated in large internal patches (Fig. 4-4C). Nevertheless, these patches/clusters failed to re-align as puncta upon treatment with TG (Fig. 4-4D) suggesting, as pointed out by other study [114], that the poly-K tail might be necessary for translocation to the cortex. Hence, we generated a 481-polyK hStim1-YFP mutant that included the last fourteen amino acids from the Stim1 C-terminus containing all seven Ks. Overexpression of 481-polyK hStim1-YFP show that it recovered the reticular distribution for hStim1 (Fig. 4-4A, E, C) and, following Ca^{2+} store depletion, it formed internal patches/clusters in addition to puncta (Fig. 4-4F). Co-expression of 481-polyK hStim1 with hOrai1-mRFP revealed co-localization with hOrai1 even at basal conditions (Fig. 4-4G), which was enhanced following TG treatment (Fig. 4-4H); the only exception was the spindle area, which seemed to exclude hStim1 despite Orai1 being localized to the PM overlaying this area.

We next determined how the aforementioned mutants affected SOCE using the TG-Ca^{2+} re-addition method. Despite its unusual distribution and perceived lacked of cortical location, expression of 482 stop-hStim1-YFP mutant increased Ca^{2+} influx as much as expression of WT hStim1-YFP (Fig. 4-4I). Remarkably, expression of 481-polyK hStim1-YFP resulted in almost two-fold increase in the amplitude of Ca^{2+} influx than other group (Fig. 4-4 J, I and K). This data supports the notion that enhanced localization of 481-polyK hStim1-YFP near the PM region, which is facilitated by removal of the C-term phosphorylation sites, enhances its function. Together, the results show that whereas the C-terminus end of hStim1-YFP is not required to activate SOCE, it is important for its regulation.

4.2.5 Substitution of Serines on the C-terminus of hStim1 leads to persistent cortical distribution and enhanced SOCE activity

The previous results using the 481-poly K hStim1-YFP mutant are consistent with the notion that the C-term domain of Stim1 with its M-phase kinase phosphorylation sites regulates SOCE activity [59]. The interpretation of our results is nevertheless somewhat compromised by the modified size of the 481-poly K hStim1 vs. the native protein. To address this, we carry out a serious of studies using a version of the protein where all ten serine within conserved phosphorylation sites were substituted by alanine, S10A hStim1-YFP, which largely prevented phosphorylation of the protein while preserving the native size of hStim1[102]. Expression of S10A hStim1-YFP resulted in accumulation of its signal near the cortex and the plasma membrane even in the presence of standard extracellular Ca^{2+} and without addition of TG (Fig. 4-5B). Such a distribution was not observed following expression of WT hStim1-YFP (Fig. 4-5A) or 481-polyK hStim1-YPF, although the latter displayed a similar organization when co-expressed with hOrai1. These results suggest that the full length of S10A hStim1-YFP confers better accessibility to the PM than the shorter 482-polyK hStim1-YFP.

Next, we examined whether the distribution of S10A hStim1-YFP was influenced by co-expression with hOrai1. We expressed S10A hStim1-YFP with E106Q hOrai1 [115] instead of WT hOrai1 to prevent the exposure of excessive influx during maturation caused when Stim1 and Orai1 are co-expressed[99]. In control cells co-expressing WT hStim1-YFP and E106A hOrai1 in the presence of regular extracellular Ca^{2+} concentrations, hStim1-YFP did not accumulate near the cortex and no apparent overlap with E106A hOrai1 was observed (Fig. 4-5C); treatment of these eggs with TG to reduce Ca^{2+} in ER levels only somewhat enhanced the co-localization of the molecules (Fig. 4-5D). On the contrary, cells co-expressing S10A hStim1 and E106Q hOrai1 showed extensive co-localization both in the presence of normal external Ca^{2+} concentrations (Fig. 4-5E) and after treatment with TG, although after the latter greater overlap was observed mainly the result of additional translocation of S10A hStim1-YFP to the plasma membrane (Fig. 4-5E and F and their insets). It is worth noting that under both conditions, eggs expressing S10A hStim1-YFP displayed extensive fluorescent signal within the spindle region, which was detected intercalated between chromosomes (Fig. 4-5F; Fig. S3); this spindle localization of hStim1 was not observed following expressing of WT or 481-polyK versions of hStim1.

We then examined how S10A hStim1-YFP expression affected basal $[Ca^{2+}]_i$ levels, Ca^{2+} release and SOCE activity. Expression of S10A hStim1-YFP alone did not impact basal $[Ca^{2+}]_i$ levels in MII eggs and addition of TG revealed it did not modify the amplitude or duration of the TG-releasable Ca^{2+} pool (Fig. 4-5G; upper panel). Nevertheless, following re- addition of Ca^{2+}, the presence of S10A hStim1-YFP clearly increased the magnitude of the Ca^{2+} influx by several folds over the WT-hStim1-YFP (Fig. 4-5G). It is worth noting that the magnitude of the Ca^{2+} influx in eggs expressing S10A hStim1-YFP was not different than the one observed following expression of 481-polyK tail, although there were differences in degree of inactivation, which was not obvious in S10A hStim1 YFP expressing eggs (Fig. 4-5G upper and lower panels). These results suggest that the consensus phosphorylation sites on the C-terminal end of hStim1 play important roles in its distribution and activity.

4.3 Discussion

Using confocal images and Ca^{2+} imaging in the live egg overexpressing fluorescence protein tagged mutants of Stim1-YFP on the carboxyl terminus; we investigated underlying mechanisms responsible for inactivation of SOCE during mouse meiotic progression. Our study clearly showed that Stim1 is phosphorylated mainly in effect of CDK1 activation, concomitant with resumption of mouse meiotic maturation. Its phosphorylations regulate Stim1 function in two ways: these phosphorylations limit Stim1 reorganization as puncta near PM in response to the ER store depletion and restrict poly-K tail interaction with PM. Furthermore, its phosphorylations also reduced the interaction with Orai1. In sum, our study provide more detailed modulatory insights of how phosphorylations of Stim1 affect the suppression during mouse meiotic progression and its regulation can be varied among cell types.

4.3.1 The effect of phosphorylations of Stim1 in regulation of Ca^{2+} influx varies among meiotic or mitotic cell types

Although the suppression of SOCE, impaired redistribution of Stim1 in response to the ER store depletion, and phosphorylations on Stim1 occurred commonly during meiotic or mitotic cells, the modulatory roles of phosphorylations in Stim1 distribution and subsequent SOCE may differ among cell types and between meiotic and mitotic cells. For example, single expression of 200 amino acid truncated mutant (485 stop) or with Orai1 in *Xenopus* oocyte formed internal aggregate of Stim1 and co-internalized with Orai1 when was co-expressed, and this internal aggregates were suppressed the influx in the oocyte [114]. Whereas in mitotic HeLa cells, co-expression of 482 stop mutant with Orai1 increase its accumulation near PM and further reverse mitotic SOCE suppression[59]. In our observation, expression of almost the same mutant (482 stop) formed large internal patches similar to the result of *Xenopus* egg but functionally maintained suppression of SOCE similar to the increase when WT Stim1 was expressed in mouse oocyte/egg. But 482 stop expressed egg did not increase the influx significantly as mitotic HeLa

cell. Partly these differences are because we tested only single expression of 482 stop but they tested co-expression this mutant with Orai1, nonetheless it is clear the same mutants exert different outcome depending on the system.

In the same context, expressing different combination of non-phosphorylated forms of Stim1 mutants also show variable effect among cell types. None of non-phosphorylated mutants in *Xenopus* egg revert cortical localization of Stim1 puncta near PM and the SOCE suppression. Then their conclusion is that Xenopus Orai1 internalization play a primary role to suppress the influx [60, 86]. On the contrary, two serine to alanine mutations on the C-terminus partially recover the formation of puncta of Stim1and SOCE in mitotic HeLa cell [59], and expression of S10A fully recover the mitotic suppression by forming Stim1 puncta near cortex [102]. Our study also showed S10A expression totally recover cortical localization and fully support the SOCE, however its magnitude is less than the immature oocytes expressing Stim1 alone. These observations tell us that regulatory modules of Stim1 during mouse meiotic maturation are more close to the mammalian mitotic cells rather than Xenopus meiotic cell. This can be triggered by different ways of measuring Ca^{2+} changes using electrophysiology versus cytoplasmic Ca^{2+}, but confocal data clearly suggest that regulatory functions of phosphorylation roles on the C-term are quite differently between Xenopus and mouse. Several factors can contribute these differences such that there are different combinations of molecular adaptor proteins to regulate SOCE or ER distribution, and the needs of Ca^{2+} influx after fertilization are quite different, therefore the system is adapted accordingly.

4.3.2 Regulatory roles of C-terminus of Stim1 in Ca^{2+} influx in mouse meiotic maturation

The removal of C-terminus of the Stim1, 482 stop mutant, resulted in large internal patches in mouse egg at resting state, which likely also co-aggregated with ER as reported in Xenopus eggs [114], and its large internal patches seemed immobile aggregate since they did not redistribute near PM after the ER store depletion. Notably, only the attachment of positive

charged 14 amino acids into 482 stop mutant (481-polyK) totally retrieved these internal patches into reticular tubular structures. Similarly in *Xenoupus* egg, substitution of 200 amino acids of C-terminus with a similar length, non-functional florescent protein reversed internal aggregation of C-term truncated mutant to the reticular structure [114]. These results suggest that C-terminus of Stim1 sterically contribute its own conformational stability; hence without C-terminus it aggregate internally. Thus C-terminus involve in regulation of intra molecular interactions of Stim1and intracellular distribution.

Furthermore our study reveals a new mechanistic insight of SOCE regulation during meiotic maturation that there is a negative correlation between phosphorylation on the C-terminus and poly K tail for Stim1 localization near PM. It is probably controlled by electrostatic interactions between the C-terminus of the Stim1 and PM. This notion is supported by several C-terminus mutants. First, single expression of S10A hStim1 increase spontaneous localization of near cortex at resting state. In case of S668A hStim1 mutant, not dramatic as S10A hStim1, but it also showed decent increase of spontaneous accumulation near cortex. Interestingly, S668 site is the most proximal phosphorylation site from poly K tail that is likely sterically close. In addition, 481polyK- Stim1 also accumulated as a cortical ring when it co-expressed with Orai1 at resting state but it did not occur in single expression of 481-polyK. It may suggest that interaction with Orai1 also contribute cortical localization of Stim1 near PM even at resting state. Based on above observations, phosphorylations on Stim1 affect negatively to its localization near PM. we propose that phosphorylations on Stim1 during maturation induce repulsive interaction between negatively charged phospholipids in PM, thus sterically hinder poly K way from PM.

This notion is underpinned by Ca^{2+} influx traces after the store depletion among these mutants. Both removal of C-terminus or non-phosphorylated S10A reverses inactivation of SOCE in MII egg and show dramatic increase in amplitudes of Ca^{2+} influx. This increase was consistent with redistributions of both mutants after the store depletion. Interestingly, the traces after the peak significantly maintained higher in egg expressing S10A than 481-polyK. As shown in

spontaneous accumulation of both mutants in PM, it may occur that the full length of S10A is more advantageous to maintain more stable interaction with negatively charged phospholipids in PM than the shorter 481-poly K mutant. These differences will be also triggered by the interaction with positive microtubule cytoskeleton, since S10A Stim1 contains the interaction domain. However, its effect might be in part in mouse egg because 481-polyK mutant, without EB1 binding site, intensively accumulated in the cortex in response to the store depletion. And also high Ca^{2+} is known to detach Stim1 from EB, and another study show that the treatment of nocodazole destructing microtubule polymers does not affect SOCE function. We could not exclude whether it is triggered by other Ca^{2+} machineries such as Ca^{2+} ATPase, but at least, removal of extracellular Ca^{2+} in S10A hstim1 expressing egg quickly recovered the basal level suggesting that this longer duration in S10A expressing egg rely on Ca^{2+} influx.

Lastly, we also showed whether distribution of Stim1 can be changed by fluctuations of endogenous M-phase. By varying the timing of cRNAs injection before and after M-phase kinases activation, we assess whether constitutively active Stim1, D76A Stim1, together with Orai1 show changes in their distribution. Advantage of this approach that we thought are that usage of D76A hStim1 ruled out another critical factor, changes of ER Ca^{2+} contents during meiotic maturation, and constitutive binding of D76A Stim1 with Orai1 may sterically hinder access of M phase kinases. Remarkably, D76A hStim1and Orai1 injected before the kinases activation, the overlay of both molecules was observed as large puncta near PM in the egg, while if they were injected after the kinase activation, it clearly showed reduction of size of D76A Stim1 puncta and orai1. These observations confirm whether the effect of phosphorylation on Stim1 assessed by molecular or physiological approaches, distribution of Stim1 near PM is regulated by phosphorylations on C-terminus.

Another significant role of phosphorylation effects on Stim1 is ER retraction in metaphase plate. We also observed that intercalation of ER in S10A, which is known to interact with EB1 and S668 A mutant is also accumulated near the metaphase plate. However the effect of

ER intercalation during mouse meiotic maturation is also elusive like mitotic cell study. We did not observed statistically significant defect in cell cycle progression between S10A expressed egg and control eggs during in vitro maturation and Sr^{2+} induced pathenogenetic activation. As it is also suggested in mitotic somatic cells, dissociation of growing microtubule end due to Stim1 phosphorylation effect on SOCE function is not critical as we saw in 481-polyK .

In this study, we show how this mammalian meiotic cell regulated its Ca^{2+} influx mediated by Stim1. Our study reveals that phosphorylations on the C-term affect its own intermolecular polymerization, negatively affect polyK tail availability for interaction with PM, and interaction with Orai1. Its modulatory regulation of Stim1during mammalian oocyte/eggs may be more complicated than we described here, since many versatile roles of Stim1 and its adaptor or regulators are found these days in somatic studies. Combined with our knowledge will help clarify to understand for suppression mechanism.

Figure 4-1.

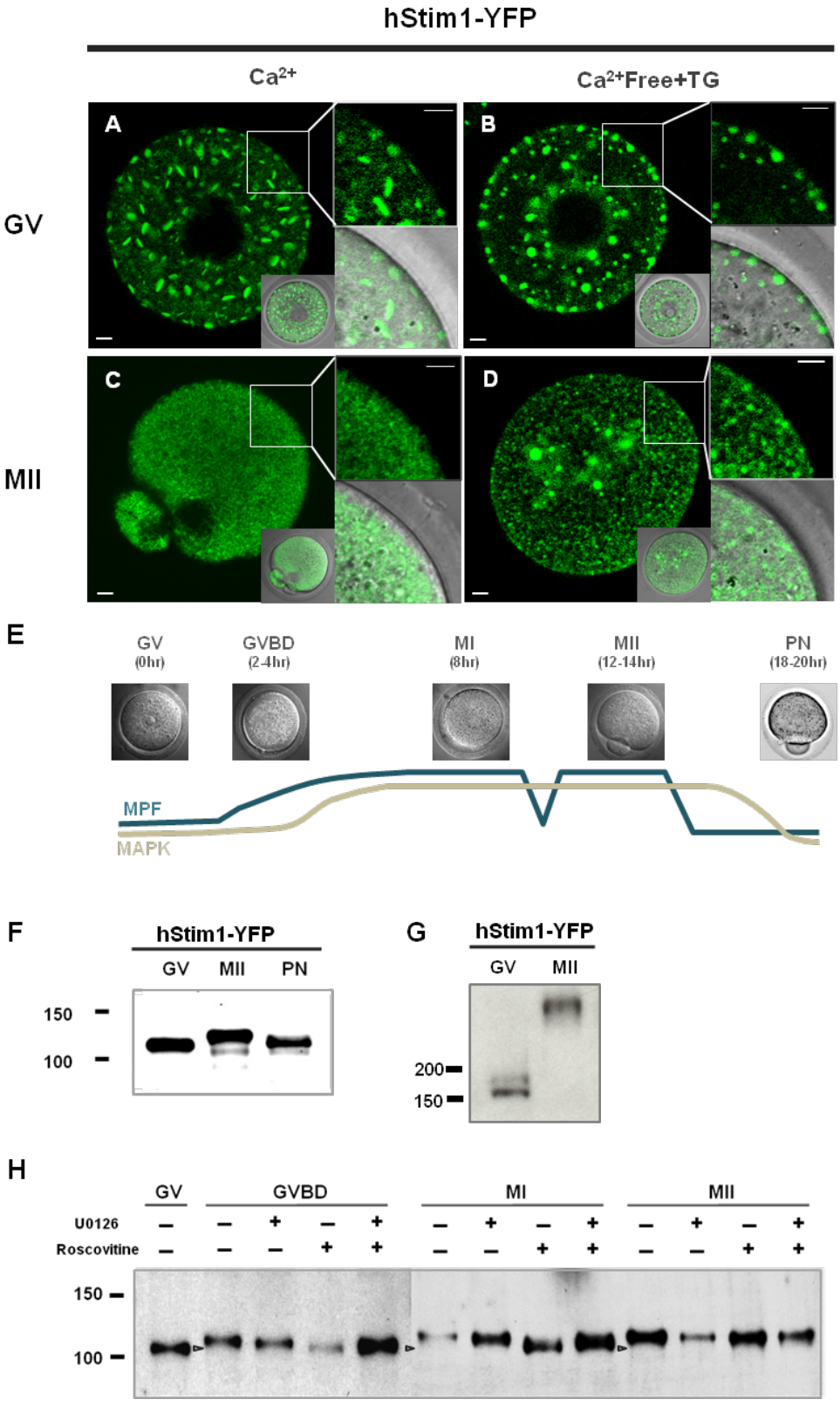
hStim1-YFP
Ca2+
Ca2+Free+TG
GV
MII
A
B
C
D
E
GV (0hr)
GVBD (2-4hr)
MI (8hr)
MII (12-14hr)
PN (18-20hr)
MPF
MAPK
F
hStim1-YFP
GV
MII
PN
150
100
G
hStim1-YFP
GV
MII
200
150
H
GV
GVBD
MI
MII
U0126
Roscovitine
150
100

Figure 4-1. Stim1 is differentially phosphorylated during mouse oocyte maturation. (A-D) Confocal images show the changes in distribution of hStim1-YFP between GV and MII stages. Images were taken at an equatorial section of live hStim1-YFP expressing GV- or MII-stage oocytes in presence of normal extracellular Ca^{2+} (A,B) or after addition of thapsigargin (TG) to reduce ER Ca^{2+} content (C,D). Insets show magnified views of cortical regions. Scale bar: 5μM. **(E-H)** Stim1 is phosphorylated by M-phase kinases active during cell-cycle transitions. (E) A schematic of the fluctuation of MAPK and MPF activities during oocyte maturation. (G) Western blots showing migration patterns of hStim1-YFP from oocytes collected at different stages of maturation. (F) Changes in migration pattern of human Stim1-YFP (n=10 eggs per lane, left panel) between GV and MII stage were enhanced by separating polypeptides in 6% Phos-tag-containing gel followed by normal immunoblotting. (G) The source of phosphorylation and change in migration patterns of hStim1-YFP was ascertained using the pharmacological inhibitors Cdk1/MPF and MAP kinases during the different stages of oocyte maturation. Arrowheads denote the expected position of hStim1-YFP at GV stage.

Figure 4-2.

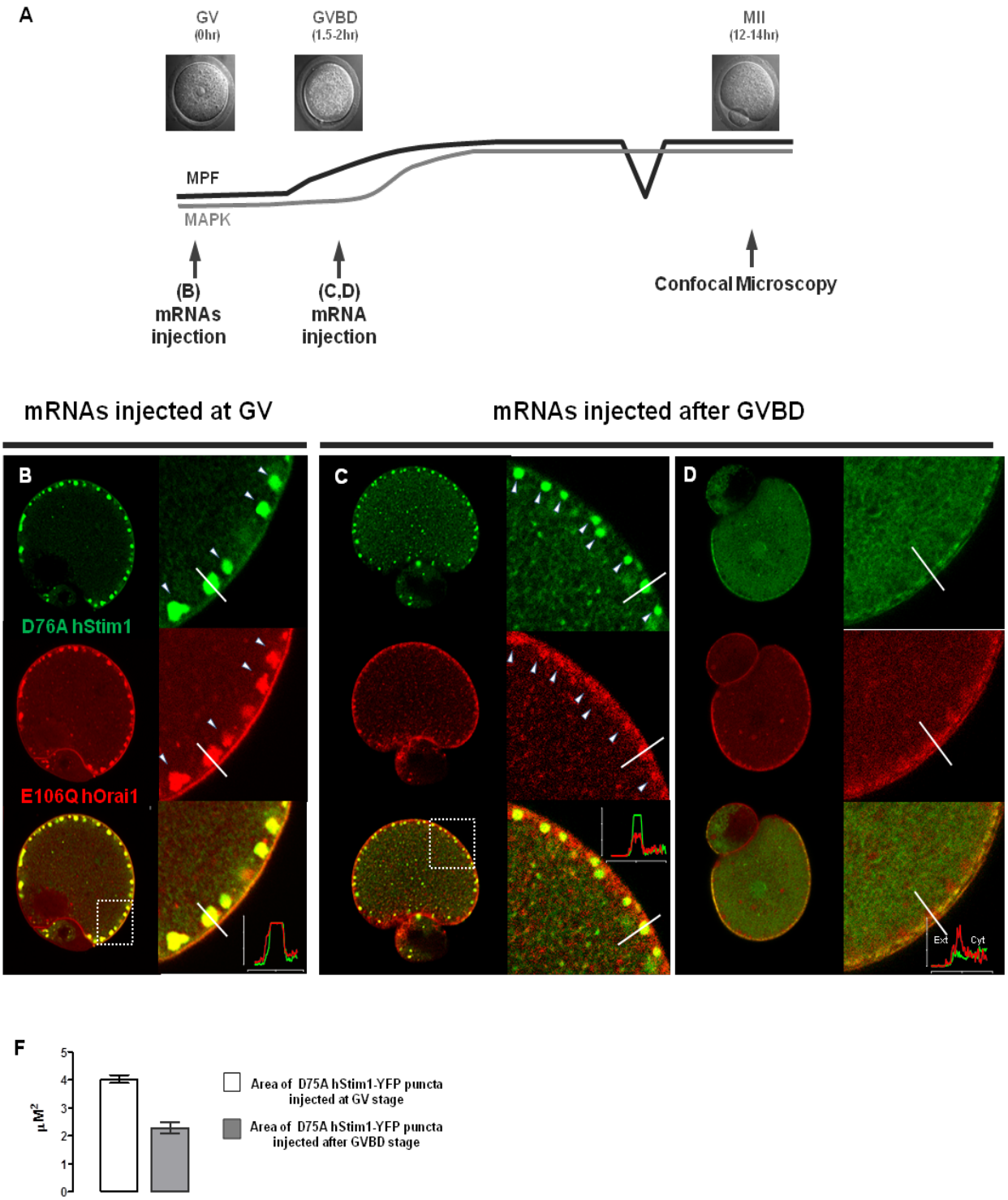
A
GV
(0hr)
GVBD
(1.5-2hr)
MII
(12-14hr)
MPF
MAPK
(B)
mRNAs
injection
(C,D)
mRNA
injection
Confocal Microscopy
mRNAs injected at GV
mRNAs injected after GVBD
B
C
D
D76A hStim1
E106Q hOrai1
Ext
Cyt
F
μM²
Area of D75A hStim1-YFP puncta injected at GV stage
Area of D75A hStim1-YFP puncta injected after GVBD stage

Figure 4- 2. hStim1-YFP phosphorylation affects hStim1-YFP's ability to co-localize with hOrai1. (A) A schematic of the experimental design where D76A hStim1-YFP and hOrai1-mRFP were co-injected at the GV stage or after GVBD. **(B-D)** Distribution of D76A hStim1-YFP and hOrai1-mRFP was examined using confocal microscopy in live MII oocytes; cRNAs were co-injected at GV (B) or at GVBD (C, D) and were translated for 12-14 hr during in vitro maturation. Arrowheads denote the position of D76A hStim1 puncta. Left panels within B, C, D show images of the whole egg, whereas right panels show magnified versions of the cortex area. The bottom panels show merged image of D76A hStim1 and hOrai1-mRFP images. Lines graphs within each image show the fluorescence the intensity of D76A hStim1-YFP and hOrai1-mRFP where the line scan was performed. **(F)** Averages sizes of puncta were quantified using image J.

Figure 4-3.

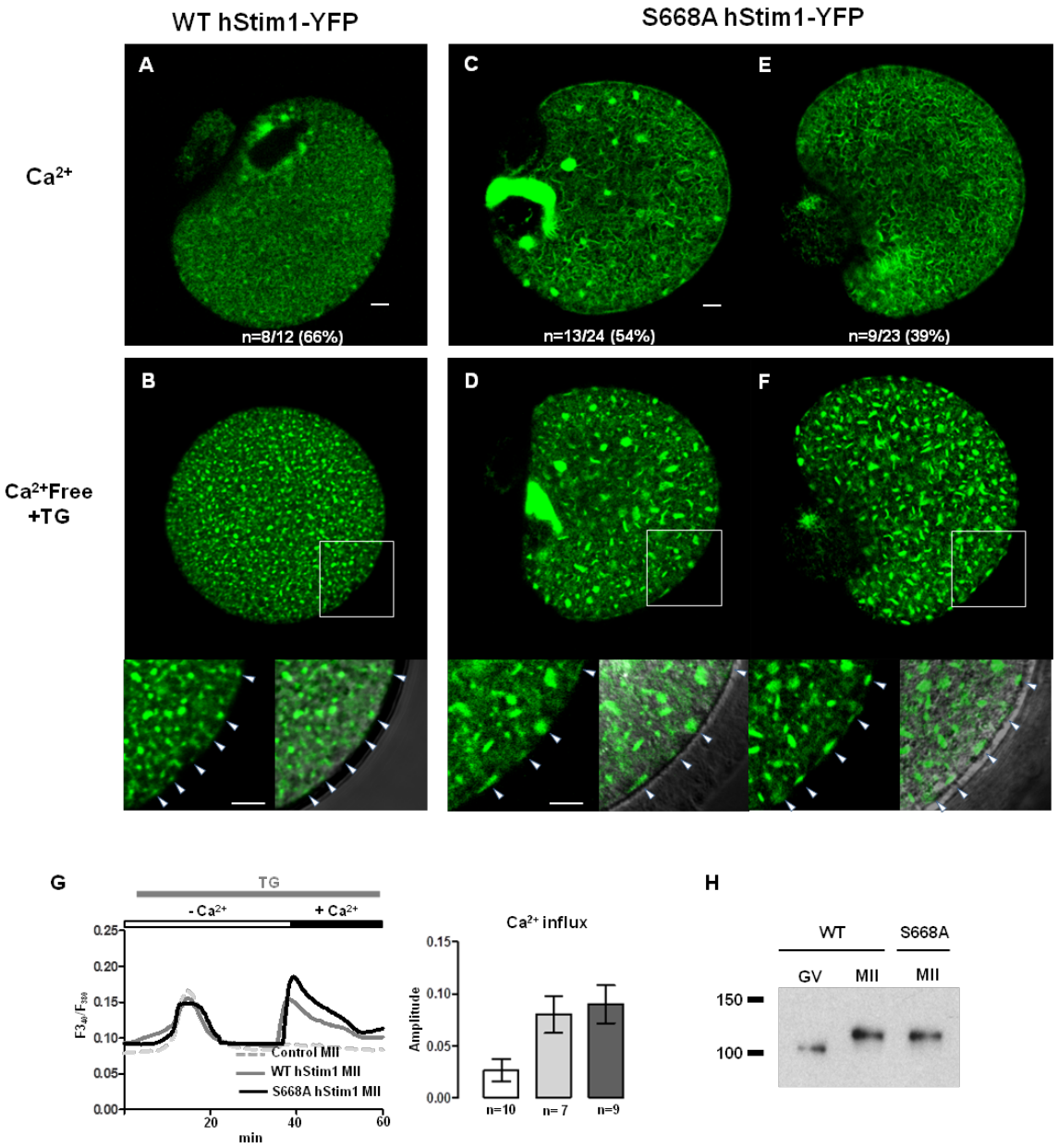

Figure 4- 3. A point mutation on a Cdk1 consensus site alters the distribution of WT hStim1-YFP in MII stage oocytes. (A-B) Distribution of WT hStim1-YFP in MII oocytes under normal Ca^{2+} conditions (A) or after treatment with TG in the absence of external Ca^{2+}(B). (C-F) Distribution of S668A hStim1-YFP in MII stage oocytes under normal conditions (C, E) and after TG treatment (D, F). Oocytes assessed for redistribution of S668A hStim1-YFP after TG (D, F) are the same oocytes at rest state (C, E, respectively). Bottom panels show magnified images of

the cortical area. Arrowheads denote the presence of hStim1-YFP and S668A hStim1-YFP puncta. (G) SOCE was examined in WT hStim1 vs. hStim1-YFP S668A expressing cells using the TG-Ca^{2+}addition method and the amplitude of Ca^{2+} influx in each group is displayed in the adjacent bar graph. (H) Immunoblot showing the migration pattern of S668A hStim1-YFP.

Figure 4-4.

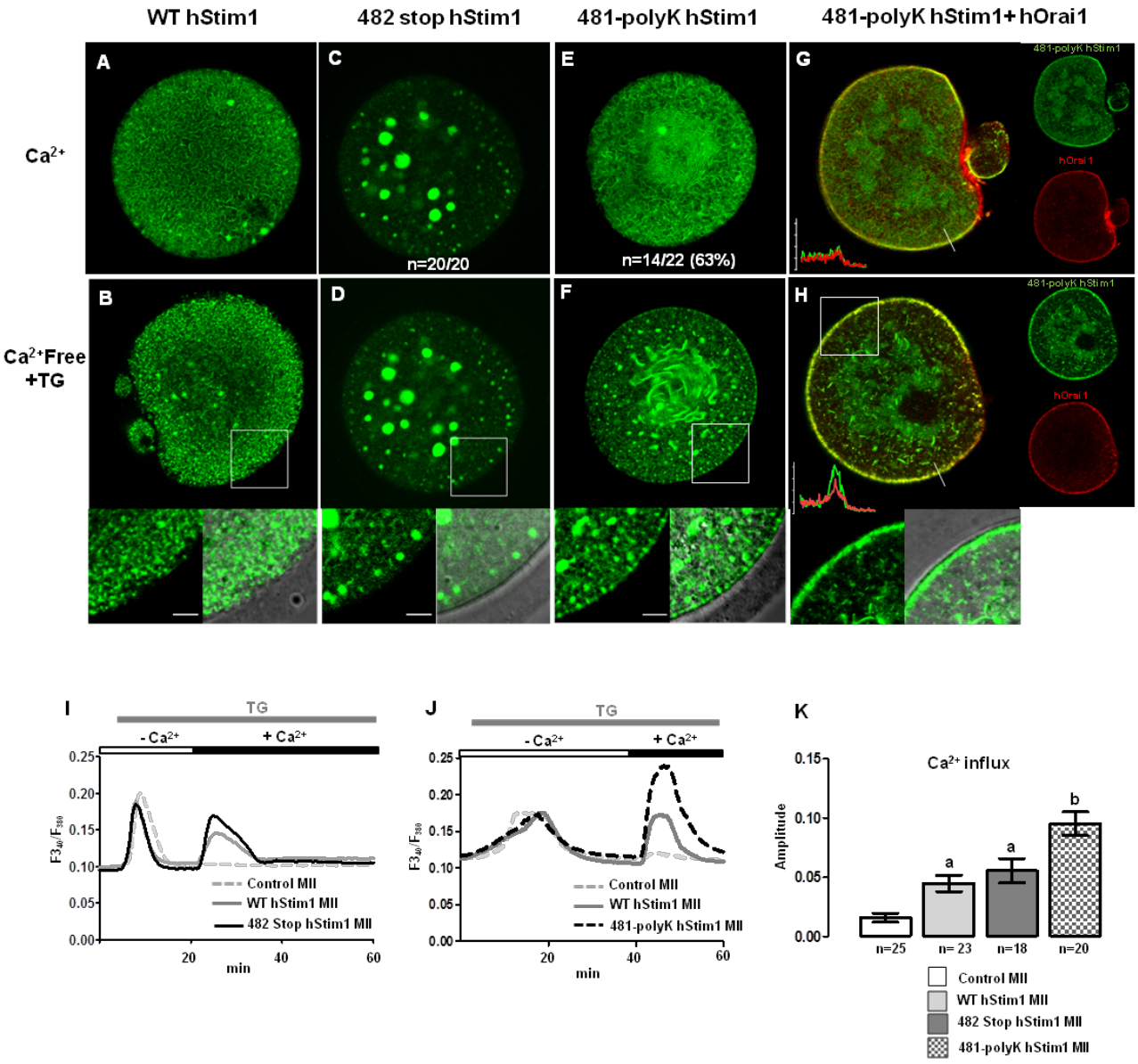

Figure 4-4. The C-terminal end of hStim1 modulates its distribution and Ca^{2+} influx-mediating ability during meiotic maturation. Distribution in MII oocytes of hStim1-YFP mutants in which portions of the C-terminal end of the molecule that contain consensus sites for M-phase kinase have been omitted. **(A-F)** Distribution of WT hStim1-YPF, 482 stop hStim1-YPF and 482-poly K hStim1 in MII oocytes in control conditions (A, C, E) or after TG treatment in the

absence of external Ca^{2+} (B, D, F). **(G, H)** Co-expression of 482-poly K hStim1 and hOrai1-mRFP cRNA in control conditions (G) or after TG treatment in the absence of external Ca^{2+} (H). The area denoted by a square in B, D, F, H is magnified in panels below (fluorescence image, left, and light image superimposed to fluorescence image, right). Insets in G and H show line scan profiles in each representative image. **(I-K)** $[Ca^{2+}]_i$ responses and influx after TG and Ca^{2+} addition in the aforementioned hStim1-YFP mutants. Representative Ca^{2+} traces for 482 Stop hStim1 and 481-poly K hStim1mutant are shown in I and J, respectively, and quantifications of amplitude of Ca^{2+} influx for both groups are shown in K.

Figure 4-5.

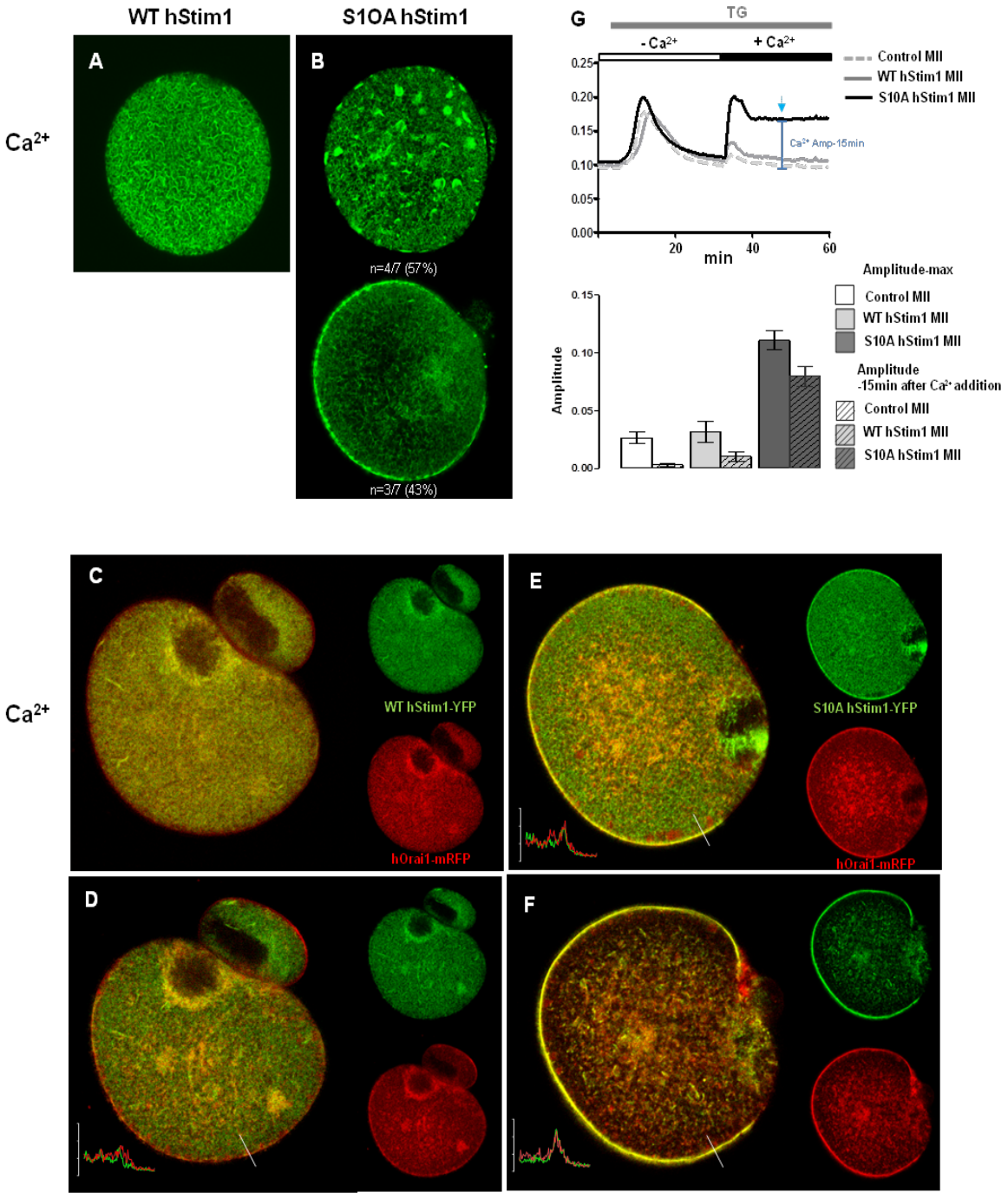
WT hStim1
S10A hStim1
Ca2+
A
B
n=4/7 (57%)
n=3/7 (43%)
G
TG
- Ca2+
+ Ca2+
Control MII
WT hStim1 MII
S10A hStim1 MII
Ca2+ Amp-15min
min
Amplitude-max
Amplitude
-15min after Ca2+ addition
C
D
E
F
WT hStim1-YFP
S10A hStim1-YFP
hOrai1-mRFP

Figure 4-5. The S10A hStim1-YFP mutant display increased SOCE activity at the MII stage and attains near PM distribution. (A) Localization of WT hStim1-YFP and **(B)** S10A hStim1-YFP in MII oocytes under control conditions. **(C-F)** Images demonstrating the co-localization of hStim1 and Orai1 signals after co-expression of WT hStim1-YFP+hOrai1-mRFP (C, D) or 481-polyK hStim1-YFP and hOrai1-mRFP (E, F) in normal Ca^{2+} condition (C, E) or after TG treatment (D, F), respectively. Same oocytes were used for images before and after addition of TG. **(G)** Ca^{2+} influx was measured in controls, WT hStim1-YFP and S10A hStim1-YFP expressing MII oocytes after TG treatment and Ca^{2+} addition. Representative traces are shown in the upper panel and the amplitude of Ca^{2+} influx following the addition of $CaCl_2$ was quantified at peak and 15 min after.

SUPPLEMENTARY FIGURES

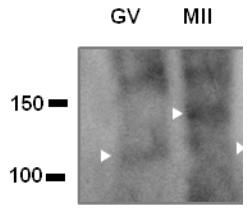

Figure S1. Changes in migration pattern of endogenous mouse Stim1 (n=150 eggs) between GV and MII stage were enhanced by separating polypeptides in 6% Phos-tag-containing gel followed by normal immunoblotting.

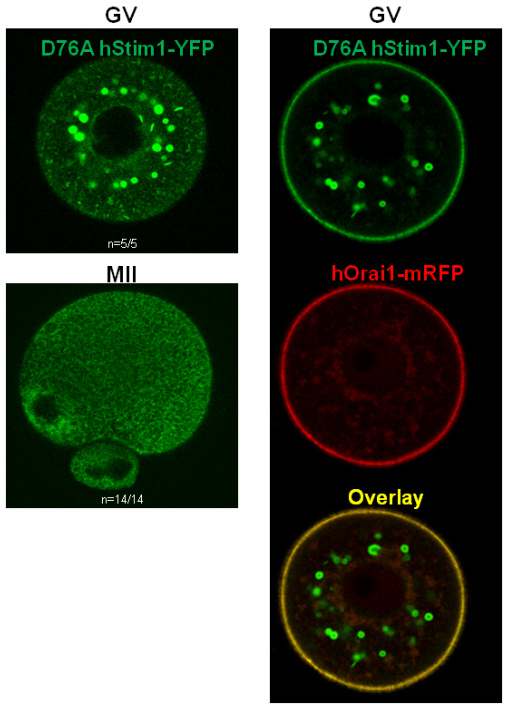

Figure S2. Distribution of D76A hStim1-YFP alone in GV oocyte and MII stage egg (left)and co-expressed with hOrai1-mRFP in GV stage oocyte (right) in normal $[Ca^{2+}]e$.

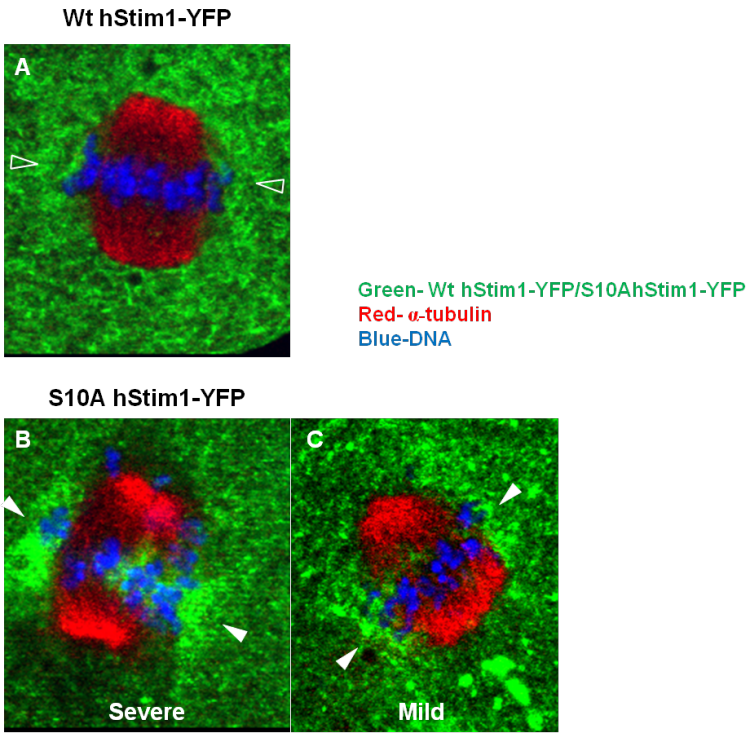

Figure S3. Distribution of WT hStim1 (A) or S10A hStim1-YFP (B, C) juxtaposed with metaphase II stage plate. S10A hStim1-YFP is interposed in metaphase II plate or accumulated next to metaphase II (white filled arrow heads), while WT hStim1 is not (empty arrow heads).

CHAPTER 5

CONCLUSIONS

Free Ca^{2+} is an important second messenger and as such controls numerous functions in cells including activating dormant oocytes/eggs from their MII arrest following sperm entry to begin early embryonic development. Hence, understanding the mechanisms that lead to the generation of Ca^{2+} responses has been regarded as an important question in the reproductive biology field as a mean to overcome infertility as well as to design now and more physiological contraceptive methods. The Ca^{2+} signal is ubiquitous and therefore oocytes have acquired the molecular toolkit present in most cells to maintain Ca^{2+} homeostasis. Nevertheless, it is also likely that they have acquired some specific mechanism(s), many of which are presently unknown, to make possible the persistent oscillations that are a hallmark of mammalian fertilization. Most studies to characterize those mechanisms in oocytes and eggs thus far have focused on the role of IP_3R1, which is the main intracellular channel responsible for Ca^{2+} release, and it optimization during maturation, as well on several changes that occur during the same process with the ER, which is the host organelle of IP_3R1 [18, 32-34]. Nevertheless, an covert Ca^{2+} toolkit in oocytes/eggs are the plasma membrane channels that make possible the filling of the $[Ca^{2+}]_{ER}$ store during maturation and its refilling during oscillations, as without Ca^{2+} influx oscillations do not persist [88]. Our study was designed to examine the Ca^{2+} influx pathway(s) that are associated with the increase in $[Ca^{2+}]_{ER}$ during mouse oocyte maturation and their regulation during this process. Our expectation is that these results will contribute to identify the Ca^{2+} influx pathway(s) that underlie the fertilization induced $[Ca^{2+}]_i$ oscillations.

The first aim of our studies focused on identifying the Ca^{2+} influx pathways associated with the spontaneous increase in $[Ca^{2+}]_{ER}$ during maturation. Given that the stores are low at the GV stage and there is increased Ca^{2+} influx at this stage, we examined the presence of SOCE, as it is a well known Ca^{2+} influx pathway modulated by levels of $[Ca^{2+}]_{ER}$ and is ubiquitously expressed. We confirmed that oocytes and eggs express the SOCE components, Stim1 and Orai1, both at the message and protein

levels. We also demonstrated that whereas Ca^{2+} influx, either induced following TG addition or simply by changing the levels of $[Ca^{2+}]_e$, was robust in GV oocytes, it was severely decreased in MII eggs. Thus, these observations show that Ca^{2+} influx is distinctly regulated during oocyte maturation, and that the levels of $[Ca^{2+}]_{ER}$ might be one of the factors involved in the modulation of Ca^{2+} influx.

We next investigated whether the regulation of Ca^{2+} influx during maturation was also observed after expression of the of ER Ca^{2+} sensor component of SOCE, hStim1-YFP. Remarkably, overexpression of hStim1-YFP greatly increased the Ca^{2+} influx triggered by ER store depletion throughout maturation. Nevertheless, and consistent with the changes observed for endogenous Ca^{2+} influx, the magnitude of Ca^{2+} influx was significantly reduced as maturation progressed and it was minimal at the MII stage. Therefore, overexpression of hStim1-YFP recapitulated the regulation of endogenous Ca^{2+} influx during maturation, suggesting that SOCE may be one of the mechanisms involved in Ca^{2+} influx during mouse oocyte maturation. Similar effects and down regulation of Ca^{2+} influx was observed when both components of SOCE, Stim1 and Orai1, were co-expressed. Importantly, the only example where the suppression of Ca^{2+} influx with meiotic progression was bypassed was when constitutively active Stim1, D76A hStim1 [48], was co-expressed with hOrai1; in this case, the increased influx rates remained throughout maturation, even at the MII stage. These results suggest that one of the mechanism mediating the inactivation of Ca^{2+} influx is the increase in $[Ca^{2+}]_{ER}$ levels, as the suppression is bypassed by expression of D76A-hStim1, which is insensitive to levels in the ER. The excessive influx following expression D76A-hStim1 had detrimental effects on maturation rates, as it prevented the progression of meiosis in many of the oocytes. In sum, we demonstrate that the components of SOCE are expressed in mouse oocytes/eggs and that Ca^{2+} influx mediated through this mechanism, and possibly through others, is downregulated during maturation. The inactivation of the influx is associated with increased $[Ca^{2+}]_{ER}$ levels, although others mechanisms are also thought to participate and will be investigated below [60, 86]. Lastly, inactivation of Ca^{2+} influx seems necessary, as it is maintained unchanged throughout maturation, compromises meiotic progression.

To better understand the mechanisms underlying the suppression of SOCE during maturation, we expressed hStim1-YFP and using confocal microscopy we monitored its distribution throughout maturation. We found that during maturation, hStim1-YFP undergoes remarkable changes in distribution such that at the GV stage hStim1-YFP displayed appears organized in large patches that are spread throughout the ooplasm. As maturation commences, these internal patches appear to dissolve and the distribution becomes nearly homogenous throughout the ooplasm, which is similar to the distribution of the ER. Upon ER Ca^{2+} depletion, hStim1 presence in the ooplasm at the GV stage decreases and this is accompanied by the appearance of distinct puncta and accumulation near the PM. Importantly, the same treatment in MII eggs does not affect the distribution hStim1-YFP. Further, if Stim1 and Orai1 are co-expressed, following TG treatment and emptying of the stores, there is extensive co-localization of these molecules at the sites of puncta formation in GV stage oocytes whereas the overlap is negligible in MII eggs. Therefore, the distribution of Stim1 undergoes significant reorganization during maturation, and the inability of Stim1 to form puncta at the MII stage might be a mechanism that underlies the inactivation of SOCE in MII eggs.

Earlier studies have reported that phosphorylation of Stim1 may be one of the mechanisms that contributes to the suppression of SOCE in mitotic cells [59, 116] and in *Xenopus* eggs [64, 65, 86]. Importantly, whereas both studies agreed that Stim1 is phosphorylated during M-phases of the cell cycle, results in somatic cells pointed at this mechanism as responsible for inhibition of puncta formation and Ca^{2+} influx (Smyth, Petranka et al. 2009), although in *Xenopus* eggs it was shown to affect Stim1 distribution but not the function of SOCE[86] . To examine the possible impact of Stim1 phosphorylation in mouse oocytes/eggs, we designed a series of studies to demonstrate whether Stim1 phosphorylation takes place in our system and how this impacts the function of SOCE. Our results show that the exogenously expressed hStim1-YFP is differentially phosphorylated during maturation, and this might also be the case for the endogenous mStim1. We confirmed that the phosphorylation was occurring on the C-terminal end of the molecule, as expression of a hStim1 mutant missing the last 200 amino acids failed to show any migration changes following western blotting. Lastly, with the use of

pharmacological inhibitors and collection of oocytes during different stages of maturation we show that the majority of Stim1 phosphorylation is mediated by CDK1, although MAPK also seems to target Stim1 during mouse oocyte maturation.

We next examined how phosphorylations affected the distribution of hStim1 and the function of SOCE. On way we tested this effect was by expressing hStim1 and hOrai1 before and after GVBD, which is before and after activation of Cdk1. We used the D76A-Stim1 mutant, so its distribution would not be affected by $[Ca^{2+}]_{ER}$ levels, and E106Q hOrai1, which is inactive so that excessive Ca^{2+} influx does not alter the progression of meiosis. The rationale for injecting post-Cdk1 activation was to allow hStim1 to become phosphorylated prior to interacting with hOrai1. We found that the distribution of D76A hStim1 was greatly affected by the timing of injection, as injection after GVBD reduced the interaction of D76A hStim1 with E106Q hOrai1, as reflected by the smaller puncta size as well as reduced overlap following the merging of their respective images. We also examined the impact phosphorylation on Stim1 distribution and function by specifically deleting/replacing residues that are targets of phosphorylation. Expression of a mutant with a large truncation of the C-terminal end of the molecule, hStim1-482-stop, showed altered organization with large internal patches, which seemed to remain largely intact following depletion of $[Ca^{2+}]_{ER}$ after addition of TG, which is radically different from the distribution of WT hStim1. Remarkably, this mutant supported Ca^{2+} influx as much as WT hStim1. A second mutant examined was similar to hStim1-482-stop, although in this case the poly-K found at the end of hStim1 was added back, 481-poly K mutant. Expression of this mutant resulted in a nearly homogenous distribution throughout the ER, although it seemed to form a series of internal parallel sheets, possibly as a consequence of ER reorganization. Upon depletion of $[Ca^{2+}]_{ER}$, 481-poly K hStim1 continued to form these internal sheets, although it formed prominent puncta near the PM. Consistent with the cortical accumulation of m481-polyK tail, it greatly enhanced Ca^{2+} influx following the re-addition of Ca^{2+} to the media. Mutation of S668 to A within a conserved CDK1 site at the very tail end of the molecule, also altered the distribution of hStim1, as puncta formation was seen even before depletion of $[Ca^{2+}]_{ER}$, although its effects on Ca^{2+} influx was comparable to that of WT hStim1.

Finally, we tested a mutant where all serine amino acids within the minimal kinase motif S/T-P in the C-terminal end of the molecule were substituted to alanine, S10A hStim1-YFP. Expression of this mutant resulted in nearly constitutive cortical distribution of the molecule, extensive overlap with Orai1 and significant enhancement of Ca^{2+} influx, which also seemed unable to be inactivated. Taken together, our results show that phosphorylation of Stim1 limits its cortical distribution, its ability to form puncta and interact with Orai1, and therefore represent one of mechanisms whereby SOCE is suppressed in M-phase stages of mitosis and meiosis.

Despite our findings, important aspects of the regulation of Ca^{2+} influx in mouse oocytes/eggs remain unknown. For example, what is the role of endogenous SOCE in the increase of $[Ca^{2+}]_{ER}$ and support of the oscillations during fertilization? This could be answered in part by performing knockdown studies as well as using tissue-specific knockouts. Our attempts using knockdown studies or dominant negative constructs have thus far being unsuccessful. Importantly, we need to identify the endogenous channel(s) that hStim1 is binding and gating in mouse oocytes. It is possible that one of the channels is Orai1, as we have shown that is expressed in mouse oocytes. Nevertheless, Stim1 has been shown to interact with others family of channels [112, 117-120], and it would be pivotal to show if these channels are expressed in mouse oocytes and if Stim1 gates them. In addition, it would be necessary how these channels contribute to Ca^{2+} homeostasis during maturation and fertilization. Ca^{2+} influx is required to maintain the fertilization-initiated oscillations and initiate embryo development. In spite of its relevance, we know nearly nothing about the mechanisms, channels and regulation of Ca^{2+} influx in these cells. Therefore, our studies are a first step in the characterization of the channels that regulate Ca^{2+} influx in oocytes and eggs. We have developed novel tools that will make possible to probe the function of SOCE but also of other channels, which should make possible the elucidation of the mechanisms that underlie Ca^{2+} influx in these cells. Such knowledge will contribute to improve conditions for *in vitro* maturation conditions, which will enhance the developmental competence

of *in vitro* matured oocytes. Lastly, these mechanisms could be utilized to design better egg activation protocols as well as serve as targets for contraception.

BIBLIOGRAPHY

1. Clapham, D.E., *Calcium signaling.* Cell, 2007. **131**(6): p. 1047-58.
2. Berridge, M.J., M.D. Bootman, and H.L. Roderick, *Calcium signalling: dynamics, homeostasis and remodelling.* Nat Rev Mol Cell Biol, 2003. **4**(7): p. 517-29.
3. Berridge, M.J., P. Lipp, and M.D. Bootman, *The versatility and universality of calcium signalling.* Nat Rev Mol Cell Biol, 2000. **1**(1): p. 11-21.
4. Parekh, A.B. and J.W. Putney, Jr., *Store-operated calcium channels.* Physiol Rev, 2005. **85**(2): p. 757-810.
5. Collins, S.R. and T. Meyer, *Evolutionary origins of STIM1 and STIM2 within ancient Ca2+ signaling systems.* Trends Cell Biol, 2011. **21**(4): p. 202-11.
6. Bootman, M.D., *Calcium signaling.* Cold Spring Harb Perspect Biol, 2012. **4**(7): p. a011171.
7. Swann, K., et al., *PLCzeta(zeta): a sperm protein that triggers Ca2+ oscillations and egg activation in mammals.* Semin Cell Dev Biol, 2006. **17**(2): p. 264-73.
8. Runft, L.L., L.A. Jaffe, and L.M. Mehlmann, *Egg activation at fertilization: where it all begins.* Dev Biol, 2002. **245**(2): p. 237-54.
9. Malcuit, C., M. Kurokawa, and R.A. Fissore, *Calcium oscillations and mammalian egg activation.* J Cell Physiol, 2006. **206**(3): p. 565-73.
10. Stricker, S.A., *Comparative biology of calcium signaling during fertilization and egg activation in animals.* Dev Biol, 1999. **211**(2): p. 157-76.
11. McGuinness, O.M., et al., *A direct measurement of increased divalent cation influx in fertilised mouse oocytes.* Development, 1996. **122**(7): p. 2199-206.
12. Ducibella, T., et al., *Egg-to-embryo transition is driven by differential responses to Ca(2+) oscillation number.* Dev Biol, 2002. **250**(2): p. 280-91.
13. Schultz, R.M. and G.S. Kopf, *Molecular basis of mammalian egg activation.* Curr Top Dev Biol, 1995. **30**: p. 21-62.
14. Saunders, C.M., et al., *PLC zeta: a sperm-specific trigger of Ca(2+) oscillations in eggs and embryo development.* Development, 2002. **129**(15): p. 3533-44.
15. Ducibella, T. and R. Fissore, *The roles of Ca2+, downstream protein kinases, and oscillatory signaling in regulating fertilization and the activation of development.* Dev Biol, 2008. **315**(2): p. 257-79.
16. Miyazaki, S., *Thirty years of calcium signals at fertilization.* Semin Cell Dev Biol, 2006. **17**(2): p. 233-43.
17. Miyazaki, S., et al., *Block of Ca2+ wave and Ca2+ oscillation by antibody to the inositol 1,4,5-trisphosphate receptor in fertilized hamster eggs.* Science, 1992. **257**(5067): p. 251-5.
18. Kline, D. and J.T. Kline, *Thapsigargin activates a calcium influx pathway in the unfertilized mouse egg and suppresses repetitive calcium transients in the fertilized egg.* J Biol Chem, 1992. **267**(25): p. 17624-30.
19. Ichijima, Y., et al., *MDC1 directs chromosome-wide silencing of the sex chromosomes in male germ cells.* Genes Dev, 2011. **25**(9): p. 959-71.
20. Johnson, J., et al., *Calcium/calmodulin-dependent protein kinase II and calmodulin: regulators of the meiotic spindle in mouse eggs.* Dev Biol, 1998. **204**(2): p. 464-77.
21. Backs, J., et al., *The gamma isoform of CaM kinase II controls mouse egg activation by regulating cell cycle resumption.* Proc Natl Acad Sci U S A, 2010. **107**(1): p. 81-6.
22. Markoulaki, S., et al., *Oscillatory CaMKII activity in mouse egg activation.* Dev Biol, 2003. **258**(2): p. 464-74.

23. Ozil, J.P., et al., *Egg activation events are regulated by the duration of a sustained [Ca2+]cyt signal in the mouse.* Dev Biol, 2005. **282**(1): p. 39-54.
24. Gordo, A.C., et al., *Injection of sperm cytosolic factor into mouse metaphase II oocytes induces different developmental fates according to the frequency of [Ca(2+)](i) oscillations and oocyte age.* Biol Reprod, 2000. **62**(5): p. 1370-9.
25. Ducibella, T., R.M. Schultz, and J.P. Ozil, *Role of calcium signals in early development.* Semin Cell Dev Biol, 2006. **17**(2): p. 324-32.
26. Mehlmann, L.M., *Stops and starts in mammalian oocytes: recent advances in understanding the regulation of meiotic arrest and oocyte maturation.* Reproduction, 2005. **130**(6): p. 791-9.
27. Kim, J.H., et al., *Orai1 and STIM1 are critical for cell migration and proliferation of clear cell renal cell carcinoma.* Biochem Biophys Res Commun, 2014. **448**(1): p. 76-82.
28. Gautier, J., et al., *Cyclin is a component of maturation-promoting factor from Xenopus.* Cell, 1990. **60**(3): p. 487-94.
29. Phillips, K.P., et al., *Inhibition of MEK or cdc2 kinase parthenogenetically activates mouse eggs and yields the same phenotypes as Mos(-/-) parthenogenotes.* Dev Biol, 2002. **247**(1): p. 210-23.
30. Racki, W.J. and J.D. Richter, *CPEB controls oocyte growth and follicle development in the mouse.* Development, 2006. **133**(22): p. 4527-37.
31. Li, R. and D.F. Albertini, *The road to maturation: somatic cell interaction and self-organization of the mammalian oocyte.* Nat Rev Mol Cell Biol, 2013. **14**(3): p. 141-52.
32. Tombes, R.M., et al., *Meiosis, egg activation, and nuclear envelope breakdown are differentially reliant on Ca2+, whereas germinal vesicle breakdown is Ca2+ independent in the mouse oocyte.* J Cell Biol, 1992. **117**(4): p. 799-811.
33. Jones, K.T., J. Carroll, and D.G. Whittingham, *Ionomycin, thapsigargin, ryanodine, and sperm induced Ca2+ release increase during meiotic maturation of mouse oocytes.* J Biol Chem, 1995. **270**(12): p. 6671-7.
34. Mehlmann, L.M. and D. Kline, *Regulation of intracellular calcium in the mouse egg: calcium release in response to sperm or inositol trisphosphate is enhanced after meiotic maturation.* Biol Reprod, 1994. **51**(6): p. 1088-98.
35. Miyazaki, S., et al., *Essential role of the inositol 1,4,5-trisphosphate receptor/Ca2+ release channel in Ca2+ waves and Ca2+ oscillations at fertilization of mammalian eggs.* Dev Biol, 1993. **158**(1): p. 62-78.
36. Mehlmann, L.M., et al., *Reorganization of the endoplasmic reticulum during meiotic maturation of the mouse oocyte.* Dev Biol, 1995. **170**(2): p. 607-15.
37. Carroll, J., et al., *Spatiotemporal dynamics of intracellular [Ca2+]i oscillations during the growth and meiotic maturation of mouse oocytes.* Development, 1994. **120**(12): p. 3507-17.
38. Carroll, J. and K. Swann, *Spontaneous cytosolic calcium oscillations driven by inositol trisphosphate occur during in vitro maturation of mouse oocytes.* J Biol Chem, 1992. **267**(16): p. 11196-201.
39. Putney, J.W., Jr., *A model for receptor-regulated calcium entry.* Cell Calcium, 1986. **7**(1): p. 1-12.
40. Penner, R., C. Fasolato, and M. Hoth, *Calcium influx and its control by calcium release.* Curr Opin Neurobiol, 1993. **3**(3): p. 368-74.
41. Limnander, A., et al., *STIM1, PKC-delta and RasGRP set a threshold for proapoptotic Erk signaling during B cell development.* Nat Immunol, 2011. **12**(5): p. 425-33.
42. Hoth, M. and R. Penner, *Calcium release-activated calcium current in rat mast cells.* J Physiol, 1993. **465**: p. 359-86.
43. Hsu, S., et al., *Fundamental Ca2+ signaling mechanisms in mouse dendritic cells: CRAC is the major Ca2+ entry pathway.* J Immunol, 2001. **166**(10): p. 6126-33.

44. Takemura, H., et al., *Activation of calcium entry by the tumor promoter thapsigargin in parotid acinar cells. Evidence that an intracellular calcium pool and not an inositol phosphate regulates calcium fluxes at the plasma membrane.* J Biol Chem, 1989. **264**(21): p. 12266-71.
45. Zweifach, A. and R.S. Lewis, *Mitogen-regulated Ca2+ current of T lymphocytes is activated by depletion of intracellular Ca2+ stores.* Proc Natl Acad Sci U S A, 1993. **90**(13): p. 6295-9.
46. Parekh, A.B., A. Fleig, and R. Penner, *The store-operated calcium current I(CRAC): nonlinear activation by InsP3 and dissociation from calcium release.* Cell, 1997. **89**(6): p. 973-80.
47. Putney, J.W., *Capacitative calcium entry: from concept to molecules.* Immunol Rev, 2009. **231**(1): p. 10-22.
48. Liou, J., et al., *STIM is a Ca2+ sensor essential for Ca2+-store-depletion-triggered Ca2+ influx.* Curr Biol, 2005. **15**(13): p. 1235-41.
49. Roos, J., et al., *STIM1, an essential and conserved component of store-operated Ca2+ channel function.* J Cell Biol, 2005. **169**(3): p. 435-45.
50. Feske, S., et al., *A mutation in Orai1 causes immune deficiency by abrogating CRAC channel function.* Nature, 2006. **441**(7090): p. 179-85.
51. Vig, M., et al., *CRACM1 multimers form the ion-selective pore of the CRAC channel.* Curr Biol, 2006. **16**(20): p. 2073-9.
52. Barr, V.A., et al., *Dynamic movement of the calcium sensor STIM1 and the calcium channel Orai1 in activated T-cells: puncta and distal caps.* Mol Biol Cell, 2008. **19**(7): p. 2802-17.
53. Stathopulos, P.B., et al., *Structural and mechanistic insights into STIM1-mediated initiation of store-operated calcium entry.* Cell, 2008. **135**(1): p. 110-22.
54. Park, C.Y., et al., *STIM1 clusters and activates CRAC channels via direct binding of a cytosolic domain to Orai1.* Cell, 2009. **136**(5): p. 876-90.
55. Penna, A., et al., *The CRAC channel consists of a tetramer formed by Stim-induced dimerization of Orai dimers.* Nature, 2008. **456**(7218): p. 116-20.
56. Parekh, A.B., *Store-operated CRAC channels: function in health and disease.* Nat Rev Drug Discov, 2010. **9**(5): p. 399-410.
57. Jha, A., et al., *The STIM1 CTID domain determines access of SARAF to SOAR to regulate Orai1 channel function.* J Cell Biol, 2013. **202**(1): p. 71-9.
58. Yuan, J.P., et al., *SOAR and the polybasic STIM1 domains gate and regulate Orai channels.* Nat Cell Biol, 2009. **11**(3): p. 337-43.
59. Smyth, J.T., et al., *Phosphorylation of STIM1 underlies suppression of store-operated calcium entry during mitosis.* Nat Cell Biol, 2009. **11**(12): p. 1465-72.
60. Yu, F., L. Sun, and K. Machaca, *Orai1 internalization and STIM1 clustering inhibition modulate SOCE inactivation during meiosis.* Proc Natl Acad Sci U S A, 2009. **106**(41): p. 17401-6.
61. Grigoriev, I., et al., *STIM1 is a MT-plus-end-tracking protein involved in remodeling of the ER.* Curr Biol, 2008. **18**(3): p. 177-82.
62. Liou, J., et al., *Live-cell imaging reveals sequential oligomerization and local plasma membrane targeting of stromal interaction molecule 1 after Ca2+ store depletion.* Proc Natl Acad Sci U S A, 2007. **104**(22): p. 9301-6.
63. Zhou, Y., et al., *Initial activation of STIM1, the regulator of store-operated calcium entry.* Nat Struct Mol Biol, 2013. **20**(8): p. 973-81.
64. Machaca, K. and S. Haun, *Induction of maturation-promoting factor during Xenopus oocyte maturation uncouples Ca(2+) store depletion from store-operated Ca(2+) entry.* J Cell Biol, 2002. **156**(1): p. 75-85.

65. Machaca, K. and S. Haun, *Store-operated calcium entry inactivates at the germinal vesicle breakdown stage of Xenopus meiosis.* J Biol Chem, 2000. **275**(49): p. 38710-5.
66. Prikoszovits, A. and M. Schuh, *[The mineral content of calcium, phosphorus and magnesium in the serum and bones and the serum activity of alkaline phosphatase in slaughtered fattening pigs].* Dtsch Tierarztl Wochenschr, 1995. **102**(1): p. 53-5.
67. Mohri, T., et al., *Analysis of Mn(2+)/Ca(2+) influx and release during Ca(2+) oscillations in mouse eggs injected with sperm extract.* Cell Calcium, 2001. **29**(5): p. 311-25.
68. Gomez-Fernandez, C., et al., *Calcium signaling in mouse oocyte maturation: the roles of STIM1, ORAI1 and SOCE.* Mol Hum Reprod, 2012. **18**(4): p. 194-203.
69. Gomez-Fernandez, C., et al., *Relocalization of STIM1 in mouse oocytes at fertilization: early involvement of store-operated calcium entry.* Reproduction, 2009. **138**(2): p. 211-21.
70. Koh, S., et al., *STIM1 regulates store-operated Ca2+ entry in oocytes.* Dev Biol, 2009. **330**(2): p. 368-76.
71. Clift, D. and M. Schuh, *Restarting life: fertilization and the transition from meiosis to mitosis.* Nat Rev Mol Cell Biol, 2013. **14**(9): p. 549-62.
72. Jones, K.T., *Meiosis in oocytes: predisposition to aneuploidy and its increased incidence with age.* Hum Reprod Update, 2008. **14**(2): p. 143-58.
73. Archacka, K., et al., *Defective calcium release during in vitro fertilization of maturing oocytes of LT/Sv mice.* Int J Dev Biol, 2008. **52**(7): p. 903-12.
74. Fuenmayor, A.J., et al., *Six mechanisms of supraventricular tachycardia in the same patient: report of a case.* Int J Cardiol, 2005. **103**(3): p. 330-4.
75. Kurokawa, M., et al., *Proteolytic processing of phospholipase Czeta and [Ca2+]i oscillations during mammalian fertilization.* Dev Biol, 2007. **312**(1): p. 407-18.
76. Chatot, C.L., et al., *An improved culture medium supports development of random-bred 1-cell mouse embryos in vitro.* J Reprod Fertil, 1989. **86**(2): p. 679-88.
77. Milder, I.E., et al., *Relation between plasma enterodiol and enterolactone and dietary intake of lignans in a Dutch endoscopy-based population.* J Nutr, 2007. **137**(5): p. 1266-71.
78. Wang, C., et al., *Orai1 mediates store-operated Ca2+ entry during fertilization in mammalian oocytes.* Dev Biol, 2012. **365**(2): p. 414-23.
79. Homa, S.T., *Neomycin, an inhibitor of phosphoinositide hydrolysis, inhibits the resumption of bovine oocyte spontaneous meiotic maturation.* J Exp Zool, 1991. **258**(1): p. 95-103.
80. Kaufman, M.L. and S.T. Homa, *Defining a role for calcium in the resumption and progression of meiosis in the pig oocyte.* J Exp Zool, 1993. **265**(1): p. 69-76.
81. Sun, L. and K. Machaca, *Ca(2+)(cyt) negatively regulates the initiation of oocyte maturation.* J Cell Biol, 2004. **165**(1): p. 63-75.
82. DeHaven, W.I., et al., *Complex actions of 2-aminoethyldiphenyl borate on store-operated calcium entry.* J Biol Chem, 2008. **283**(28): p. 19265-73.
83. Bird, G.S., et al., *Methods for studying store-operated calcium entry.* Methods, 2008. **46**(3): p. 204-12.
84. Darbellay, B., et al., *STIM1L is a new actin-binding splice variant involved in fast repetitive Ca2+ release.* J Cell Biol, 2011. **194**(2): p. 335-46.
85. Balghi, H., et al., *Enhanced Ca2+ entry due to Orai1 plasma membrane insertion increases IL-8 secretion by cystic fibrosis airways.* FASEB J, 2011. **25**(12): p. 4274-91.
86. Yu, F., L. Sun, and K. Machaca, *Constitutive recycling of the store-operated Ca2+ channel Orai1 and its internalization during meiosis.* J Cell Biol, 2010. **191**(3): p. 523-35.
87. Putney, J.W., *Pharmacology of store-operated calcium channels.* Mol Interv, 2010. **10**(4): p. 209-18.

88. Miao, Y.L., et al., *Calcium influx-mediated signaling is required for complete mouse egg activation.* Proc Natl Acad Sci U S A, 2012. **109**(11): p. 4169-74.
89. Takahashi, T., et al., *Ca(2+) influx-dependent refilling of intracellular Ca(2+) stores determines the frequency of Ca(2+) oscillations in fertilized mouse eggs.* Biochem Biophys Res Commun, 2013. **430**(1): p. 60-5.
90. Lee, K., C. Wang, and Z. Machaty, *STIM1 is required for Ca2+ signaling during mammalian fertilization.* Dev Biol, 2012. **367**(2): p. 154-62.
91. Russa, A.D., et al., *Microtubule remodeling mediates the inhibition of store-operated calcium entry (SOCE) during mitosis in COS-7 cells.* Arch Histol Cytol, 2008. **71**(4): p. 249-63.
92. Manji, S.S., et al., *STIM1: a novel phosphoprotein located at the cell surface.* Biochim Biophys Acta, 2000. **1481**(1): p. 147-55.
93. Pozo-Guisado, E., et al., *Phosphorylation of STIM1 at ERK1/2 target sites modulates store-operated calcium entry.* J Cell Sci, 2010. **123**(Pt 18): p. 3084-93.
94. Bayles, S.W., et al., *Demonstration that phosphorescent 6-bromo-2-naphthyl sulfate can be used to probe heme accessibility in heme proteins.* Photochem Photobiol, 1991. **54**(2): p. 175-81.
95. Jones, K.T., et al., *Repetitive sperm-induced Ca2+ transients in mouse oocytes are cell cycle dependent.* Development, 1995. **121**(10): p. 3259-66.
96. Marangos, P., G. FitzHarris, and J. Carroll, *Ca2+ oscillations at fertilization in mammals are regulated by the formation of pronuclei.* Development, 2003. **130**(7): p. 1461-72.
97. Mehlmann, L.M., K. Mikoshiba, and D. Kline, *Redistribution and increase in cortical inositol 1,4,5-trisphosphate receptors after meiotic maturation of the mouse oocyte.* Dev Biol, 1996. **180**(2): p. 489-98.
98. Kline, D., et al., *The cortical endoplasmic reticulum (ER) of the mouse egg: localization of ER clusters in relation to the generation of repetitive calcium waves.* Dev Biol, 1999. **215**(2): p. 431-42.
99. Cheon, B., et al., *Ca2+ influx and the store-operated Ca2+ entry pathway undergo regulation during mouse oocyte maturation.* Mol Biol Cell, 2013. **24**(9): p. 1396-410.
100. Putney, J.W., Jr., et al., *Mechanisms of capacitative calcium entry.* J Cell Sci, 2001. **114**(Pt 12): p. 2223-9.
101. Lewis, R.S., *Store-operated calcium channels: new perspectives on mechanism and function.* Cold Spring Harb Perspect Biol, 2011. **3**(12).
102. Smyth, J.T., et al., *Phosphoregulation of STIM1 leads to exclusion of the endoplasmic reticulum from the mitotic spindle.* Curr Biol, 2012. **22**(16): p. 1487-93.
103. Palty, R., et al., *SARAF inactivates the store operated calcium entry machinery to prevent excess calcium refilling.* Cell, 2012. **149**(2): p. 425-38.
104. Mullins, F.M., et al., *STIM1 and calmodulin interact with Orai1 to induce Ca2+-dependent inactivation of CRAC channels.* Proc Natl Acad Sci U S A, 2009. **106**(36): p. 15495-500.
105. Kinoshita, E., E. Kinoshita-Kikuta, and T. Koike, *Separation and detection of large phosphoproteins using Phos-tag SDS-PAGE.* Nat Protoc, 2009. **4**(10): p. 1513-21.
106. Kinoshita-Kikuta, E., E. Kinoshita, and T. Koike, *Phos-tag beads as an immunoblotting enhancer for selective detection of phosphoproteins in cell lysates.* Anal Biochem, 2009. **389**(1): p. 83-5.
107. Yamamoto, T.M., et al., *Regulation of Greatwall kinase during Xenopus oocyte maturation.* Mol Biol Cell, 2011. **22**(13): p. 2157-64.
108. Yu, J., et al., *Greatwall kinase participates in the Cdc2 autoregulatory loop in Xenopus egg extracts.* Mol Cell, 2006. **22**(1): p. 83-91.

109. Zheng, L., et al., *Biophysical characterization of the EF-hand and SAM domain containing Ca2+ sensory region of STIM1 and STIM2.* Biochem Biophys Res Commun, 2008. **369**(1): p. 240-6.
110. Stathopulos, P.B., et al., *Stored Ca2+ depletion-induced oligomerization of stromal interaction molecule 1 (STIM1) via the EF-SAM region: An initiation mechanism for capacitive Ca2+ entry.* J Biol Chem, 2006. **281**(47): p. 35855-62.
111. Spassova, M.A., et al., *STIM1 has a plasma membrane role in the activation of store-operated Ca(2+) channels.* Proc Natl Acad Sci U S A, 2006. **103**(11): p. 4040-5.
112. Huang, G.N., et al., *STIM1 carboxyl-terminus activates native SOC, I(crac) and TRPC1 channels.* Nat Cell Biol, 2006. **8**(9): p. 1003-10.
113. Holt, L.J., et al., *Global analysis of Cdk1 substrate phosphorylation sites provides insights into evolution.* Science, 2009. **325**(5948): p. 1682-6.
114. Yu, F., et al., *Role of the STIM1 C-terminal domain in STIM1 clustering.* J Biol Chem, 2011. **286**(10): p. 8375-84.
115. Prakriya, M., et al., *Orai1 is an essential pore subunit of the CRAC channel.* Nature, 2006. **443**(7108): p. 230-3.
116. Preston, S.F., R.I. Sha'afi, and R.D. Berlin, *Regulation of Ca2+ influx during mitosis: Ca2+ influx and depletion of intracellular Ca2+ stores are coupled in interphase but not mitosis.* Cell Regul, 1991. **2**(11): p. 915-25.
117. Zeng, W., et al., *STIM1 gates TRPC channels, but not Orai1, by electrostatic interaction.* Mol Cell, 2008. **32**(3): p. 439-48.
118. Yuan, J.P., et al., *STIM1 heteromultimerizes TRPC channels to determine their function as store-operated channels.* Nat Cell Biol, 2007. **9**(6): p. 636-45.
119. Park, C.Y., A. Shcheglovitov, and R. Dolmetsch, *The CRAC channel activator STIM1 binds and inhibits L-type voltage-gated calcium channels.* Science, 2010. **330**(6000): p. 101-5.
120. Wang, Y., et al., *The calcium store sensor, STIM1, reciprocally controls Orai and CaV1.2 channels.* Science, 2010. **330**(6000): p. 105-9.